Synthesis of NiO-SDC Based Composite and Influence of La and H_2O_2 Addition on its Structural and Thermal Performance for Intermediate Temperature SOFCs

By

MUHAMMAD NAVEED AKBAR

Reg. #: NUST201260723MCES64112F

Session 2012-14

Supervised by

Dr. Zuhair S. Khan

This thesis is submitted to the U.S Pakistan Center for Advanced Studies in Energy in partial fulfillment of the requirements for the degree of

MASTERS of SCIENCE

in

ENERGY SYSTEMS ENGINEERING

U.S Pakistan Center for Advanced Studies in Energy (USPCAS-E),

National University of Sciences and Technology (NUST),

Main Campus Sector H-12, Islamabad 44000, Pakistan

February 2016

Certificate

This is to certify that work in this thesis has been carried out by **Mr. Muhammad Naveed Akbar** and completed under my supervision in Advanced Energy Materials and Fuel Cells Lab, U.S Pakistan Centre for Advanced Studies in Energy, National University of Sciences and Technology, Main Campus Sector H-12, Islamabad, Pakistan.

Supervisor:

_____
Dr. Zuhair S. Khan
USPCAS-E
NUST, Islamabad

GEC member # 1:

_____
Dr. Mrs. Naveed K. Janjua
Department of Chemistry
QAU, Islamabad

GEC member # 2:

_____
Dr. Muhammad Bilal Khan
USPCAS-E
NUST, Islamabad

GEC member # 3:

_____
Dr. Nasir Mehmood Ahmad
SCME
NUST, Islamabad

HoD-CES:

_____
Dr. Zuhair S. Khan
USPCAS-E
NUST, Islamabad

Principal / Dean:

_____
Dr. Muhammad Bilal Khan
USPCAS-E
NUST, Islamabad

I dedicated this thesis to my beloved Parents, Siblings, Teachers and dear Friends

Abstract

Solid oxide fuel cells (SOFCs) conventionally operate in the temperature range of 800 – 1000 °C. The barriers for full-scale commercialization of SOFCs are the high cost and relatively poor long-term stability due to the high temperatures used in current state-of-the-art SOFCs. One solution is to decrease the operating temperature from high to intermediate, e.g. to 550-750 °C but this requires developing new electrolytes and electrode materials. Also, to increase efficiency and practicality, the anode should be able to internally reform hydrocarbon fuels especially methane because it is the most common hydrocarbon in natural gas. In this respect, Nickel Oxide-Samarium Doped Ceria (NiO-SDC) is the suitable candidate for its robust stability and performance in the recent past for SOFC applications.

Various parameters were studied, such as pH, NiO concentration by volume, calcination temperature, addition of Lanthanum (La) and Hydrogen Peroxide (H_2O_2), to develop enhanced NiO-SDC composite. Observations from the X-ray diffraction results demonstrates that crystallites show an increment in their size with the rise in pH and calcination temperature but the alteration of NiO concentration influenced the average crystallite size. The average crystallite size in both the phases (NiO and SDC) show an increment at higher concentration of NiO. Furthermore, no impurity phases have been found in the crystalline structure of synthesized NiO-SDC composite material. SEM results demonstrated that NiO-SDC powder samples are well dispersed but the particles exhibit irregular shape and size of the particles ranges from 50-65 nm.

Two different methods have been used to improve the NiO-SDC cermet. Firstly, NiO-SDC composite anode material by adding Lanthanum (La), Ni(La)O-SDC, was prepared by co-precipitation route. Cubic fluorite structure was observed and crystallite sizes, of both NiO and SDC, fall in the size ranges of 25 nm – 48 nm. La mix and disperse in the compound finely and no chemical reaction was observed with 10 mol% La or even with 15 mol% La. However, with 20 mol% La, there appears the onset formation of La_2NiO_4 and $LaNiO_3$. Secondly, NiO-SDC was synthesized via altered co-precipitation method with the inclusion of Hydrogen Peroxide (H_2O_2). Cubic fluorite structures was also observed in NiO-SDC prepared using H_2O_2 and crystallites of NiO and SDC were found in the size ranges of 20 nm - 48 nm. Addition of H_2O_2 promotes somewhat earlier crystallization and it also resulted in formation of

refined crystals. Furthermore, the conductivity of NiO-SDC was also calculated at 650 °C and found to be 3.494×10^{-3} S/cm.

Last part contains chemical compatibility test of Neodymium Doped Ceria (NDC) electrolyte composite material and NiO-SDC. XRD characterization showed that both NDC and NiO-SDC remained separate at the elevated temperature of 800 °C and no mixed phase was found between the two composites. That is why it can be depicted that both of these materials can be used in SOFC applicaitons. Therefore, these research results can broaden the opportunities for applications in intermediate temperature solid oxide fuel cells (IT-SOFCs).

Keywords: ITSOFC, Nanocomposite Anode, Doping, Microstructural Analysis, Thermal Analysis

Table of Contents

List of Figures

List of Tables

List of Journals/Conference Papers

Journal Arcticle (Under Review):

1. M. N. Akbar, Mustafa Anwar, M. A. Rana, S. Shakir, Kamal Mustafa, Naveed K. Janjua, Zuhair S. Khan, Preparation of NiO-SDC Composites by a Modified Co-Precipitation Synthesis Method for Solid Oxide Fuel Cell (SOFC) Applications.

Conference Papers from other work not included:

1. M. N. Akbar, Mustafa Anwar, M. A. Rana, S. Shakir, Kamal Mustafa, Naveed K. Janjua, Zuhair S. Khan, Synthesis of NiO-SDC by co-precipitation for anode applications in low temperature solid oxide fuel cells, Conference on Frontiers of Nanoscience & Nanotechnology, June 03-05, 2014, PINSTECH Islamabad, Pakistan.
2. Mustafa Anwar, M. N. Akbar, Naveed K. Janjua, M. A. Rana, Kamal Mustafa, S. Shakir, Z. S. Khan, Development of Samarium-doped ceria based electrolytes for use in Intermediate Temperature Solid Oxide Fuel Cells (IT-SOFCs), Conference on Frontiers of Nanoscience & Nanotechnology, June 03-05, 2014, PINSTECH Islamabad, Pakistan (Attached to Annexure-A).
3. M. Akmal Rana, Mustafa Anwar, M. N. Akbar, Kamal Mustafa, S. Shakir, Zuhair S. Khan, Investigations on doped ceria electrolytes and their structural and electrical properties for applications in low temperature solid oxide fuel cells, Conference on Frontiers of Nanoscience & Nanotechnology, June 03-05, 2014, PINSTECH Islamabad, Pakistan.
4. Kamal Mustafa, M. A. Rana, Mustafa Anwar, M. N. Akbar, S. Shakir, Zuhair S. Khan, Synthesis of cobalt doped lithiated NiO cathode material and investigation on corrosion performance of LiAlO2 matrices for MCFCs applications, Conference on Frontiers of Nanoscience & Nanotechnology, June 03-05, 2014, PINSTECH Islamabad, Pakistan.
5. Sehar Shakir, Abdur Rehman, M. A. Rana, M. N. Akbar, Mustafa Anwar, Kamal Mustafa, Zuhair S. Khan, Sol-gel fabrication of TiO_2 Nanoparticles and investigations on Cu doping effects for application in dye sensitized solar cells, Conference on Frontiers of Nanoscience & Nanotechnology, June 03-05, 2014, PINSTECH Islamabad, Pakistan.

List of Abbreviations

PEMFC	Proton Exchange Membrane Fuel Cell
PAFC	Phosphoric Acid Fuel Cell
MCFC	Molten Carbonate Fuel Cell
AFC	Alkaline Fuel Cell
LTFC	Low Temperature Fuel Cell
HTFC	High Temperature Fuel Cell
SOFC	Solid Oxide Fuel Cell
ITSOFC	Intermediate Temperature Solid Oxide Fuel Cell
LTSOFC	Low Temperature Solid Oxide Fuel Cell
Ni-YSZ	Nickel Yttria Stabilized Zirconia
Ni-GDC	Nickel Gadolinium Doped Ceria
Ni-SDC	Nickel Samarium Doped Ceria
LSM	Lanthanum Strontium Manganite
XRD	X-Ray Diffraction
SEM	Scanning Electron Microscope
DC	Direct Current
NiLaO-SDC	Nickel Lanthanum Oxide Samarium Doped Ceria

Chapter 1

Introduction

1.1 The Beginning of Fuel Cell

Swiss scientist C. F. Schönbein discovered the fundamentals of the fuel cell during mid-1830s of 19th century and Sir W. Grove laid down the foundation of the first fuel cell in the late 1830s [1]. In 20th century, Francis B. of Cambridge University presented an alkali-based fuel cell system to produce electricity (~6 kW) for the first time. After the break through demonstration of alkali-based fuel cell systems, NASA required a portable energy station to provide power for the spacecraft applications. In the early mid-1960s, the researchers and developers were centered to further exploit various fuel cell applications like static power generation. IFC developed a ~11 kilowatt capacity fuel cell in early 1970s for space shuttle orbiter of NASA to provide dependable power without employing any secondary source like battery [2]. However, many countries after 50 years significantly reduced the development of fuel cells, as it required a high budget for installation. In the light of this, currently most of the developers are focused to reduce the higher installation cost of fuel cell.

1.2 What is a Fuel Cell?

Like a battery, a fuel cell is an electricity generator that transforms electrochemical reactions directly into electrical power. In other words, it is such an energy-producing device, which converts the chemical energy stored in the fuels instantly into electricity and heat without the use of any secondary process and the byproduct is only water making it tremendously environment friendly. While the commonly used engines/ energy systems generate electricity by using mechanical energy, which leads to scaled down efficiency when compared with fuel cells. Fuel cells are combination of conventional engines and batteries because like an engine fuel cells can work as long as fuel supply is available and fuel cell behaves like a battery under load conditions[3].

A typical fuel cell includes three most important components:

i. A positive electrode (anode)
ii. A negative electrode (cathode)
iii. electrolyte

1.3 How Fuel Cell Works?

The construction of a typical fuel cell is demonstrated in Figure 1.1 [4]. The fuel cell comprises an electrolyte layer sandwiched between electrodes (an anode and a cathode) on its sides. The hydrogen fuel is pumped at anode and the oxidizing agent (commonly oxygen) is provided at the cathode. While at the positive electrode (anode), the fuel breaks down as cations and anions. The intermediate electrolyte, being an ionic conductor, permits only the cations to pass through anode to cathode side and resists the flow of electrons through it. As a result, the electrons use the external circuit as a passage towards the cathode. The recombination of cations and anions with the oxidizing agent happens at the negative electrode (cathode) to produce water as byproduct. The chemical reactions happening at electrodes are given as:

Anode reaction: $H_2 \rightarrow 2H^+ + 2e^-$ (1.1)

Cathode reaction: $½\ O_2 + 2H^+ + 2e^- \rightarrow H_2O$ (1.2)

Overall reaction: $H_2 + ½O_2 \leftrightarrow H_2O$ + Waste Heat (1.3)

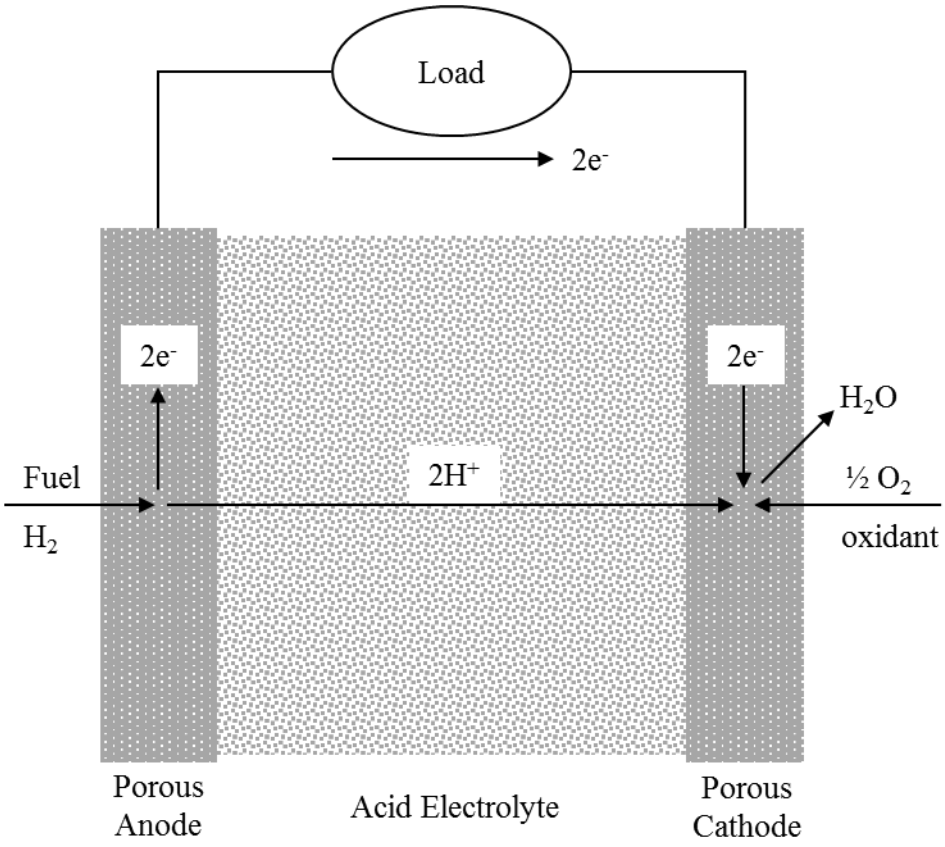

Figure 1.1: A typical acid electrolyte fuel cell

1.4 Fuel Cell Performance

As long as the fuel is being fed, the fuel cell should ideally maintain a constant voltage. This ideal voltage (the reversible voltage) can be determined using the Nernst equation.

$$E = E_{H_2}^0 + \frac{RT}{4F}\ln(\rho_{O_{2e}}) + \frac{RT}{4F}\ln\left(\frac{\rho_{H_{2a}}}{\rho_{H_2O_a}}\right) \quad (1.4)$$

In the case of hydrogen/air fuel cell, the reversible voltages are 1.16V and 1.11V at 100 ºC and 900 ºC, respectively. In contrast, the voltage output of a real fuel cell decreases as the current load increases due to the irreversible voltage losses. These losses (or overpotentials) are attributed to three causes: activation, ohmic and concentration polarizations, discussed in next section. Thus, the net cell voltage E_{cell} can be expressed as:

$$E_{cell} = E - \eta \quad (1.5)$$

where η is the overpotential which can be expanded as the following equation:

$$\eta = \eta_{act} + \eta_{ohm} + \eta_{conc} \quad (1.6)$$

where η_{act}, η_{ohm} and η_{conc} are the activation, ohmic and concentration overpotentials, respectively [5]. The overall effects of these overpotentials as a function of current density are indicated on the performance curve shown in Figure 1.2.

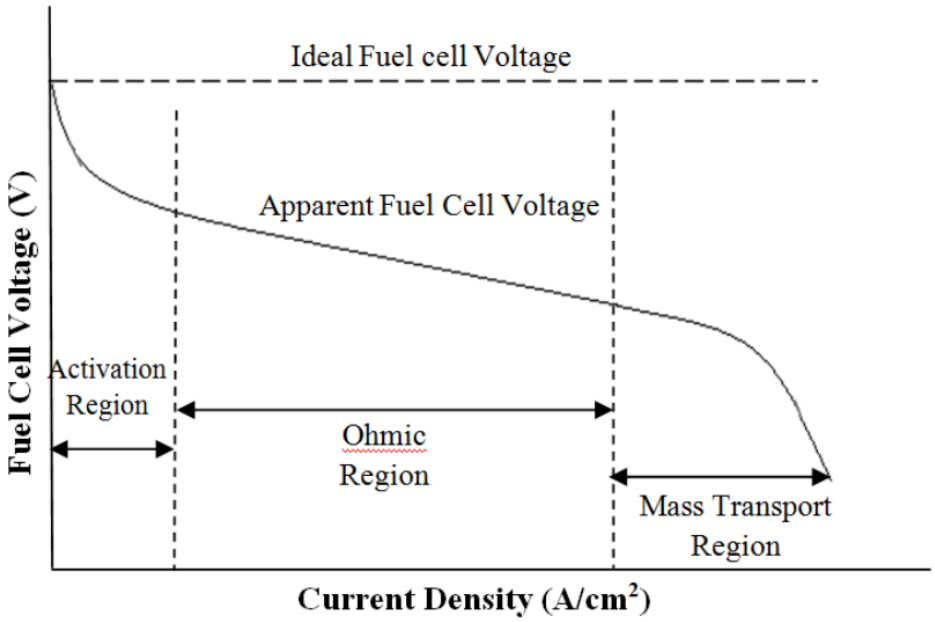

Figure 1.2: Overall effects of various polarizations on the performance curve

1.5 Fuel Cell Types

Although fuel cells of all types operate with similar overall reactions, they can be classified depending on the electrolyte [6]. Primarily, fuel cells are categorized into following main types:

i. AFC – Alkaline fuel cell
ii. DMFC – Direct methanol fuel cell
iii. MCFC – Molten carbonate fuel cell
iv. PAFC – Phosphoric acid fuel cell
v. PEMFC – Proton exchange membrane fuel cell
vi. SOFC – Solid oxide fuel cell

Generally, the option/ type of the electrolyte prescribes the working temperature of the fuel cell. The operating temperature of a fuel cell demonstrates the physical stability and thermal efficiency of materials used for construction of cell components (i.e., electrodes, electrolyte, interconnect, current collector, etc.). Liquid electrolytes are restricted to temperatures up to 200 °C or lesser due to the high vapor pressure and quick degradation at elevated temperatures. The operating temperature has a vital function in determining the need for fuel reforming. In LTFCs, the hydrogen (fuel) must be pure before feeding the cell. Moreover, the anode Pt-catalyst in LTFCs is greatly toxicated in the presence of carbon monoxide. In HTFCs, carbon monoxide and even certain hydrocarbons are possible to reform internally to hydrogen. Table 1.1 contains a summary of differences in each type of fuel cell [7].

Table 1.1 Types of Fuel Cells with various Characteristic Properties

Item/ Property		Type of Fuel Cell				
	AFC	**DMFC**	**MCFC**	**PAFC**	**PEMFC**	**SOFC**
Electrolyte	Alkaline	Solid Polymer Membrane	Alkali Carbonate mixtures	Phosphoric acid	Ion exchange membrane	Stabilized zirconia and ceria
Operating Temperature (°C)	50-250	60-200	600-700	160-220	50-85	800-1000
Charge Carrier	OH^-	H^+	CO_3^{2-}	H^+	H^+	O^{2-}
Electrolyte State	Liquid	Solid	Immobilized Liquid	Immobilized Liquid	Solid	Solid
Corrosiveness	High	None	High	High	None	None
Fuel	H_2	CH_3OH	Synthesis gas, CH_4	H_2	H_2	Synthesis gas, CH_4
Anode Reaction	$H_2 + 2OH^- \rightarrow 2H_2O + 2e^-$	$CH_3OH + H_2O \rightarrow CO_2 + 6H^+ + 6H^-$	$H_2O + CO_3^{2-} \rightarrow H_2O + CO_2 + 2e^-$	$H_2 \rightarrow 2H^+ + 2e^-$	$H_2 \rightarrow 2H^+ + 2e^-$	$H_2 + O^{2-} \rightarrow H_2O + 2e^-$
Cathode Reaction	$½\ O_2 + H_2O + 2e^- \rightarrow 2(OH)^-$	$O_2 + 4H^+ + 4e^- \rightarrow 2H_2O$	$½\ O_2 + CO_2 + 2e^- \rightarrow 2CO_3^{2-}$	$½\ O_2 + 2H^+ + 2e^- \rightarrow H_2O$	$½\ O_2 + 2H^+ + 2e^- \rightarrow H_2O$	$½\ O_2 + 2e^- \rightarrow O^{2-}$
Catalyst	Pt/Au, Pt, Ag for cathode and anode	Ni, Ag, Metal Oxides, Spinels, Noble Metals	Cathode: Li/NiO Anode: Ni, Ni/Cr	Cathode: Pt/Cr/Co, Pt/Ni; Anode: Pt	Cathode: Pt, Pt/Ru Anode: Pt	Cathode: $LaSrMnO_3$ Anode: Ni/ZrO_2
Cogeneration Heat	None	None	High	Low quality	None	High
Size (MW)	Very small (0.1)	1	2	1.3	0.25	1-2
Application	Small power in aerospace	Mobiles, Laptops & other portable devices	Power generation, CHP	Power generation, CHP	Transport, small appliances	Power generation, CHP
Efficiency (%)	>60	~40	50-60	40-45	<40	50-60

1.5.1 Alkaline Fuel Cell (AFC)

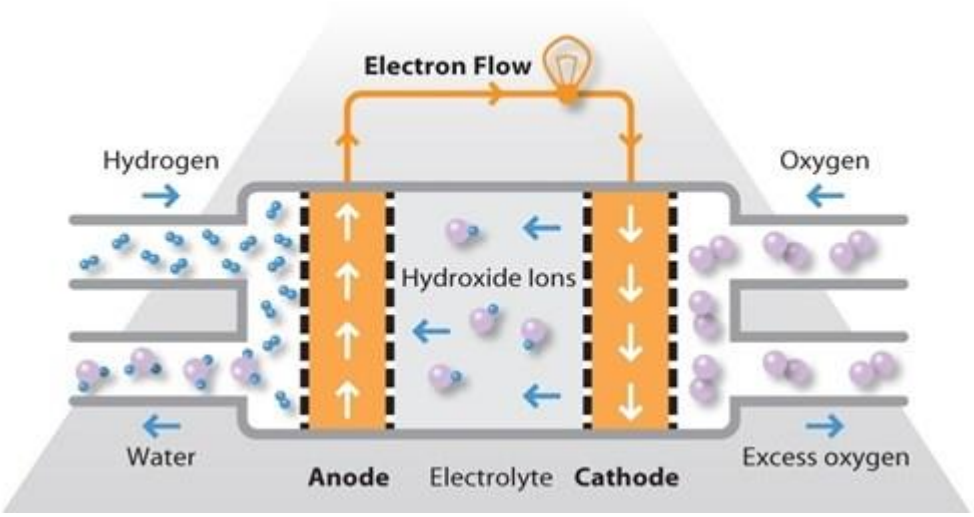

Figure 1.3: Alkaline Fuel Cell

The electrolyte in AFC is ~80 wt% KOH for high temperature (~250 °C) operation, or ~45 wt% KOH for low temperature (<120 °C) operation. The electrolyte is kept normally in asbestos, and a wide range of electro-catalysts can be used (e.g., Nickel, Silver, metal-oxides, and noble metals). The fuel provision is restricted to non-reactive components except for H_2. CO is a toxicant, and CO_2 reacts with KOH to form K_2CO_3, thus modifying the chemistry of electrolyte. Even a little quantity of CO_2 in air is taken a potential toxic material for AFC. Normally, H_2 is preferred as fuel for AFC [7].

Chemical reactions [3] in a simplified AFC (Figure 1.3) are as follows:

Anode: $H_2 + 2OH^- \rightarrow 2H_2O + 2e^-$ (1.7)

Cathode: $½\ O_2 + H_2O + 2e^- \rightarrow 2(OH)^-$ (1.8)

These were one of the earliest advanced fuel cells to originate, in the 1960s. The objective at that time was to develop static electricity device for the Apollo spacecraft. The AFC received significant success in space applications, but its application is greatly challenged by its sensitivity to CO_2. However, U.S. and European researchers pursue AFC mobile and closed-system applications[8].

AFC has high performance on H_2 and O_2 compared to other fuel cells due to its active O_2 dynamics and its ability to use a variety of electro-catalysts. The sensitiveness of the KOH to CO_2 implies the use of very pure H_2 fuel. As a result, the reformer system must be capable of removing CO and CO_2 effectively. Moreover, CO_2 purified ambient air can be used as oxidant.

1.5.2 Direct Methanol Fuel Cell (DMFC)

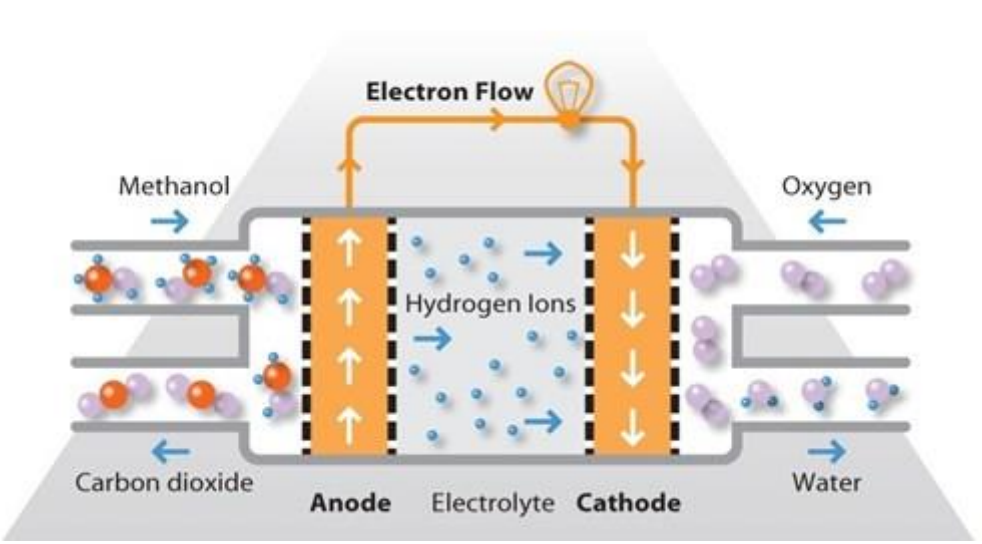

Figure 1.4: Direct Methanol Fuel Cell

The DMFC knowledge is comparatively emerging unlike the other fuel cells. DMFC makes use of polymer electrolyte similar to a PEM fuel cell. But DMFC makes use of methanol (CH_3OH)/ other alcohols as fuel in lieu of rectified H_2. During operation (Figure 1.4), the anode take up hydrogen by diffusing liquid CH_3OH in H_2O in order to eradicate the necessity of a reformer. At the cathode, the oppositely charged ions combine, which anode had supplied via electrical circuit and it reacts with oxidant giving out water as a byproduct [9].

Chemical reactions [10] in a typical DMFC (Figure 1.4) are as follows:

Anode: $CH_3OH + H_2O \rightarrow CO_2 + 6H^+ + 6e^-$ (1.9)

Cathode: $O_2 + 4H^+ + 4e^- \rightarrow 2H_2O$ (1.10)

Features of DMFC and PEM fuel cell are alike, however DMFC's performance is restrained by important elements like, and crossover of methanol from electrodes lowers the method efficiency and the slow reaction dynamics of the electrochemical oxidation of fuel. Usually a single unit of DMFC renders ~0.5 V. Main application of DMFC includes batteries for small portable electronic devices up to one kilowatt electrical capacity. The main benefit of DMFC is that the anode itself acts as a catalyst while bringing down the overall cost of the system. DMFC is just like PEM fuel cell, but its performance is restricted due to two factors; first the low cell efficiency and the slow oxidation reaction at the anode [11].

1.5.3 Molten Carbonate Fuel Cell (MCFC)

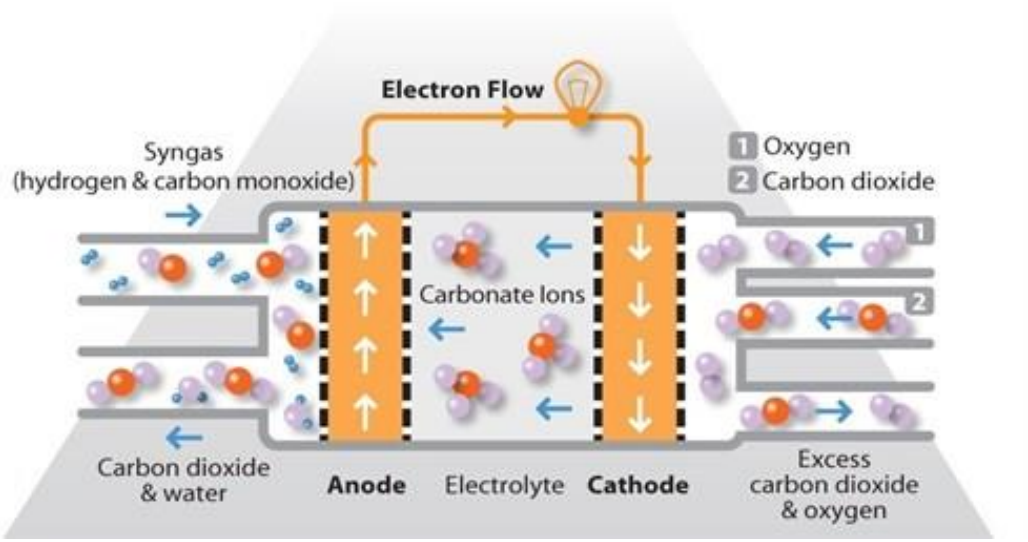

Figure 1.5: Molten Carbonate Fuel Cell

MCFCs are high-temperature fuel cells, which operates in range of 600 – 700 °C. It contains an electrolyte in the form of molten carbonate salt mixture. During chemical reaction at the anode, the electrolyte melts and turns conductive to carbonate ions. Then the ions react with H_2 to form H_2O on the negative electrode (cathode) side. In the meantime, electrons are released with emission of CO_2. During the chemical reaction at the cathode, oxygen and carbon dioxide produce carbonate ions, which then moves towards the anode to complete the reaction [12].

The chemical reaction equations [13] of the MCFC are:

Anode: $H_2O + CO_3^{2-} \rightarrow H_2O + CO_2 + 2e^-$ (1.11)

Cathode: $\frac{1}{2} O_2 + CO_2 + 2e^- \rightarrow 2CO_3^{2-}$ (1.12)

When hydrogen fuel is pumped into MCFC, the electrons released during reaction moves from anode to cathode through the external electrical circuit. These electrons combine with carbon dioxide at cathode and the carbonate ions are formed. In this way, the current will continue to flow as long as fuel and oxidant is available.

The comparatively high temperature of the MCFC has several benefits like inexpensive electro-catalysts can be used in combination of number of fuels like CO and some hydrocarbons for sufficient activity. The main challenge for MCFC development is high corrosive nature of electrolyte due to which nickel and high-grade stainless steel is required as the cell frame. The higher temperature put certain

restrictions on cell materials like having high mechanical stability and stack life. In addition, continuous CO_2 source must be provided for carbonate ion formation [14].

1.5.4 Phosphoric Acid Fuel Cell (PAFC)

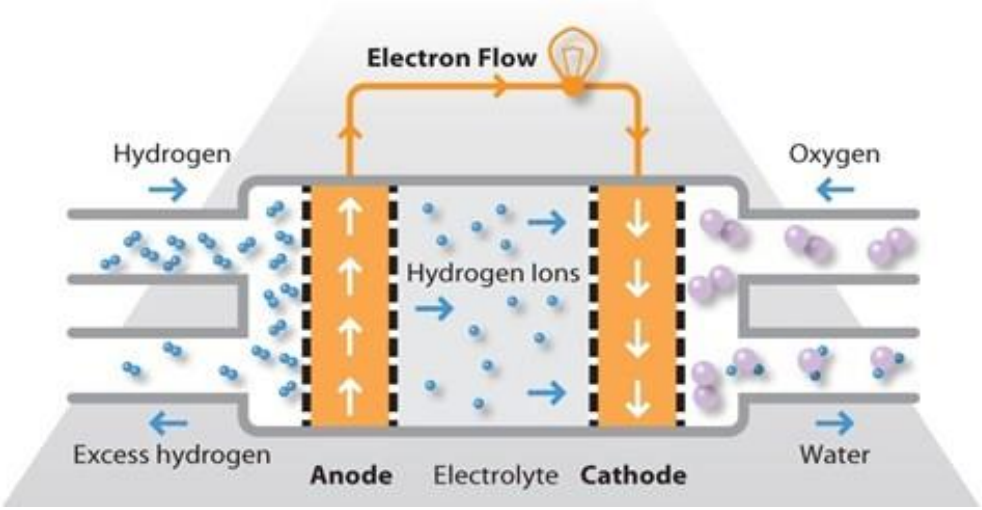

Figure 1.6: Phosphoric Acid Fuel Cell

100% concentrated phosphoric acid (H_3PO_4) is the electrolyte in PAFC and it normally works in the temperature range of 160 to 220 °C. At low temperature, H_3PO_4 has poor ionic activity, and CO poisons the electro-catalyst, which sometimes becomes very severe. However, concentrated phosphoric acid is most stable than other acids due to which PAFC can operate in the temperature range (160 to 220 °C). Moreover, the concentrated acid makes the water management easy as it reduces the water vapor pressure to a neglect-able amount. Silicon carbide is usual the matrix to contain the acid in PAFC, and the electro-catalyst in both the electrodes is Pt [15].

Chemical reactions of the cell are:

Anode: $H_2 \rightarrow 2H^+ + 2e^-$ (1.13)

Cathode: $½\ O_2 + 2H^+ + 2e^- \rightarrow H_2O$ (1.14)

PAFCs can tolerate the presence CO (about one percent) unlike the other cells like PEFCs and AFCs. The low operating temperature permits the use of ordinary materials and makes thermal management easy. PAFCs are 40 – 45% efficient, which is much greater in value as compared to PEFCs but lesser than most of the SOFC and MCFC energy systems. Cathode reaction is slower as compared to AFC, and requires the use of Pt as catalyst [16]. Moreover, PAFCs needs initial fuel reforming, generally a water-

gas shift reaction for reasonable performance. Lastly, the high corrosive electrolyte needs costly stack composition.

1.5.5 Proton Exchange Membrane Fuel Cell (PEMFC)

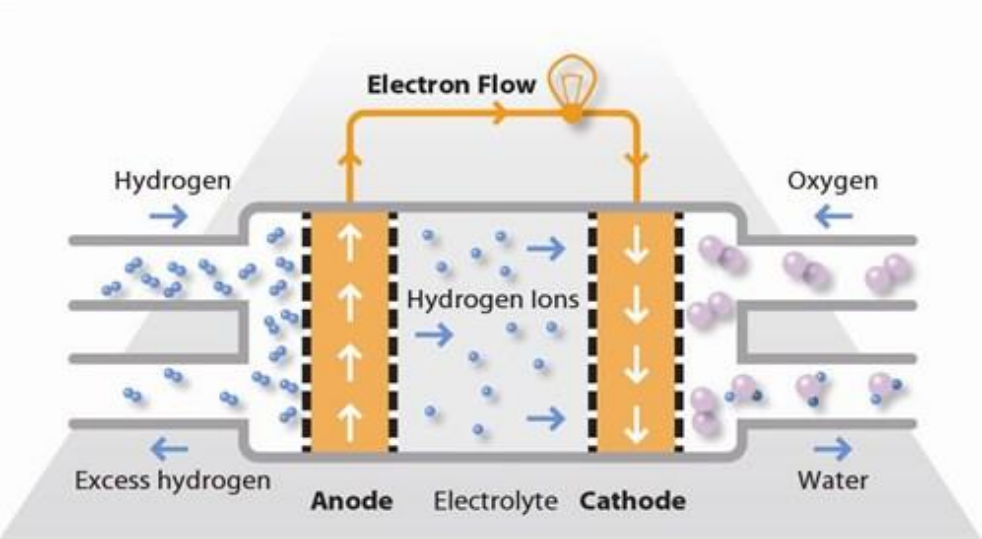

Figure 1.7: Proton Exchange Membrane Fuel Cell

PEMFC has an ion exchange membrane as electrolyte that has high proton conductivity. Corrosion issues are neglect-able as water is the only liquid in this cell. Usually, carbon electrodes (both anode and cathode) with Pt as a catalyst. Effective performance depends on the vital water management in the membrane. The fuel cell temperature must be in such a range that the by-product water does not vaporize quicker than its production, as the membrane must remain hydrated. Water balance impose the operation of PEMFC under 100 °C usually 50 – 85 °C and it also develops the need of pure H_2 as fuel. High Pt catalyst loading is used than PAFCs for both electrodes. Moreover, initial fuel processing required for fuels other than H_2, because of the poisoning of anode by even traces of CO, sulfur, halogens etc [17].

Chemical reactions [3] of the cell are:

Anode: $H_2 \rightarrow 2H^+ + 2e^-$ (1.15)

Cathode: $\frac{1}{2} O_2 + 2H^+ + 2e^- \rightarrow H_2O$ (1.16)

PEMFCs have diverse applications especially fuel cell vehicles (FCVs). Because of the rising interest in FCVs the development of PEMFCs very well exceeds every other fuel cell type. PEMFC can be applied in static energy systems but mostly research in PEMFC centers around automotive and portable devices. The low operating temperature of PEMFCs allow quick start-up and, non-corrosive nature of electrolyte

eliminates the need of high-grade materials for the cell. Simulations of PEMFCs have shown that high current densities can be acheived. The temperature range of 50 – 85 °C makes thermal management challenging due to which it is nearly impossible to use rejected heat for cogeneration. Water management is also difficult in PEMFC, as a balance must be ensured for the electrolyte to be properly hydrous. Moreover, disadvantages of PEMFCs can be countered at low current density and with high catalyst loading [18].

1.5.5 Solid Oxide Fuel Cell (SOFC)

A solid oxide fuel cell (SOFC), conventionally operating at 800 to 1000ºC, consists of three solid components: two porous electrodes (an anode and a cathode) and a dense electrolyte (Figure 1.8) [19]. It operates by passing air through the porous cathode and fuel through the anode. Oxygen molecules receive electrons at the cathode/electrolyte interface and are reduced to oxide ions. The oxide ions are conducted through the electrolyte between the two electrodes from the cathode side to the anode side. Then, the oxide ions interact with the fuel at the anode/electrolyte interface where the gaseous fuel, active metal and electrolyte meet known as the three phase boundary (TPB) [20].

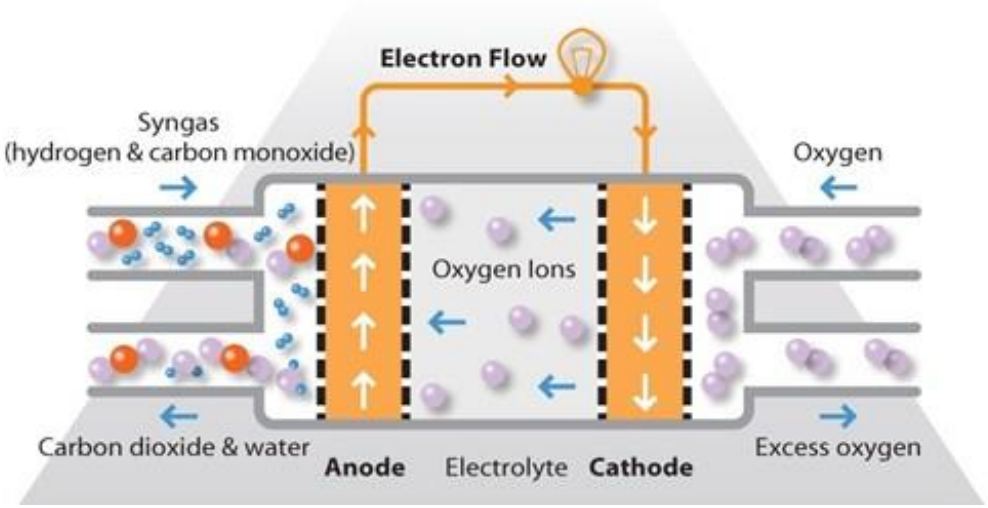

Figure 1.8: Typical Solid Oxide Fuel Cell

According to the thermodynamics of the system, many possible reactions can occur when hydrogen or methane is used as a fuel. The reactions that are most likely to occur under direct internal reforming of methane are showed as follows [3,19,20]:

$H_{2(g)} + ½O_{2(g)} \leftrightarrow H_2O_{(g)}$		1.17
$CO_{(g)} + ½O_{2(g)} \leftrightarrow CO_{2(g)}$		1.18
$CH_{4(g)} + 2O_{2(g)} \leftrightarrow CO_{2(g)} + 2H_2O_{(g)}$	(CH_4 oxidation)	1.19
$CH_{4(g)} + H_2O_{(g)} \leftrightarrow CO_{(g)} + 3H_{2(g)}$	(CH_4 steam reforming)	1.20
$CH_{4(g)} + CO_{2(g)} \leftrightarrow 2CO_{(g)} + 2H_{2(g)}$	(CH_4 dry reforming)	1.21
$CO_{(g)} + H_2O_{(g)} \leftrightarrow CO2_{(g)} + H_{2(g)}$	(Water-gas shift)	1.22
$2CO_{(g)} \leftrightarrow C(s) + CO2(g)$	(CO disorptionation)	1.23
$CH_{4(g)} \leftrightarrow C_{(s)} + 2H_{2(g)}$	(CH_4 pyrolysis)	1.24
$CO_{(g)} + H_{2(g)} \leftrightarrow C_{(s)} + H_2O_{(g)}$	(CO hydrogenation)	1.25

Equations (1.17), (1.18), and (1.19) are direct electrochemical oxidations. The reforming reactions (1.20) and 1.21) are the steam and dry reforming reactions, respectively. When a mixture of methane and steam is used as a fuel, equation (1.20) is normally followed by the water-gas shift reaction (equation (1.22)). If the amount of steam is not high enough, reactions (1.23) and (1.24) are more favored. Consequently, carbon may deposit on the active site or clog gas flow channels, causing loss of TPB.

The SOFC is the fuel cell, which is the leader when it comes to research and development, emerging in the early 1960s, long before the demonstration of AFC. Having the solid electrolyte, the cell can be constructed in various shapes/ figures, such as tubular, planar, or monolithic. The solid cermet construction of the fuel cell eliminates any corrosion issues for the cell. The solid electrolyte also permits advanced development of the triple-phase boundary and nullify any electrolyte flooding in the electrodes. The dynamics of the fuel cell are comparatively rapid, and CO is a directly usable as a fuel like in the MCFC. There is no need of CO_2 at the cathode unlike the MCFC. Inexpensive materials are used for construction of SOFC components. Thin-electrolyte planar SOFCs have been developed to be capable of power capacity close to the as attained with PEFC. Like the MCFC, the high operating temperature allows use rejected heat for cogeneration. Efficiencies fall in the range of 40% (small scale systems) to over 50% (hybrid/ large scale systems) have been recorded [21].

The high operating temperature of the SOFC also has some disadvantages. The thermal expansion coefficient matching within the materials is very critical, and perfectly sealed structure is very hard to build in the flat plate shape. Also, the high temperature require the use of high-tech materials and efficient fabrication process.

1.6 Some Challenges in SOFCs Development

It is a major challenge to pick materials for each SOFC component because each component has individual material requirements. As shown in Table 1.2, a match between thermal expansion coefficients of the various components is also a necessity to prevent cracks and delamination in the cell.

Table 1.2: Material Requirements

Component	Requirements				
	Conductivity		Stability	Porosity	Thermal Expansion
	Ionic	Electronic			
Electrolyte	High	Nil	In reducing and oxidizing environment	Fully Dense	Matches Others
Cathode	Low	High	In oxidizing environment	Porous	Matches Others
Anode	Low	High	In reducing environment	Porous	Matches Others

1.6.1 Anode Materials

Requirements for the anode material include stability under operating conditions, high electrical conductivity, minimum chemical reactivity and diffusivity with other cell components, thermal expansion similar to that of the electrolyte, stable pore structure, stable reactivity for steam reforming and electro-catalysis. The porosity of the electrodes not only provides the transport of fuel and products, but also increases the number of active sites [19].

Originally, platinum and certain transition metals were tested as anodes. However, no pure metal meets all requirements of an anode. For example, platinum tends to delaminate from the cell over long operating times, while nickel also agglomerates at high temperatures. Nonetheless, nickel has been considered as an active metal species because of its electrical conductivity, catalytic activity and cost. Furthermore, the addition of YSZ lowers its agglomeration tendency and the adjustment of thermal expansion between Ni anode and YSZ electrolyte [22].

To mend the overall performance or fabricate stabilized Ni-YSZ, the Ni-based anode can be modified or changed using the following methods [23–33]:

- Addition of some transition metals (Ti, Cr, Mn and Pd), a small amount of some precious metals, or some alkali oxides to prevent carbon deposition and/or to promote reforming reaction

- Addition of a functional layer to reduce electrode interface resistance and/or to inhibit carbon deposition
- Replacement of YSZ by doped ceria for IT-SOFCs to achieve acceptable ionic conductivity at intermediate temperatures
- Using/ modification of synthesis process for anode materials like with H_2O_2 for better structural morphology
- Use of new materials such as La-based anode to improve fuel cell structural stability and thermal performance

Details about improving the anode will be discussed the subsequent chapters.

1.6.2 Electrolyte Materials

Oxygen ions produced from the reduction reaction of oxygen molecules at the cathode/electrolyte interface must diffuse through the electrolyte and react with the fuel at the TPB. Therefore, the electrolyte material must possess high ionic conductivity without electronic conductivity to provide a high diffusion rate of oxide ions, but must inhibit the transfer of electrons. The electrolyte must also be stable in reducing and oxidizing atmospheres. Moreover, to minimize resistive losses and to prevent the short circuiting of reacting gases within the cell, electrolyte materials must be formed as a fully dense thin film with no gas leaks. Furthermore, the electrolyte has to be chemically and thermally compatible with the other cell components. To date, two predominant types of electrolytes have been used: doped zirconia and doped ceria.

The most common fluorite structure for an electrolyte is stabilized zirconia. Yttria-stabilized zirconia (ZrO_2-Y_2O_3; YSZ) and scandia-stabilized zirconia (ZrO_2-Sc_2O_3; SSZ or ScSZ) have shown high ionic conductivity with a reasonable cost and processing time; however, degradation of ScSZ has been reported at high temperatures (1000°C). Stabilized zirconia materials possess inappropriately low ionic conductivity at temperatures below 750 °C. Therefore, they are replaced by doped-ceria materials for IT-SOFCs because ceria-based electrolytes provide much higher ionic conductivity at intermediate temperatures. Doped ceria, the other preferred structure, has higher oxygen ion conductivity compared to doped zirconia at intermediate temperatures, especially samaria-doped ceria (CeO_2-Sm_2O_3; SDC) and gadolinia-doped ceria (CeO_2-Gb_2O_3; GDC or CGO) [34–38].

Below are some works aimed at improving the conductivity of doped ceria [39–43]:

- A composite of calcium-doped ceria (CCO) and carbonate has been synthesized. For this material, Ca^{2+} was used instead of Gd^{3+} or Sm^{3+} and the calcium-doped ceria was mixed with $66Li_2CO_3$:$34Na_2CO_3$. The conductivity of the composite was approximately two orders of magnitude higher than that of pure CCO. The use of the CCO-composite electrolyte in the SOFC demonstrated a performance as high as 600 $mW.cm^{-2}$ at 600 °C.
- When small amounts of alkali elements or alkali-earth elements are dissolved in SDC, the ionic conductivity increased. Also, the addition of alkali or alkali-earth elements can inhibit large volume expansion.
- $La_{0.9}Sr_{0.1}Ga_{0.8}Mg_{0.2}O_{3-d}$ (LSGM)/$Ce_{0.8}Sm_{0.2}O_{2-d}$ (SDC) composite was deposited on the anode substrate to form a 400 nm thin layer. The 5 μm of LSGM was then deposited on top of the SDC film and it showed better performance than other electrolyte materials.

1.6.3 Cathode Materials

The properties of the cathode must cover all requirements described in Table 1.1. Platinum was the first cathode material used but it is too expensive for commercial application. Perovskite oxides are low-cost alternative cathodes. Since 1965 many perovskite cathodes have been studied; for example, $La_{1-x}Sr_xCoO_{3-\delta}$ (LSC) was one of the earliest studied. This research led to studies of other perovskites: $La_{1-x}Ca_xCoO_{3-\delta}$ and $La_{1-x}Sr_xMO_{3\pm\delta}$ (M= Cr, Mn (LSM), Fe (LSF), Co). Besides electrochemical performance, chemical compatibility of the cathode material with the electrolyte is also critical. Interactions between the cathode/electrolyte can limit electrochemical reactions at the cathode side [5].

The perovskite structure can be represented by $ABO_{3-\delta}$, the large cations are located at the corner of a cube, while the small cation located at the centre of the cube. The oxide ions occupy the face-centered positions. δ is the number of oxygen ion vacancies. In the case where a transition metal (such as Mn or Fe) occupies a B-site, whereas the A-site is a mixture, the materials yield high electronic conductivity because the mixture can introduce a charge imbalance and the transition metal has a vacancy d-orbital. For example, LSM: Mn atoms occupy B-sites while La and Sr are placed at A-sites.

To date, LSM has been the most common cathode because of its high electronic conductivity, relatively low cost and thermal expansion match with YSZ. Although

many transition metals could be located at B-sites, Mn has the lowest reducibility that prevents large expansion during operation. In addition, LSM is the most thermodynamically stable of the mixed conductors containing cobalt or iron [20].

Even though LSM is one of the most promising cathode materials for conventional SOFCs, its performance decreases when the operating temperature decreases. Although LSM has been modified by adding doped ceria such as GDC, the oxygen surface exchange coefficient and oxygen diffusion coefficient values of LSM are relative low for intermediate temperatures. Certain alternative materials have been used as cathodes [44–49]:

- $La_{0.6}Sr_{0.4}Co_{0.2}Fe_{0.8}O_3$-$Ce_{0.7}Bi_{0.3}O_{0.2}$ (LSCF-CBO) composite shows very low specific resistivity at about 700°C.
- Composite cathodes consisting of $Sm_{0.5}Sr_{0.5}CoO_3$ (SSC) and SDC cathode and a dense SDC electrolyte resulted in a significant reduction in the interfacial resistance to 0.18 $V.cm^2$ at 600 °C under open circuit condition.
- At 700 °C, in humidified H_2, a maximum power density of 250 $mW.cm^{-2}$ was obtained when Ni-YSZ, YSZ, and $La_{0.75}Sr_{0.25}CuO_{2.5-\delta}$ (LSCu) were used as an anode, electrolyte, and cathode (Ni-YSZ//YSZ//LSCu), respectively.
- LSCu was replaced by $La_{0.6}Sr_{0.4}CoO_{3-\delta}$ (LSC) resulting in a maximum power density of 100 $mW.cm^{-2}$ at 700 °C.
- $Ln_{0.6}Sr_{0.4}Co_{0.2}Fe_{0.8}O_{3-\delta}$ (Ln = Ce, Sm, Gd, Dy) compounds were prepared by glycine-nitrate process. All compounds had a good chemical compatibility with SDC. The highest catalytic activity was obtained with $Dy_{0.6}Sr_{0.4}Co_{0.2}Fe_{0.8}O_{3-\delta}$ (Dy-SCF). A good cathode material for ITSOFCs would then be Dy-SCF.

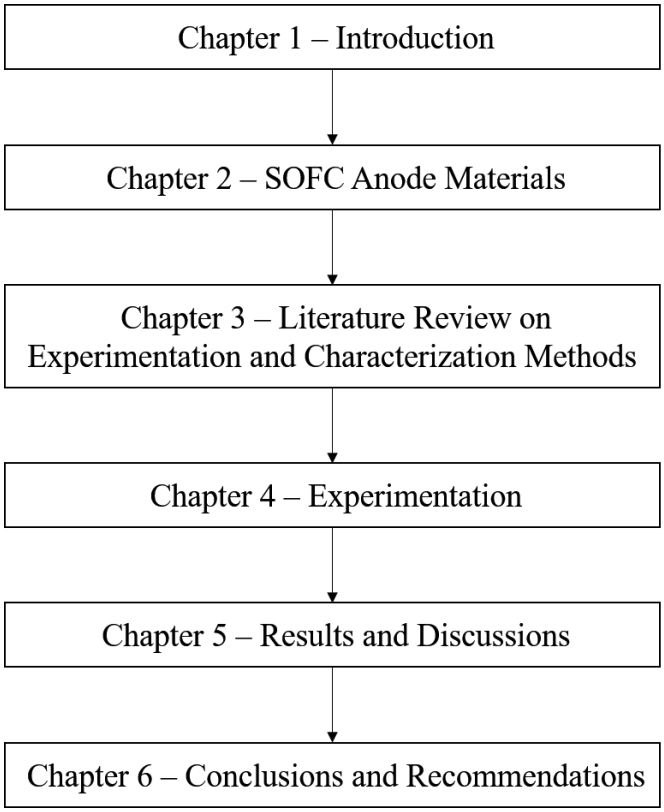

Figure 1.9: Figurative Flow of the Thesis

Summary

Like a battery, a fuel cell is an electricity generator that transforms electrochemical reactions directly into electrical power. In other words, it is such an energy-producing device, which converts the chemical energy stored in the fuels instantly into electricity and heat without the use of any secondary process and the byproduct is only water making it tremendously environment friendly. While the commonly used engines/ energy systems generate electricity by using mechanical energy, which leads to scaled down efficiency when compared with fuel cells. Although fuel cells of all types operate with similar overall reactions, they can be classified depending on the electrolyte. Amongst all, MCFC and SOFC stand at the top because of high efficiency and fuel flexibility. It operates by passing air through the porous cathode and fuel through the anode. Oxygen molecules receive electrons at the cathode/electrolyte interface and are reduced to oxide ions. The oxide ions are conducted through the electrolyte between the two electrodes from the cathode side to the anode side. Then, the oxide ions interact with the fuel at the anode/electrolyte interface where the gaseous fuel, active metal and electrolyte meet known as the three phase boundary (TPB).

References

[1] A. Boudghene Stambouli, E. Traversa, Fuel cells, an alternative to standard sources of energy, Renew. Sustain. Energy Rev. 6 (2002) 295–304.

[2] B. Cook, Introduction to fuel cells and hydrogen technology, Eng. Sci. Educ. J. (2002).

[3] A. Kirubakaran, S. Jain, R.K. Nema, A review on fuel cell technologies and power electronic interface, Renew. Sustain. Energy Rev. 13 (2009) 2430–2440.

[4] X. Huang, Z. Zhang, J. Jiang, Fuel Cell Technology for Distributed Generation: An Overview, in: 2006 IEEE Int. Symp. Ind. Electron., IEEE, 2006: pp. 1613–1618.

[5] R. O'Hayre, S.-W. Cha, W. Colella, F.B. Prinz, Fuel Cell Fundamentals, Wiley, 2009.

[6] X. Li, Principles of Fuel Cells, Taylor & Francis, 2005.

[7] NETL, Seventh Edition Fuel Cell Handbook, Pittsburgh, PA, and Morgantown, WV, 2004.

[8] M. Farooque, H.C. Maru, Fuel Cells - The Clean and Efficient Power Generators, Proc. IEEE. 89 (2001) 1819–1829.

[9] N.K. Shrivastava, S.B. Thombre, R. V. Motghare, Wire mesh current collectors for passive direct methanol fuel cells, J. Power Sources. 272 (2014) 629–638.

[10] R.K. Mallick, S.B. Thombre, N.K. Shrivastava, Vapor feed direct methanol fuel cells (DMFCs): A review, Renew. Sustain. Energy Rev. 56 (2016) 51–74.

[11] N.K. Shrivastava, S.B. Thombre, R.K. Mallick, Effect of diffusion layer compression on passive DMFC performance, Electrochim. Acta. 149 (2014) 167–175.

[12] A.A.A. Agll, Y.M. Hamad, T.A. Hamad, M. Thomas, S. Bapat, K.B. Martin, et al., Study of a molten carbonate fuel cell combined heat, hydrogen and power system: Energy analysis, Appl. Therm. Eng. 59 (2013) 634–638.

[13] S. Mekhilef, R. Saidur, A. Safari, Comparative study of different fuel cell technologies, Renew. Sustain. Energy Rev. 16 (2012) 981–989.

[14] J.J. de-Troya, C. Álvarez, C. Fernández-Garrido, L. Carral, Analysing the possibilities of using fuel cells in ships, Int. J. Hydrogen Energy. 41 (2015) 2853–2866.

[15] R. Raza, N. Akram, M.S. Javed, A. Rafique, K. Ullah, A. Ali, et al., Fuel cell technology for sustainable development in Pakistan – An over-view, Renew. Sustain. Energy Rev. 53 (2016) 450–461.

[16] S. Ganguly, S. Das, K. Kargupta, D. Bannerjee, 11th International Symposium on Process Systems Engineering, Elsevier, 2012.

[17] S. Authayanun, K. Im-orb, A. Arpornwichanop, A review of the development of high temperature proton exchange membrane fuel cells, Chinese J. Catal. 36 (2015) 473–483.

[18] S. Bose, T. Kuila, T.X.H. Nguyen, N.H. Kim, K. Lau, J.H. Lee, Polymer membranes for high temperature proton exchange membrane fuel cell: Recent advances and challenges, Prog. Polym. Sci. 36 (2011) 813–843.

[19] Y. Zhao, C. Xia, L. Jia, Z. Wang, H. Li, J. Yu, et al., Recent progress on solid oxide fuel cell: Lowering temperature and utilizing non-hydrogen fuels, Int. J. Hydrogen Energy. 38 (2013) 16498–16517.

[20] S.C. Singhal, K. Kendal, High-temperature Solid Oxide Fuel Cells: Fundamentals, Design and Applications, Elsevier, 2003.

[21] M. Yu, S. Muy, F. Quader, A. Bonifacio, R. Varghese, E. Clerigo, et al., Combined Hydrogen, Heat and Power (CHHP) pilot plant design, Int. J. Hydrogen Energy. 38 (2013) 4881–4888.

[22] S.P.S. Shaikh, A. Muchtar, M.R. Somalu, A review on the selection of anode materials for solid-oxide fuel cells, Renew. Sustain. Energy Rev. 51 (2015) 1–8.

[23] J. Myung, T. ho Shin, S.-D. Kim, H.-G. Park, J. Moon, S.-H. Hyun, Optimization of Ni–zirconia based anode support for robust and high-performance 5 × 5 cm2 sized SOFC via tape-casting/co-firing technique and nano-structured anode, Int. J. Hydrogen Energy. 40 (2015) 2792–2799.

[24] S. Souentie, M. Athanasiou, D.K. Niakolas, A. Katsaounis, S.G. Neophytides,

C.G. Vayenas, Mathematical modeling of Ni/GDC and Au–Ni/GDC SOFC anodes performance under internal methane steam reforming conditions, J. Catal. 306 (2013) 116–128.

[25] B.B. Patil, S. Basu, Synthesis and Characterization of PdO-NiO-SDC Nano-powder by Glycine-Nitrate Combustion Synthesis for Anode of IT-SOFC, Energy Procedia. 54 (2014) 669–679.

[26] Q. Jeangros, A.B. Aebersold, C. Hébert, J. Van Herle, A. Hessler-Wyser, A TEM study of Ni interfaces formed during activation of SOFC anodes in H2: Influence of grain boundary symmetry and segregation of impurities, Acta Mater. 103 (2016) 442–447.

[27] M. V. Sandoval, A. Matta, T. Matencio, R.Z. Domingues, G.A. Ludwig, M. De Angelis Korb, et al., Barium-modified NiO–YSZ/NiO–GDC cermet as new anode material for solid oxide fuel cells (SOFC), Solid State Ionics. 261 (2014) 36–44.

[28] K. Sugihara, M. Asamoto, Y. Itagaki, T. Takemasa, S. Yamaguchi, Y. Sadaoka, et al., A quantitative analysis of influence of Ni particle size of SDC-supported anode on SOFC performance: Effect of particle size of SDC support, Solid State Ionics. 262 (2014) 433–437.

[29] M.S. Khan, W. Wahyudi, S.-B. Lee, R.-H. Song, J.-W. Lee, T.-H. Lim, et al., Effect of various sintering inhibitors on the long term performance of Ni-YSZ anodes used for SOFCs, Int. J. Hydrogen Energy. 40 (2015) 11968–11975.

[30] D. Papurello, A. Lanzini, S. Fiorilli, F. Smeacetto, R. Singh, M. Santarelli, Sulfur poisoning in Ni-anode solid oxide fuel cells (SOFCs): Deactivation in single cells and a stack, Chem. Eng. J. 283 (2016) 1224–1233.

[31] A. Lanzini, C. Guerra, P. Leone, M. Santarelli, F. Smeacetto, S. Fiorilli, et al., Influence of the microstructure on the catalytic properties of SOFC anodes under dry reforming of methane, Mater. Lett. 164 (2016) 312–315.

[32] A. Yan, M. Phongaksorn, D. Nativel, E. Croiset, Lanthanum promoted NiO–SDC anode for low temperature solid oxide fuel cells fueled with methane, J. Power Sources. 210 (2012) 374–380.

[33] T. Ryll, P. Reibisch, L. Schlagenhauf, A. Bieberle-Huetter, M. Döbeli, J.L.M. Rupp, et al., Lanthanum nickelate thin films deposited by spray pyrolysis: Crystallization, microstructure and electrochemical properties, J. Eur. Ceram. Soc. 32 (2012) 1701–1709.

[34] C. Alves, T. Marcelo, F.A.C. Oliveira, L.C. Alves, J. Mascarenhas, B. Trindade, On the influence of silica type on the structural integrity of dense La9.33Si2Ge4O26 electrolytes for SOFCs, J. Eur. Ceram. Soc. 33 (2013) 2251–2258.

[35] D.S. Khaerudini, G. Guan, P. Zhang, X. Hao, Y. Kasai, K. Kusakabe, et al., Structural and conductivity characteristics of Bi4MgxV2−xO11−δ (0⩽x⩽0.3) as solid electrolyte for intermediate temperature SOFC application, J. Alloys Compd. 589 (2014) 29–36.

[36] L. Fan, Y. Wang, Z. Jia, Y. Xiong, M.E. Brito, Nanofiber-structured SSC–GDC composite cathodes for a LSGM electrolyte based IT-SOFCs, Ceram. Int. 41 (2015) 6583–6588.

[37] R.K. Singh, P. Singh, Electrical conductivity of barium substituted LSGM electrolyte materials for IT-SOFC, Solid State Ionics. 262 (2014) 428–432.

[38] C. Jin, Y. Mao, N. Zhang, K. Sun, Fabrication and characterization of Ni-SSZ gradient anodes/SSZ electrolyte for anode-supported SOFCs by tape casting and co-sintering technique, Int. J. Hydrogen Energy. 40 (2015) 8433–8441.

[39] H. Sun, Y. Zhang, H. Gong, Q. Li, Y. Bu, T. Li, Anode-supported SOFCs based on Sm0.2Ce0.8O2−δ electrolyte thin-films fabricated by co-pressing using microwave combustion synthesized powders, Ceram. Int. 42 (2016) 4285–4289.

[40] T. Van Gestel, D. Sebold, H.P. Buchkremer, Processing of 8YSZ and CGO thin film electrolyte layers for intermediate- and low-temperature SOFCs, J. Eur. Ceram. Soc. 35 (2015) 1505–1515.

[41] N. Tian, J. Yu, Y. Deng, G. Li, X. Zhang, Electrical properties of Ce0.85Sm0.15O1.925–Fe2O3 electrolytes for IT-SOFCs, J. Alloys Compd. 655 (2016) 215–219.

[42] Y. Ma, N. Fenineche, O. Elkedim, Ab initio study of La10−xSrx(Si,Ge)6O27−0.5x apatite for SOFC electrolyte, Comput. Mater. Sci. 109 (2015) 25–33.

[43] D.A. Medvedev, J.G. Lyagaeva, E.V. Gorbova, A.K. Demin, P. Tsiakaras, Advanced materials for SOFC application: Strategies for the development of highly conductive and stable solid oxide proton electrolytes, Prog. Mater. Sci. 75 (2015) 38–79.

[44] N. Schrödl, E. Bucher, A. Egger, P. Kreiml, C. Teichert, T. Höschen, et al., Long-term stability of the IT-SOFC cathode materials La0.6Sr0.4CoO3−δ and La2NiO4+δ against combined chromium and silicon poisoning, Solid State Ionics. 276 (2015) 62–71.

[45] M. Perz, E. Bucher, C. Gspan, J. Waldhäusl, F. Hofer, W. Sitte, Long-term degradation of La0.6Sr0.4Co0.2Fe0.8O3-δ IT-SOFC cathodes due to silicon poisoning, Solid State Ionics. (2016).

[46] L.-N. Xia, Z.-P. He, X.W. Huang, Y. Yu, Synthesis and properties of SmBaCo2−xNixO5+δ perovskite oxide for IT-SOFC cathodes, Ceram. Int. 42 (2016) 1272–1280.

[47] N. Schrödl, E. Bucher, C. Gspan, A. Egger, C. Ganser, C. Teichert, et al., Phase decomposition in the chromium- and silicon-poisoned IT-SOFC cathode materials La0.6Sr0.4CoO3-δ and La2NiO4+δ, Solid State Ionics. (2016).

[48] E. Djurado, A. Salaün, G. Mignardi, A. Rolle, M. Burriel, S. Daviero-Minaud, et al., Electrostatic spray deposition of Ca3Co4O9+δ layers to be used as cathode materials for IT-SOFC, Solid State Ionics. 286 (2016) 102–110.

[49] S.-W. Baek, J. Jeong, H. Schlegl, A.K. Azad, D.S. Park, U.B. Baek, et al., Metal-supported SOFC with an aerosol deposited in-situ LSM and 8YSZ composite cathode, Ceram. Int. 42 (2016) 2402–2409.

Chapter 2

SOFC Anode Materials

2.1 Overview of Anode Requirements

To develop SOFCs with operating for intermediate temperature range (500 – 800 °C), all SOFC components including electrodes, electrolyte, interconnects etc., must perform similar to one another at desired temperature range. Development of innovative anode materials for intermediate temperature range needs carefully engineered anode prerequisites that will in turn enhance fuel cell functioning. Performance calculations have been discussed in the Chapter 1.

Anode materials must meet certain specific criteria to show improved performance out of which few are [1]:

- Must be electronically conductive
- Electro-catalytic towards fuel reforming
- Lower ionic conduction
- Thermal Expansion Matching with other SOFC components
- Non-reactive to contacting components

Fabrication of anode material with such prerequisites needs to be carefully developed, however the synthesizing a composite material can merge all the requirements for an anode. Electrical conductivity is vital for SOFC anode to perform well for electron movement through external circuit. Ordinarily, conductivity of ~1 Scm^{-1} is enough for some fuel cells as anode-supported SOFCs configurations demands high electronic conduction towards the current accumulator [2]. Catalytic reactions for the fuel reforming are one of the other main requirement for an efficient SOFC. Chemical reactions at the anode promote by oxidizing the fuel, explained in following equations [3]:

Hydrogen Fuel: $H_2 + O_2 \rightarrow H_2O + 2e^-$ (2.1)

Hydrocarbon Fuel: $C_nH_{2n+2} + (3n+1)O^{2-} \rightarrow nCO_2 + (n+1)H_2O + (6n+2)e^-$ (2.2)

The ionic conductivity is not of much importance for SOFC anode, catalytic activity maxmize at the triple phase boundary, where the H_2 reacts with oxidant (Figure 2.1). This results in enhancement of anode efficiency and inhibits anode polarization. Ionic

conduction can be can be controlled by using a single phase conductor material for ions and electrons [4].

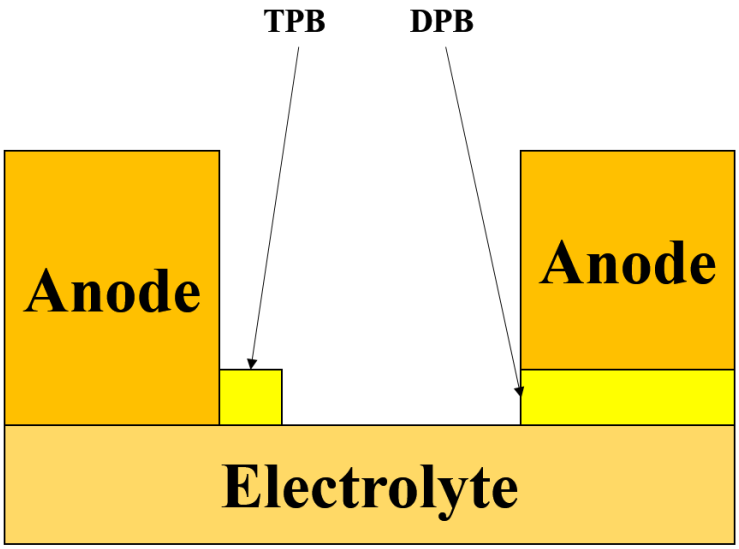

Figure 2.1: Graphical representation of TPB (triple phase boundary) and DPB (double phase boundary)

Anode materials must be capable to work under SOFC operating conditions. This demands the use of such materials, which do not decompose at elevated temperatures, means materials with high thermal performance. These are the materials, which also do not form undesirable phases at the SOFC component interfaces (physio-chemically stable) and withstand reducing and oxidizing cycles. Thermal stability of fuelcell components plays vital role for determining useful life cycle of an SOFC [5]. Materials with mismatched thermal expansion co-efficient (TEC), degradations starts to evolve and can lead stack cracking. Another characteristic is the anode microstructure, which demonstrates the transport of fuel and oxidants in the TPB. The anodic microstructure depends on the manufacturing process and anodes with high performance can be developed with different microstructural configurations [6]. As the anode is depended on the electrolyte material as well for high thermal performance and chemical stability, so for developing novel anode materials we also keep in mind the properties of electrolyte. Commonly used electrolyte materials include yttrium stabilized zirconia (YSZ, samarium and gadolinium-doped ceria (SDC & GDC respectively), carbonate composite doped ceria (like SDC-K_2CO_3) etc [7].

In this perspective, a diverse range of materials can be used to developed advanced anode composites. The most common and state of the art anode material nickel yttrium stabilized zirconia (Ni-YSZ) because of electrical conductivity, however materials like

nickel samarium-doped ceria (Ni-SDC) and lanthanum added nickel samarium-doped dera (Ni(La)O-SDC) gained popularity for their higher electronic conduction at intermediate temperatures (500 °C – 800 °C). In addition, for same materials researches are modifying development process for better physio-chemical performance towards hydrocarbon fuels.

2.2 Ni-YSZ

Generally, metals are employed for fabrication of electrode materials for both positive and negative electrodes in the SOFC, but with the progression of time materials development became more engineered, and the use of metal oxide support has been demonstrated. As explained in the previous section, the metal oxide can enhance propagation through the TPB which improves anode efficiency, while eliminating other various issues related to pure metal anode. Ni (nickel) and YSZ (yttrium stabilized zirconia) composite has a numerous factors needed for a high performance anode [8]. Ni-YSZ have high electrical conductivity, fair ionic conductivity and good catalytic activity for pure hydrogen fuel. However, Ni-YSZ composite has few drawbacks for commercial applications: coking/carbon deposition is worst issue with Ni-YSZ when fuels are hydrocarbons, sulphur toxication and nickel degradation when used for long terms. Also, it is not stable during redox cycles [9].

Coking and Sulphur toxication can be avoided by the use of metals from the transition metal group instead of nickel, but this lead mainly in reducing the anode efficiency. Moreover, anode was found unstable during redox cycles and it resulted in the enlargement of nickel to nickel oxide, which promoted stresses at the electrode and electrolyte port. Furthermore, it was found later that this problem can be solved by altering the fine structure of material and particle dispersion of the nickel and YSZ phases in the composite material [10-11]. However, a reasonable solution and answer to one of these issues is still need to be proposed. Nevertheless, Nickel Yttrium Stabilized Zirconia (Ni-YSZ) still the benchmark of all materials in this field because of its high performance and fewer alternates. Research on these composite anodes is still actively progressing rather a lot of well known drawbacks and issues related to these materials for their practical application and commercialization. Primarily, common electrolyte materials in SOFC are centered on the metal fluorite structure based composites, as doped ZrO_2 or doped CeO_2, thus various emerging anode materials can be developed using these microstructures as a standard [12].

A study was conducted previously using nickel-yttria stabilized zirconia and nickel-doped ceria separately as anode candidates. The study was done using different anodes and it described that at least ~20 wt% of Ni was a basic requirement for low electric resistance. With doped ceria Ni and CeO_2 phases co-existed and shown chemical stability. Moreover, cell polarization resistance significantly reduced and it was related to increasing ceria content, which in turn gave improved performance [13]. However, as performance is coupled directly with metal oxide formed during the fabrication, hence, homogenous distribution of nickel particles on the yttria stabilized zirconia electrolyte plays a critical role than the CeO_2 and the system showed good performance using other fuels [14].

A recent study also demonstrated that the fabrication of nickel-yttria stabilized zirconia with addition of CeO_2 delivered good performance towards hydrogen fuel containing impurities like sulhpur etc., and cell voltage was totally regained by using pure hydrogen with ~400 h of operation under toxicated environment. Still, this performance is the collateral result through homogenous dispersion of Ni anode on the electrolyte rather with direct ceria doping [15]. Using titanium as dopamt, the YSZ shows an enhanced electrical performance with low ionic conduction in a reducing environment. Composites with high Yttrium concentration with low Ti concentration proved better conductors with air and hydrogen as fuels. However, LST-YSZ and Palladium/Ceria-doped YSZ recorded low ionic conduction when compared with only ceria-doped YSZ that is because of Ti content present in the composite. Regarding the addition of other metals, another study demonstrated new dimensions of research for coking issues related to hydrocarbon fuels. Copper impregnated composite when exposed to ethanol fuel showed no degradation after prolonged operation of ~300 h with no coking overall; but applying a Cu/Co catalyst on ZDC, it was found that although the cell performance was low in case of alcohols as compared to pure hydrogen[16]. However, carbon deposition can be controlled within ~1 day time and for achieving the required performance the cell is to be exposed to pure wet hydrogen which laid the foundation that anode was not disturbed by carbon deposition [17].

Besides Cu, it was found that Sn/Ni catalyst is more tolerant to coking than in case of single Ni catalyst during hydrocarbon reforming. This is actually the consequence of supported Sn/Ni catalyst and its activity towards carbon oxidization and resistance for coking [1].

2.3 Ni-SDC

The operating conditions and temperature ranges of SOFC requires quick reaction dynamics. This opens a new window of opportunity for abundantly available hydrocarbon fuels like methane, octane, solid carbon etc. Primary objective of using such fuels is through direct electrochemical oxidation (DEO) without the need of fuel reforming internally or externally [18]. This approach has benefits like high fuel efficiency and comparatively simplified cell design. Moreover, storing of hydrocarbon fuels is reliable than hydrogen which can cut down the capital costs.

The DEO approach for alternate fuels like hydrocarbons directly into electrical energy using SOFCs is very promising, however certain number of issues still need to be addressed [19,20]. The worst and vital issue is the reduced activity of the distinctive Ni catalyst in the nickel yttria-stabilized zirconia (Ni-YSZ) anode composite as a result of the coking. Generally Ni-YSZ has high catalytic performance for fuel reforming and high electron transfer capability. This catalytic activity of Ni not only catalyzes the breakage of carbon–hydrogen bonding in hydrocarbons but after this reaction it also promotes carbon–carbon bonding which is the indirect effect of Ni catalyst, and this contributes towards deposition of carbon which in turn covers active sites of Ni catalyst [21,22]. In addition, the coking fills up the porous anode, inhibiting fuel diffusion and build up stresses on the anode microstructure, which can result to cracking and delamination of the cell structure.

Coking process activity can be reduced by feeding steam and carbon dioxide at the positive electrode (anode) to reform fuel and get rid of the carbon deposition. Meanwhile, introduction of such diluents toxicates the fuel and decrease the overall fuel efficiency. Also, highly endothermic steam reforming process can increase the operating costs resulting in challenging temperature configuration and pre-heat requirement for steam formation indicating the need of extra energy costs [23].

That is why; there is a significant requirement for fabricating new, advanced, and coking resistant SOFC anode composites for the DEO reaction in case of hydrocarbon fuels. A lot of work has been carried out in this field and researchers are trying to achieve this goal. A study was carried out for rare earth metals and doped ceria with Cu impregnation for demonstration of such an anode cermet, which can directly utilize common fuels like hydrocarbon fuels including methane and octane in the SOFC. This

study showed proven feasibility of DEO for hydrocarbon fuels usage in SOFCs, but, catalytic process was not found satisfactory and high enough for commercialization [24.25]. Normally, mixed metal alloys are anticipated to contribute more towards coking resistance. Like, another study used a Copper Nickel support as SOFC anode material to directly oxidize the hydrocarbon fuel which surprisingly result in gaining resonable power density with neglectable coking. Furthermore, dual metallic support Sn-Ni just like Cu-Ni was tested as promising material for SOFC anode when methane and octane are fuels. The results for dual metallic support lead to findings, which demonstrated resistance of the SOFC anode for coking and their high performance [26].

Moreover, some developers tested anode diffusion layers. Lin et al. used a cermet of stabilized zirconia, doped ceria as barrier layer, and showed the improved stability of NiO-YSZ anode material for SOFCs working on hydrocarbon fuels. Another approach is to utilize multi valent perovskite materials for anode to improve electronic conductivity and enhancing electro-catalysis during redox cycles. Tao et al. and some other researchers reported that these materials like $La_{0.75}Sr_{0.25}Cr_{0.5}Mn_{0.5}O_{3-\delta}$ (LSCM) performed very well for DEO in case of methane [27]. But, this composite shows low electrical conduction during redox cycles and comparatively reduced catalytic activity. Huang et al. demonstrated a dual-perovskite material $Sr_2MMoO_{6-\delta}$ (M = Mg, Co, Ni) for SOFC anode both for hydrogen and methane fuels. The study showed that magnesium inculcation in $Sr_2MMoO_{6-\delta}$ exhibited good structural stability. For hydrogen and methane as fuel, cobalt addition in $Sr_2MMoO_{6-\delta}$ gave better cell performance and $Sr_2MMoO_{6-\delta}$ with nickel addition gave the considerable power densities for hydrocarbon fuels. Li et al. reported high stability and good performance with $Sr_2Fe_{1-x}Mo_{1+x}O_6$ for DEO alcohols and hydrocarbons [28–30].

However, almost every method and material mentioned previously need high temperature >850 °C for stable operation. This demands higher capital cost with performance drawbacks including system start and shutdown timings [31,32]. In this study, nickel samarium doped ceria is demonstrated for high structural and thermal performance and a stable link of Ni and SDC. This anode material comparatively performs well in the intermediate temperature range (500 – 800 °C) and studies has proved for achieving good and stable performance. We also demonstrated addition of

lanthanum and hydrogen peroxide addition to investigate the effects on the structural and thermal performance of NiO-SDC.

2.4 Ni(La)O-SDC

SOFCs gained popularity relatively more than other fuel cell types especially low and intermediate temperature SOFCs [33,34]. This is because SOFC show enhanced and stable performance with lower capital and operating costs. Working of SOFC at intermediate temperature range (500 – 800 °C) making it more stable and reliable with rapid start and shutdown of the system. It also makes it a likely candidate to utilize cheap materials for components in turn reducing overall cost of the systems. Ceria based SOFC anode (like Ni-SDC) have higher electronic conductivity than the typical Ni-YSZ for lower temperature ranges and it is predicted to take a place in SOFC anode materials as a promising and more reliable candidate [35, 36].

The high temperature range (500–1000 °C) of SOFC gives us a benefit of fuel reforming before the main chemical reaction in the cell. SOFC running on hydrocarbon fuels such as methane is considered very promising and have attained great popularity amongst other fuel cell types because this fuel is readily and abundantly available. It also makes the cell less prone to difficult and controllable factors than other fuels like octane, diesel etc. One challenge is the reforming of natural gas and it needs more energy than as the pure hydrogen fuel requires specifically at low temperature range [37,38]. Moreover, benchmark Ni-based anode material is not an effective carbon resistant composite as the carbon deposition inhibits the Ni catalytic activity and changes the SOFC structure mechanically unstable. To resolve and address these problems, efforts are being made for alternate materials but objective is focused on fabricating such novel anode materials, which do not promote carbon deposition and have high catalytic activity. Gorte's and co-workers [39, 40] used copper instead of nickel that developed resistance towards carbon deposition and catalytic activity did not promote carbon–cabon bonding. Murray *et al.*, [41] developed ceria-based anodes and used low working temperatures to resist carbon formation through catalyzation. Zhan et al., [42] used a dual-metal supported Ru–CeO_2 operational layer for the typical anode and it showed stable cell voltage in gasoline fuel. Irvine's et al., [43, 44] fabricated perovskite-based anode that performed actively for natural gas oxidation at elevated temperatures. All the above-mentioned procedures and schemes proved an

increase in resistance for carbon formation but it leads to reduced catalytic activity with higher system costs [45].

Nickel based anode materials has proved in previous studies to be very promising nominees for SOFCs because they have the capability to improve their catalytic activity and stable performance for fuels like natural gas or other hydrocarbons[43]. Various configurations are under consideration, research is ongoing for developing advanced anode materials like addition of alkali and rare earth compounds including MgO, CaO, La2O3, and Li_2O_3 into the state of the art nickel based anode. Normally it is a perception that the addition of these materials reduce nickel agglomeration and help in homogeneous dispersion of nickel [46].

Lanthanum is a widely accepted used element as additive in metal catalysts that alters structural performance of the catalyst. Addition of La in Ni–YSZ anode greatly improves the nickel activity and linkage between Ni and YSZ. It also helps in diminution of polarization resistance and showed improved catalytic performance for chemical oxidation of fuels [47]. Since, all the above-mentioned work was carried out for Ni-YSZ anode fuel cell. In this study, we added 10, 15 & 20 mol% La into a NiO–SDC composite in order to improve structural and thermal performance NiO-SDC anode material.

2.5 NiO-SDC using Hydrogen Peroxide

Commercialization of the energy technology depending on hydrogen fuel for transportation and mobile energy requirements need the fabrication of a fuel cell along with development of high activity electro-catalysts to produce pure hydrogen fuel [31]. Regarding this, rare earth (Sm, Gd, Y, La) doped ceria materials show considerable performance and are attaining growth in the field of fuel cell electrolytes and electrodes operating at intermediate temperature range (500 – 800 °C) [48]. The chemical stability and thermal performance of these materials largely affected the synthesis/ manufacturing process used to prepare them. Modification of synthesis process is a very growing concern for researchers as well as developers to produce inexpensive materials for commercial applications [49]. Co-precipitation synthesis process is primarily used for production of rare earth based materials coupled with sintering process [50]. Using this idea of process modification, structural properties can be configured and altered by either altering the whole synthesis process or by addition of

certain reagents [51]. Peroxides are suitable candidates for this purpose as in the past hydrogen peroxide was added for homogenous dispersions. Recent studies also show fabrication of nano-crystalline ceria with the help of peroxide [52,53].

Peroxide helps oxidizing cerium cations and produce hydro active Ce^{4+} instead of Ce^{3+}. In addition, it forms cerium complexes in place of simple OH^- as O^{-2} precursors. These complexes disturb the shaping of a closely linked M–O–M [54], during crystal growth, in the favor of highly distributed and homogenous structure formation of nano-crystallites. Hydrogen peroxide, in the recent past, is found to be better additive for a stable tetragonal phase formation of ZrO_2 [55]. Recently, addition of peroxide demonstrated an improvement in redox reactions and stability in the thermal performance of rare earth-ceria mixed oxides [56].

In this present work, NiO-SDC is synthesized with typical co-precipitation method and using an alternative route by adding H_2O_2 before precipitation. The outcome of certain parameters like the concentration of H_2O_2, effects on morphology, and thermal stability were investigated. The objective of this work was introduce a flexible process through which with the simple addition of a reagent enables us to develop materials with different functionalities.

Summary

Ni-YSZ is the state of the art anode material for SOFC and have the highest electronic conductivity and reasonable ionic conductivity. But this material cannot be used for wide range of fuels due to carbon deposition and low catalytic activity due to coking. Ceria based anode materials are promising because they provide better catalytic environment for chemical reactions at the triple phase boundary. In this study, two different methods have been used to improve the NiO-SDC cermet. Firstly, NiO-SDC based composite anode material with addition of Lanthanum (La), Ni(La)O-SDC, was prepared by co-precipitation route. Secondly, NiO-SDC was synthesized via altered co-precipitation method with the inclusion of Hydrogen Peroxide (H_2O_2). Both alterations were made to investigate effects on structural and thermal performance of NiO-SDC cermet.

References

[1] P.I. Cowin, C.T.G. Petit, R. Lan, J.T.S. Irvine, S. Tao, Recent Progress in the Development of Anode Materials for Solid Oxide Fuel Cells, Adv. Energy Mater. 1 (2011) 314–332.

[2] R. O'Hayre, S.-W. Cha, W. Colella, F.B. Prinz, Fuel Cell Fundamentals, Wiley, 2009.

[3] X. Li, Principles of Fuel Cells, Taylor & Francis, 2005.

[4] B. Cook, Introduction to fuel cells and hydrogen technology, Eng. Sci. Educ. J. (2002).

[5] Y. Zhao, C. Xia, L. Jia, Z. Wang, H. Li, J. Yu, *et al.*, Recent progress on solid oxide fuel cell: Lowering temperature and utilizing non-hydrogen fuels, Int. J. Hydrogen Energy. 38 (2013) 16498–16517.

[6] X. Huang, Z. Zhang, J. Jiang, Fuel Cell Technology for Distributed Generation: An Overview, in: 2006 IEEE Int. Symp. Ind. Electron., IEEE, 2006: pp. 1613–1618.

[7] NETL, Seventh Edition Fuel Cell Handbook, Pittsburgh, PA, and Morgantown, WV, 2004.

[8] A. Iio, H. Ikeda, S.A. Anggraini, N. Miura, Sensing characteristics of YSZ-based oxygen sensors attached with BaxSr1-xFeO3 sensing-electrode, Solid State Ionics. (2015).

[9] I.E. Achouri, N. Abatzoglou, N. Braidy, S. Bastien, New insights on the role of YSZ in a NiAl2O4/Al2O3–YSZ catalyst, Appl. Catal. A Gen. 497 (2015) 42–50.

[10] A. Cubero, J.I. Peña, M.A. Laguna-Bercero, Optimization of Ni–YSZ solid oxide fuel cell anodes by surface laser melting, Appl. Surf. Sci. 335 (2015) 39–43.

[11] N. Narimani, M. Saremi, A study on the oxidation resistance of electrodeposited and nanostructured YSZ thermal barrier ceramic coatings, Ceram. Int. 41 (2015) 13810–13816.

[12] X. Cheng, C. Wang, B. Wang, R. Sun, Y. Guan, Y. Sun, et al., Mixed-potential-type YSZ-based sensor with nano-structured NiO and porous TPB processed

with pore-formers using coating technique, Sensors Actuators B Chem. 221 (2015) 1321–1329.

[13] F.J. Garcia-Garcia, F. Yubero, A.R. González-Elipe, S.P. Balomenou, D. Tsiplakides, I. Petrakopoulou, et al., Porous, robust highly conducting Ni-YSZ thin film anodes prepared by magnetron sputtering at oblique angles for application as anodes and buffer layers in solid oxide fuel cells, Int. J. Hydrogen Energy. 40 (2015) 7382–7387.

[14] W.S. Jablonski, S.M. Villano, A.M. Dean, A comparison of H2S, SO2, and COS poisoning on Ni/YSZ and Ni/K2O-CaAl2O4 during methane steam and dry reforming, Appl. Catal. A Gen. 502 (2015) 399–409.

[15] A. Buyukaksoy, S.P. Kammampata, V.I. Birss, Effect of porous YSZ scaffold microstructure on the long-term performance of infiltrated Ni-YSZ anodes, J. Power Sources. 287 (2015) 349–358.

[16] R. Konar, J. Mukhopadhyay, A. Das Sharma, R.N. Basu, Synthesis of Cu-YSZ and Ni-Cu-YSZ cermets by a novel electroless technique for use as solid oxide fuel cell anode: Application potentiality towards fuel flexibility in biogas atmosphere, Int. J. Hydrogen Energy. (2015).

[17] X. Wu, X. Zhou, Y. Tian, X. Kong, J. Zhang, W. Zuo, et al., Preparation and electrochemical performance of silver impregnated Ni-YSZ anode for solid oxide fuel cell in dry methane, Int. J. Hydrogen Energy. 40 (2015) 16484–16493.

[18] X.B. Li, H.Y. Wang, H.X. Gu, J. Wang, W.J. Zhang, T.G. Wang, Preparation of gradient Ni-SDC anode by tape casting and co-sintering, Sci. Sinter. 42 (2010) 153–159.

[19] K. Sugihara, M. Asamoto, Y. Itagaki, T. Takemasa, S. Yamaguchi, Y. Sadaoka, et al., A quantitative analysis of influence of Ni particle size of SDC-supported anode on SOFC performance: Effect of particle size of SDC support, Solid State Ionics. (2014).

[20] B.B. Patil, S. Basu, Synthesis and Characterization of PdO-NiO-SDC Nano-powder by Glycine-Nitrate Combustion Synthesis for Anode of IT-SOFC, Energy Procedia. 54 (2014) 669–679.

[21] M. Chen, B.H. Kim, Q. Xu, O.J. Nam, J.H. Ko, Synthesis and performances of Ni–SDC cermets for IT-SOFC anode, J. Eur. Ceram. Soc. 28 (2008) 2947–2953.

[22] B.B. Patil, V. Ganesan, S.H. Pawar, Studies on spray deposited NiO–SDC composite films for solid oxide fuel cells, J. Alloys Compd. 460 (2008) 680–687.

[23] T. Skalar, K. Zupan, M. Marinšek, B. Novosel, J. Maček, Microstructure evaluation of Ni–SDC synthesized with an innovative method and Ni–SDC/SDC bi-layer construction, J. Eur. Ceram. Soc. 34 (2014) 347–354.

[24] K. Sugihara, M. Asamoto, Y. Itagaki, T. Takemasa, S. Yamaguchi, Y. Sadaoka, et al., A quantitative analysis of influence of Ni particle size of SDC-supported anode on SOFC performance: Effect of particle size of SDC support, Solid State Ionics. 262 (2014) 433–437.

[25] M. Asamoto, S. Miyake, K. Sugihara, H. Yahiro, Improvement of Ni/SDC anode by alkaline earth metal oxide addition for direct methane–solid oxide fuel cells, Electrochem. Commun. 11 (2009) 1508–1511.

[26] X. Fang, Synthesis and properties of Ni–SDC cermets for IT–SOFC anode by co-precipitation, Solid State Ionics. 168 (2004) 31–36.

[27] M. Kawano, H. Yoshida, K. Hashino, H. Ijichi, S. Suda, K. Kawahara, et al., Synthesis of matrix-type NiO–SDC composite particles by spray pyrolysis with acid addition for development of SOFC cermet anode, J. Power Sources. 173 (2007) 45–52.

[28] M. Chen, B.H. Kim, Q. Xu, O.J. Nam, J.H. Ko, Synthesis and performances of Ni–SDC cermets for IT-SOFC anode, J. Eur. Ceram. Soc. 28 (2008) 2947–2953.

[29] Z. Wang, Y. Li, J.W. Schwank, Evaluation of Ni/SDC as anode material for dry CH4 fueled Solid Oxide Fuel Cells, J. Power Sources. 248 (2014) 239–245.

[30] N. Tian, J. Yu, Y. Deng, G. Li, X. Zhang, Electrical properties of Ce0.85Sm0.15O1.925–Fe2O3 electrolytes for IT-SOFCs, J. Alloys Compd. 655 (2016) 215–219.

[31] M. NI, M. LEUNG, D. LEUNG, Technological development of hydrogen production by solid oxide electrolyzer cell (SOEC), Int. J. Hydrogen Energy. 33 (2008) 2337–2354.

[32] H. Sun, Y. Zhang, H. Gong, Q. Li, Y. Bu, T. Li, Anode-supported SOFCs based on Sm0.2Ce0.8O2−δ electrolyte thin-films fabricated by co-pressing using microwave combustion synthesized powders, Ceram. Int. 42 (2016) 4285–4289.

[33] B. Zhu, X.T. Yang, J. Xu, Z.G. Zhu, S.J. Ji, M.T. Sun, et al., Innovative low temperature SOFCs and advanced materials, J. Power Sources. 118 (2003) 47–53.

[34] M. SHIONO, K. KOBAYASHI, T. LANNGUYEN, K. HOSODA, T. KATO, K. OTA, et al., Effect of CeO2 interlayer on ZrO2 electrolyte/La(Sr)CoO3 cathode for low-temperature SOFCs, Solid State Ionics. 170 (2004) 1–7.

[35] N.Q. Minh, Ceramic Fuel Cells, J. Am. Ceram. Soc. 76 (1993) 563–588.

[36] R.M. Ormerod, Solid oxide fuel cells, Chem. Soc. Rev. 32 (2003) 17–28.

[37] M. Mogensen, K. Kammer, C ONVERSION OF H YDROCARBONS IN S OLID O XIDE F UEL C ELLS, Annu. Rev. Mater. Res. 33 (2003) 321–331.

[38] R.J. Gorte, S. Park, J.M. Vohs, C. Wang, Anodes for Direct Oxidation of Dry Hydrocarbons in a Solid-Oxide Fuel Cell, Adv. Mater. 12 (2000) 1465–1469.

[39] R.J. Gorte, S. Park, J.M. Vohs, Direct oxidation of hydrocarbons in a solid-oxide fuel cell, Nature. 404 (2000) 265–267.

[40] S. McIntosh, R.J. Gorte, Direct Hydrocarbon Solid Oxide Fuel Cells, Chem. Rev. 104 (2004) 4845–4866.

[41] S.A. Barnett, E.P. Murray, T. Tsai, A direct-methane fuel cell with a ceria-based anode, Nature. 400 (1999) 649–651.

[42] Z. Zhan, S.A. Barnett, An octane-fueled solid oxide fuel cell., Science. 308 (2005) 844–7.

[43] J.C. Ruiz-Morales, J. Canales-Vázquez, C. Savaniu, D. Marrero-López, W. Zhou, J.T.S. Irvine, Disruption of extended defects in solid oxide fuel cell anodes for methane oxidation, Nature. 439 (2006) 568–571.

[44] S. Tao, J.T.S. Irvine, A redox-stable efficient anode for solid-oxide fuel cells., Nat. Mater. 2 (2003) 320–3.

[45] Y. SHIRATORI, Y. TERAOKA, K. SASAKI, Ni1−x−yMgxAlyO–ScSZ anodes for solid oxide fuel cells, Solid State Ionics. 177 (2006) 1371–1380.

[46] W. Wang, C. Su, R. Ran, Z. Shao, A new Gd-promoted nickel catalyst for methane conversion to syngas and as an anode functional layer in a solid oxide fuel cell, J. Power Sources. 196 (2011) 3855–3862.

[47] Z. Zhang, X.E. Verykios, Carbon dioxide reforming of methane to synthesis gas over Ni/La2O3 catalysts, Appl. Catal. A Gen. 138 (1996) 109–133.

[48] C. Ding, T. Hashida, Synthesis and evaluation of NiO–Ce0.8Sm0.2O1.9 nanocomposite powders for low-temperature solid oxide fuel cells, Int. J. Hydrogen Energy. 36 (2011) 5567–5573.

[49] S.-P. Li, J.-Q. Lu, P. Fang, M.-F. Luo, Effect of powder thermal treatment on the microstructure and electrical properties of doped ceria ceramics, Mater. Lett. 63 (2009) 1689–1692.

[50] Y. Fu, L. Cao, G. Guo, T.S. Huang, Multiple feature fusion by subspace learning, in: Proc. 2008 Int. Conf. Content-Based Image Video Retr. - CIVR '08, ACM Press, New York, New York, USA, 2008: p. 127.

[51] K. Higashi, K. Sonoda, H. Ono, S. Sameshima, Y. Hirata, Synthesis and sintering of rare-earth-doped ceria powder by the oxalate coprecipitation method, J. Mater. Res. 14 (2011) 957–967.

[52] P. Yu, S.A. Hayes, T.J. O'Keefe, M.J. O'Keefe, J.O. Stoffer, The Phase Stability of Cerium Species in Aqueous Systems, J. Electrochem. Soc. 153 (2006) C74.

[53] B. Djuričić, S. Pickering, Nanostructured cerium oxide: preparation and properties of weakly-agglomerated powders, J. Eur. Ceram. Soc. 19 (1999) 1925–1934.

[54] F.H. Scholes, C. Soste, A.E. Hughes, S.G. Hardin, P.R. Curtis, The role of hydrogen peroxide in the deposition of cerium-based conversion coatings, Appl. Surf. Sci. 253 (2006) 1770–1780.

[55] T.I. Panova, V.P. Popov, V.B. Glushkova, A. V. Domanskii, Preparation of nanodisperse solid solutions based on ZrO2 and HfO2 from hydroperoxides, Glas. Phys. Chem. 33 (2007) 652–657.

[56] B.P. Mandal, V. Grover, M.R. Pai, A.K. Tyagi, Improvement of physico-chemical properties by addition of H2O2: An extensive case study on the RE-doped ceria system (RE = Gd, Sm), J. Mater. Res. 24 (2011) 2845–2854.

Chapter 3

Literature Review on Some Experimental and Characterization Methods

This chapter is a demonstration of various synthesis techniques as well as a comprehensive review on characterization tools and methods commonly utilized for material testing and analysis.

3.1 Solid State Synthesis Method

Sythesis of ceramic compounds is carried out via solid-state fabrication process chiefly because it is a very simple process rather than a complex one like solution combustion synthesis. In solid state chemical reaction process, direct reaction of solids occurs to form the final products and principally no decomposition is involved. The reactants must have large surface area in order to maximize the contact between them. Generally, solids do not react with solids at low temperatures even if thermodynamics is favorable so high temperature must be employed to increase the rate of diffusion or decrease the diffusion lengths between the reactants. The rate of nucleation of such type of reactions may be enhanced by providing a structural similarity between the reactants and products. The major steps in conventional solid state synthesis are given below [1]:

- The selection of the appropriate starting materials e.g., reactive starting materials are better than inert and the reactants must be in the form of fine grain powders to maximize the surface area.
- Weigh out the starting materials in proper ratio according to the stoichiometric calculations.
- Then thorough mixing of the reactants by using agate mortar and pestle or ball mill. Organic solvent may be used to facilitate the mixing process.
- After thorough mixing, heat treatment is done at a suitable temperature to achieve the desired phase. The heating must be done in an inert crucible/container and/or in a specific environment.
- At the end, grinding of the product is done to obtain the fine particles.

The major advantages include the solid state reactions are simple to perform; the starting materials for such type of reactions are readily available at low cost and such reactions are clean i.e. they do not involve other chemical elements. However, the main drawbacks of solid state reaction method are homogeneous distribution is difficult to achieve especially for dopants, high calcination temperature, particle size is difficult to control, low surface area and reaction with containers/crucibles etc. In order to overcome the drawbacks of solid state reaction method, some wet chemistry based routes are developed. In the next section of this chapter, we will discuss the properties and different types these wet chemistry routes.

3.2 Wet Chemistry Synthesis

The major characteristics of wet chemistry routes are the atomic scale mixture homogeneity of precursors and the particle size, surface morphology as well as surface area can be controlled by the use of such routes. The basic approach is to decrease the diffusion lengths through the intimate mixing of cations. Primary advantages include lower reaction temperatures, elimination of intermediate impurity phases and the products obtained are of high surface area. Major examples of such routes are co-precipitation, sol-gel process and hydrothermal etc. In the next two sections, a brief review of co-precipitation and sol-gel process is given.

3.2.1 Co-precipitation Methode

Co-precipitation reaction consists of nucleation, growth coarsening and/or agglomeration processes. All these processes occur simultaneously. Co-precipitation method shows the following properties:

- The products formed are commonly insoluble species and formed under the conditions of high degree of supersaturation.
- The key step during co-precipitation method is nucleation. In this step, the formation of a large number of small particles will occur.
- The particle size, surface morphology and the properties of the products during synthesis mainly depend upon the secondary processes e.g., Ostwald ripening and aggregation.
- In order to induce the precipitation, the supersaturation conditions are necessary. These conditions will occur as a result of the following chemical reaction,

Typical co-precipitation synthetic methods include the formation of metals from aqueous solutions, by reduction from nonaqueous solutions, electrochemical reduction, and decomposition of metalorganic precursors; formation of oxides from aqueous and nonaqueous solutions; formation of metal chalconides by reactions of molecular precursors; microwave/sonication-assisted coprecipitation [2].

3.2.2 Sol-gel Method

The sol-gel process is a wet chemistry base route in which an integrated network usually known as gel is formed by the combination of sol. Sol is the colloidal particles for the formation of nanoscale particles. Sol may be a chemical solution (sol short for solution). Commonly used precursors for sol-gel process are metal alkoxides and metal chlorides. Sol is formed when the precursors undergo hydrolysis and polycondensation reactions to form a colloid. Sol is basically a system composed of nanoparticles which are completely dispersed in a solvent. The sol evolves then towards the formation of an inorganic continuous network containing a liquid phase (gel).

Formation of a metal oxide involves connecting the metal centers with oxo (M – O – M) or hydroxo (M – OH – M) bridges, therefore generating metal-oxo or metal-hydroxo polymers in solution.

Drying is carried out to remove the liquid phase from the integrated network i.e., gel. In order to enhance the mechanical properties and favor further polycondensation reaction a heat treatment (calcination) of the dried sample may be performed.

In addition to these wet chemistry routes some advanced synthetic methods are also exploited and studied in literature. Primarily, such methods include the deposition techniques for the formation of thin films of desired compounds over the substrates.

3.3 Vapor Phase Synthesis/ Deposition Technique

3.3.1 Physical Vapor Deposition

In physical vapor deposition (PVD), film is formed by atoms directly transported from source/target to the substrate. PVD processes take place in a vacuum chamber, and by one mean or another, create a low-pressure vapor of the material to be deposited. Some of this vapor will condense on the work piece and thereby start to deposit as a thin film. Simply melting a material in vacuum, depending on its vapor pressure, may sometimes produce a useful deposit of material. Sublimation furnaces are engaged to

efficiently evaporate selenides, sulfides, and some other oxides. The evaporative materials are sintered and pressed to form pellets that are then subjected to radiant heat source. The most common example of these kind of evaporative materials include graphite and refractory metals, mostly formed by hot pressing of powder to form pellets.

The heating is normally done by external tungsten wire resistance heating elements. The heating of evaporant source by resistive heating element (in conventional evaporation process) include disadvantages like contamination caused by the supportive materials, crucibles, and heaters that hinders the deposition of pure films. It also includes the drawback of evaporating high melting point materials at high rates. Electron beam evaporation overcomes these limitations and therefore it is a better vacuum based evaporative film deposition technique. This technique has the advantage of evaporating a wide range of materials at practical rates. The technique works by placing the evaporative material in water cooled crucible or copper hearth. A small fraction of evaporant sublimes or melts that assured the purity of evaporative material as the crucible is water cooled that hinders its melting and contamination with the source evaporant [3].

Major types of physical vapor deposition processes are given below:

- Evaporation
    - Thermal evaporation
    - Electron beam evaporation
- Sputtering
    - DC sputtering
    - DC magnetron sputtering
    - Radio frequency sputtering
    - Reactive PVD

3.3.2 Chemical Vapor Deposition

In chemical vapor deposition (CVD), the film is formed by chemical reaction on the surface of a substrate. It does not require vacuum or unusual levels of electric power. CVD has the ability to deposit films or coatings of metals, ceramics and semi-conductors. Major advantages of CVD processes are high growth rate with good reproducibility, it can deposit materials which are hard to deposit e.g., by evaporation,

can grow epitaxial films and more conformal coverage. However, CVD processes also offer some disadvantages such as high process temperature, it is a complex process i.e. toxic of corrosive gases and produced films may not be pure e.g., hydrogen incorporation. The examples of CVD processes are given below [4]:

- Atmospheric chemical vapor deposition (APCVD)
- Low pressure chemical vapor deposition (LPCVD)
- Plasma enhanced chemical vapor deposition (PECVD)

The factors that distinguished PVD from the CVD are:

- In PVD, solid and/or molten sources are used while in CVD gaseous precursors are commonly used.
- Source atoms enter into the gas phase by some physical mechanisms, such as, evaporation or collisional impact.
- Gaseous species are transported through the reduced pressure environment.
- Generally, no chemical reaction occurs in the gas phase and at the surface of the substrate.

After the successful synthesis of nanoparticles and/or thin films the detailed analysis is done by employing different characterization techniques. In the next section, a brief overview of some characterization tools are given which are mostly used in order to analyze the ceramic compounds in this thesis.

3.4 Characterization Tools and Methods

3.4.1 X-ray Diffraction (XRD)

X-rays are electromagnetic radiation with a wavelength of ~1Å. Their wavelength is shorter than ultraviolet and longer than γ-rays in the electromagnetic spectrum. X-rays are commonly used to study the phase and morphological arrangement on the atomic and molecular scale in a broad range of materials since the X-rays wavelength is comparable to the atomic and molecular size range. These rays are generated when a high-energy charged electron beam is accelerated through a high voltage field bombards on a solid target, normally copper or molybdenum. As incident electrons collide with atoms in the target, the inner shell electrons in atoms can be ejected through ionization process by the high energy electrons. A free electron in an outer orbital will immediately fill the vacant site and an X-ray photon is emitted due to the energy released in the transition. The relationship between the energy E of X-ray

radiation and its wavelength is given by the equation Eq. (3.1) where h is Planck's constant and c is the speed of light in vacuum [5].

$$E = \frac{hc}{\lambda} \tag{3.1}$$

After the collision of X-rays with the crystals, some of them will be deflected away from the direction they originally travel and these deflected X-rays are measured in diffraction experiments. The scattered X-rays carry information about the electron distribution in materials and each crystalline solid has its unique X-ray pattern, therefore it can be used as a 'fingerprint' for identification. Bragg's Law is a simple and straightforward description for crystal diffraction.

The derivation of Bragg's Law is shown in Figure 3.1. The incident beams 1&2 are always in phase and parallel up to the points A&D, where x-ray 1 hits the top layer at point D, while x-ray 2 travels to the next layer where it spreads by atom B. Therefore, x-ray 2 must go ahead a further length of distance (AB + BC) before the two x-rays continue to travel adjacent and parallel as 1'&2'. This further length of distance must equate the integral (n) times the wavelength (λ) for the two x-rays to exist in phase.

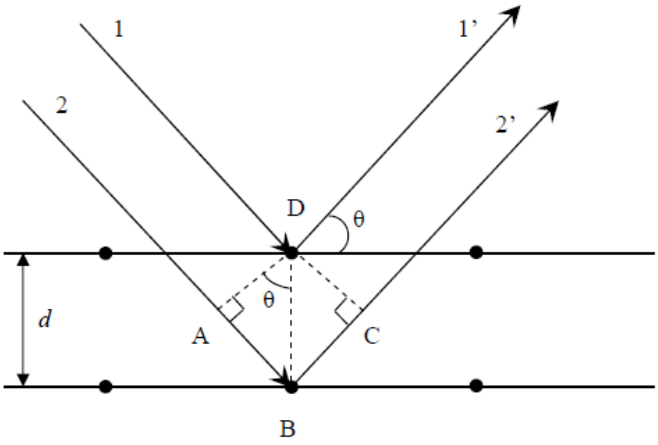

Figure 3.1: Description of Bragg's Law

d is the perpendicular distance between pairs of adjacent planes and θ is the angle of incidence, therefore:

$$AB = BC = d \sin \theta \tag{3.2}$$

$$2AB = n\lambda \tag{3.3}$$

$$2d\sin \theta = n\lambda \tag{3.4}$$

The unit cell parameter of a crystal can be calculated by the distance between adjacent atomic planes d. For cubic crystals (α = β =γ = 90°), the d-spacing for any set of planes is given by,

$$\frac{1}{d_{hkl}^2} = \frac{h^2}{a^2} + \frac{k^2}{b^2} + \frac{l^2}{c^2} \tag{3.5}$$

here h, k and l are the miller indices while the unit cell parameters are a, b and c.

The equation will be simplified if the crystal are cubic i.e. a = b = c

$$\frac{1}{d_{hkl}^2} = \frac{h^2 + k^2 + l^2}{a^2} \tag{3.6}$$

Powder X-ray Diffraction is the most widely used X-ray diffraction technique for materials characterization. Using Debye-Scherrer equation we can calculate the crystallite size of the crystals. Scherrer equation;

$$D_{XRD} = 0.9\,\lambda / \beta.\, cos\,\theta \tag{3.7}$$

λ indicates the X-rays wavelength in nanometers, θ in degrees being the tilting angle of diffraction, and β (degrees) shows the adjusted full width at half maximum (FWHM) intensity. Peaks with significant intensities were used for the calculations.

The density is an important factor for ceramics as it can greatly affect the material property especially the conductivity for electroceramics. The well densified ceramics would have higher conductivity compared to the less densified ones, in which pinholes and cracks could separate and /or block the conduction path. The theoretical density (D) of ceramics is calculated using the following equation:

$$D = \frac{MZ}{N_{av}V} \tag{3.8}$$

'M' indicates atomic weight in grams per mole, 'V' symbolizes the volume of a unit cell ($Å^3$) which can be calculated by the lattice parameter (a), of the unit cell, N_{Av} is Avogadro's constant and Z is the formula unit and for cubic fluorite based structures like CeO_2 and ZrO_2 the value of Z is 4.

3.4.2 Scanning Electron Microscopy (SEM)

Electron microscopes are microscopes that use electron beams to illuminate the specimen and take highly magnified images. They can achieve much higher resolution

than the light-powered optical microscopy, because the wavelength of electron is about 100,000 times shorter than visible light.

A Scanning Electron Microscope (SEM) takes images by scanning across a rectangular area of the sample with a focused electron beam. Particularly, an electron gun is used for the thermionic emission of the electron beam. This electron firing mechanism is accommodated with a tungsten (W) filament electrode. W is used for pre-heating in high temperature subatomic particle electron guns to produce an electron beam because of its highest melting point and lowest vapor pressure among metals. The electron beams are focused by several condenser lenses to a spot with ~4–50 Å diameters and are adjusted and controlled by the deflection coils before finally incident onto the sample. The electrons lose energy when the electron beam interacts with the specimen and the lost energy will be converted into other forms such as heat, emission of secondary electrons and emission of light or X-rays, which can be detected by specialized detectors. Figure 3.2 shows a schematic diagram of an SEM.

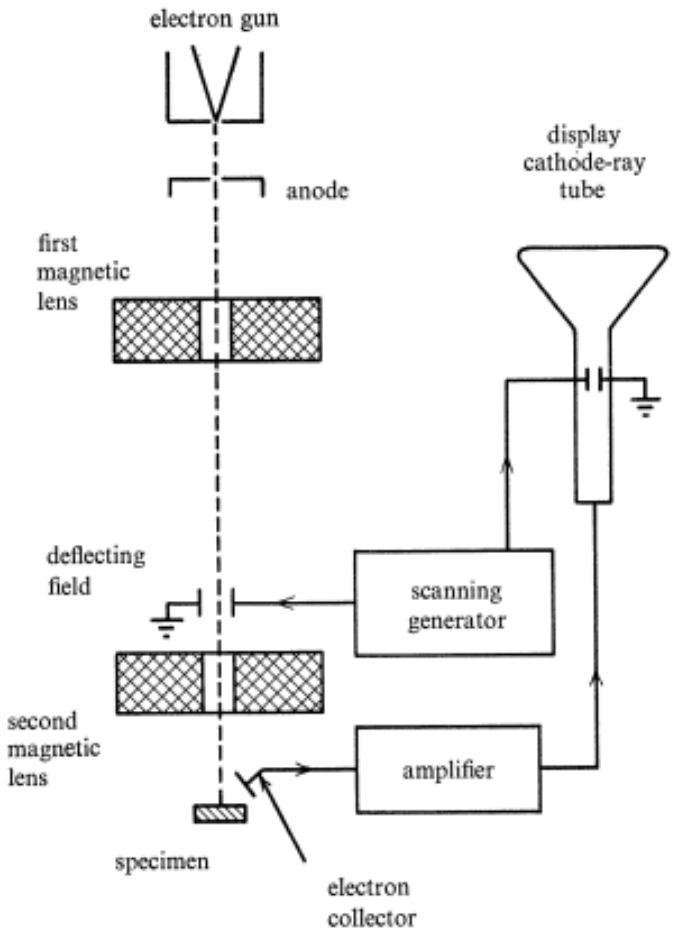

Figure 3.2: Schematic representation of SEM [3]

The major steps for the sample preparation in order to carry out SEM analysis are:

- Sectioning
- Mounting
- Grinding
- Polishing
- Etching

3.4.3 Energy Dispersive Spectroscopy

Energy Dispersive Spectroscopy (EDS) or Energy Dispersive X-ray analysis (EDX) is a compositional elemental analysis technique for chemical characterization of the specimen. EDS is always used in conjunction with TEM and/or SEM. The principle of EDS is described as when focused beam of high energy electrons is bombarded onto a solid sample, X-rays are emitted. The detector in make use of these x-rays to obtain localized chemical analysis. Typical resolution is of 150 eV. Quantitative analysis and elemental mapping are also possible through EDS.

When electrons strike the specimen, the electrons contained in specimen are excited creating vacant places in the atomic shells. Electrons in the higher shells fill these vacancies. The energy is released in this process in form of x rays. All elements emit X-rays with characteristic energy values. Each element in periodic table has its specific energy value which makes elemental analysis through EDS possible. Kα X-rays are emitted when an electron from L shell fills the vacancy in K shell of the atom. Letters K, L, M represents the shell from where electrons are emitted and α, β, γ represents the shell where they are substituted. Sample preparation is same as for SEM. In principle, all elements in periodic table from beryllium to uranium (atomic number 4 to 92) can be detected by EDS.

3.4.4 Thermo Gravimetric Analysis (TGA)

TGA is the acronym of Thermo gravimetric analysis. It is a technique for thermally analyzing that demonstrates the weight loss or weigh gain of the sample powder is observed as a function of time or increasing temperature. The sample is subjected to a controlled atmosphere and controlled temperature conditions. In other words the changes in chemical like dehydration, solid-gas reactions, chemisorption, decomposition etc. and physical properties like desorption, absorption, adsorption, vaporization, sublimation etc. are determined.

When materials are subjected to heat, physical and chemical changes occur. The weight of the material is either increased or decreased. Thermo gravimetric analyzer consists of a pan placed in a programmable furnace. This pan is supported by a sensitive precision balance. The specimen is placed onto the pan and a heat rate and a temperature range up to which changes is the material is to be observed is given to the furnace. The furnace is heated from lower limit of temperature range (usually from room temperature), reaches the maximum point and then it is cooled. The mass change is monitored during the heating and cooling process. The environment of furnace is controlled by an inert or a reactive gas [6].

The data obtained from TG analysis of the sample enables the interpretation of loss of volatile components in the sample, its thermal stability and decomposition. The data obtained is plotted in form of a graph between increasing temperature on x-axis and weight loss percentage on y-axis. In the given temperature range, if a graph shows a straight line meaning no weight change, this means that the specie is thermally stable. Sometimes an initial weight loss is shown in the graph and then the line becomes straight which means the specie is thermally unstable at low temperature and then becomes stable. The data from TG analysis also provides information about the maximum use temperature of the material beyond which the material will degrade. It also provides information about reaction kinetics, degradation mechanism, presence of inorganic content in material and decomposition patterns [7].

3.4.5 Differential Thermal Analysis

Differential thermal analysis is another thermal analysis technique that notes the temperature difference between a reference material and a sample as a function of temperature or time. Both the sample as well reference material is subjected to same conditions of temperature and environment. DTA records the changes in energy of the sample during a transformation as a function of time or temperature. From the data we can determine the phase change or transition temperature of the sample like crystallization temperature, glass transition temperature, sublimation temperature, melting temperature etc [8].

This DTA apparatus is mostly hybrid with TGA apparatus. DTA apparatus consists of a device for measurement of heat of reaction (recording system), a programmable furnace (source of heat), and a sample holder. Sample holder contains a metallic or a

ceramic block, sample containers and two thermocouples. One thermocouple is placed in sample and the other in an inert material (usually Al_2O_3) as a reference and both thermocouples are joined to a voltmeter. When the sample undergoes a phase change with increasing temperature, a deflection in voltmeter occurs. The deflection is because of the temperature differences between reference material and sample material because heat input raises the temperature of reference material and the heat is consumed as latent heat in changing the phase of sample material. This deflection is recorded and a graph between temperature or time on x-axis and heat flow on y-axis. The graph curve thus formed is called thermogram or DTA curve. Exothermic and endothermic reactions occurring in sample material are thus analyzed [9].

3.4.6 Electrical Conductivity

Conductivity for un-doped and cobalt doped samples were obtained using four point probe measurements. Figure 3.3 shows the typical arrangement used for this method. A constant current is supplied via two external probes and change in voltage as a function of temperature is measured through two central probes using a voltmeter. For best results, the amperage of the sample must be maintained at a constant level as rise in temperature can shift the equilibrium which would distort the resulting voltage. Resistance (R) is calculated using Ohm's law while pellet thickness (L) is used to calculate resistivity using following equation.

$$\rho = \frac{R_{pellet} \times A_{pellet}}{T_{pellet}} \tag{3.9}$$

R_{pellet} = *Resistance;*

A_{pellet} = *Area;*

T_{pellet} = *Thickness.*

To investigate the electrical conductivity behavior, the temperature dependency of the electrode conductivity was studied. The temperature dependency of conductivity for semi-conducting materials can be determined using the traditional Arrhenius equation. Pellet of fabricated sample was formed for measurement of electrical conductivity then conductivity of NiO-SDC pellet was calculated by using following formula:

$$\sigma(T) = \sigma_o e^{(\frac{-E}{kT})} \tag{3.10}$$

where,

Conductivity (σ) = 1 / Resistivity (ρ),

σ_o = Exponential factor (constant);

E = Activation Energy,

k = Boltzmann's Constant;

and

T = Temperature

Conductivity of electrode primarily relies on temperature conditions, and Arrhenius' law is applied to explain relation among conductivity and temperature. A typical 4 probe setup for conductivity measurement is show in Figure 3.3.

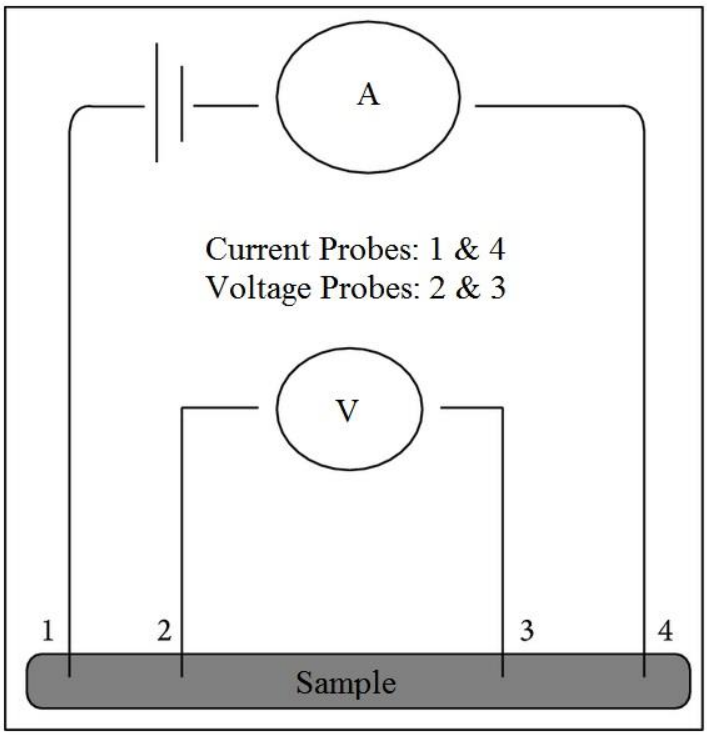

Figure 3.3: Four probe assembly for electrical conductivity measurements

Summary

In this chapter, a brief review of different experimental and characterization methods is given for the synthesis and analysis of ceramic materials for the use in fuel cell components. Conventionally, solid state reaction method is employed because of its simplicity; however, this method also offers some drawbacks like high calcination temperature, inhomogeneity and uncontrollable particle size distribution. Therefore, some wet chemistry routes such as co-precipitation, sol-gel process and hydrothermal etc. are exploited in order to overcome the drawbacks of solid state reaction method. The major characteristics of wet chemistry routes are the atomic scale mixture homogeneity of precursors and the particle size, surface morphology as well as surface area can be controlled by the use of such routes. In addition to wet chemistry routes some thin film deposition processes like physical vapor deposition and chemical vapor deposition are also developed in order to form a thin layer of desired ceramic compound on a substrate. Characterization techniques like X-ray diffraction, scanning electron microscopy and energy dispersive spectroscopy (EDX) are used for the microstructure analysis of the ceramic compounds.

References

[1] Z. Shao, W. Zhou, Z. Zhu, Advanced synthesis of materials for intermediate-temperature solid oxide fuel cells, Prog. Mater. Sci. 57 (2012) 804–874.

[2] I.M. Kolthoff, Theory of Coprecipitation - The formation and properties of crystalline precipitates, in: n.d.

[3] M. Ohring, Materials Science of Thin Films - Deposition & Structure, Second, n.d.

[4] R.M. Ormerod, Solid oxide fuel cells, Chem. Soc. Rev. 32 (2003) 17–28.

[5] J. George, Preparation of Thin Films, Marcel Dekker, INC., 1992.

[6] P. Gabbott, "Principles and applications of thermal analysis", Blackwell Pub., 2008.

[7] J. R. Newton and E. Atkins, "Report on differential thermal and thermogravimetric analysis", U.S. Dept. of Interior; [for sale by the Supt. of Docs., U.S. Govt. Print. Off.], 1969.

[8] R. C. MacKenzie, "Differential Thermal Analysis: Fundamental aspects", Academic Press, 1970.

[9] W. J. Smothers and Y. Chiang, "Differential thermal analysis: theory and practice", Chemical Pub. Co., 1958.

Chapter 4

Experimental Methods

A number of experiments were carried out to achieve certain objectives previously detailed in Chapter 2. However, the major experiments include:

- Synthesis of Nickel Oxide-Samarium Doped Ceria (NiO-SDC).
- Synthesis of NiO-SDC with variants like pH, concentration and calcination temperaure
- Synthesis of NiO-SDC with Lanthanum addition
- Synthesis of NiO-SDC using modified co-precipitation with H_2O_2
- Chemical compatibility test of NDC (electrolyte) with NiO-SDC (anode)

4.1 Synthesis and Characterization of NiO-SDC/ Base Material

The ceramic electrode material NiO-SDC was synthesized through co-precipitation process (Figure 4.1) method using nickel nitrate hexahydrate, cerium nitrate hexahydrate and samarium nitrate hexahydrate as the precursors. Stoichiometric amounts of nickel nitrate hexahydrate were dissolved in de-ionized water and separately cerium nitrate hexahydrate and samarium nitrate hexahydrate were thoroughly mixed in de-ionized water. Both solutions were then mixed with the concentration of the precursor solution was 0.5 M. This solution was stirred to obtain a transparent homogenous solution. Then poured 25% Ammonia Solution in the precursor solution until the precipitates are formed with a thick white slurry type resemblance. Now again stirred the solution consisted of precipitates and dried it on a hot plate at 200 ºC for 2 hrs. Pale yellow matter was obtained after the complete drying. Then ground that matter to form a fine powder and afterwards calcined the dried sample in a furnace at 800 ºC for 2 hrs with the heating rate of 5ºC/min.

Phase identification and crystal structure of the synthesized anode material was determined by X-ray diffractometer (STOE & Cie GmbH Germany). XRD of powder sample was recorded using micro beam of CuKα radiation (λ = 1.5425 Å), with variable 2θ in the range of 10 to 80 degrees. The diffraction pattern was scanned in steps of 0.015°. The morphological analysis and the particle size distribution of the prepared sample was observed by scanning electron microscopy (JEOL Analytical

SEM). Thermal performance was analyzed by thermogravimetric and differential thermal analysis. For determining the conductivity of the anode, composite poweder was transformed into a pellet by using hydraulic press and was sintered at 1100 °C for ~3 hours. LCR meter (W. Kerr Electronics) was used to mearure DC conductivity up to an elevated 650 °C temperature environment.

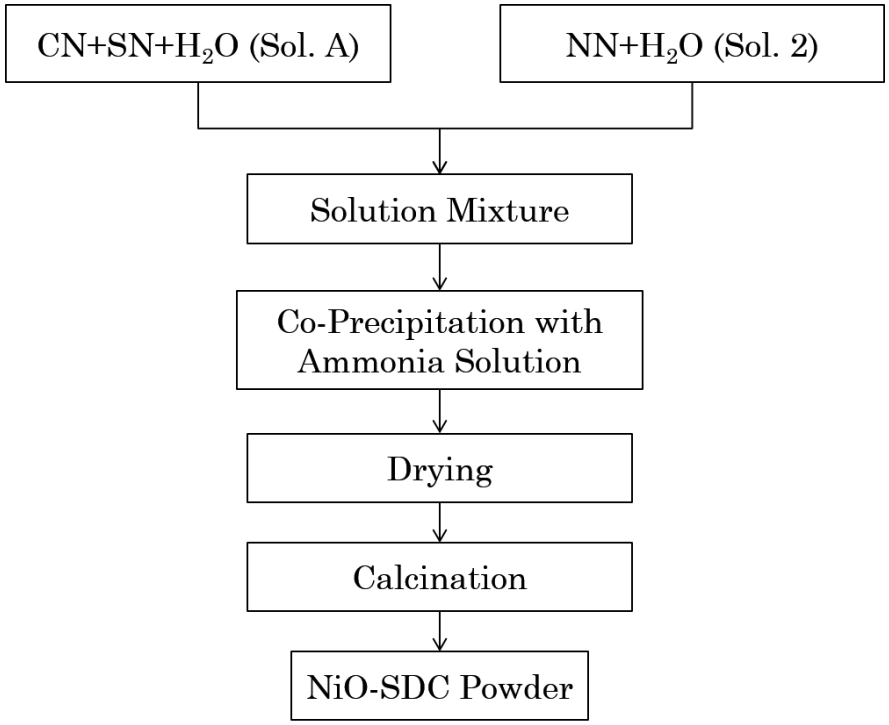

Figure 4.1: Flow Diagram of NiO-SDC Synthesis where CN, SN and NN are Cerium, Samarium and Nickle Nitrate Hexahydrates respectively

4.2 Study of Effects of Various Process Parameters on NiO-SDC

4.2.1 Synthesis with Variable Concentration of NiO in NiO- SDC

Three samples were prepared with NiO concentration of 45, 55 and 65% by volume.

The ceramic electrode material NiO-SDC was synthesized through co-precipitation process (Figure 4.1) method using nickel nitrate hexahydrate, cerium nitrate hexahydrate and samarium nitrate hexahydrate as the precursors. Stoichiometric amounts of nickel nitrate hexahydrate were dissolved in de-ionized water and separately cerium nitrate hexahydrate and samarium nitrate hexahydrate were thoroughly mixed in de-ionized water. Both solutions were then mixed with the concentration of the precursor solution was 0.5 M. This solution was stirred to obtain a transparent homogenous solution. Then poured 25% Ammonia Solution in the precursor solution until the precipitates are formed with a thick white slurry type

resemblance. Now again stirred the solution consisted of precipitates and dried it on a hot plate at 200 ºC for 2 hrs. Pale yellow matter was obtained after the complete drying. Then ground that matter to form a fine powder and afterwards calcined the dried sample in a furnace at 800 ºC for 2 hrs with the heating rate of 5ºC/min.

4.2.2 Synthesis of NiO-SDC at Different pH Value

Three samples were prepared pH values 9.5, 10 and 10.5. pH of medium of NiO-SDC was set to desired value before precipiation.

The ceramic electrode material NiO-SDC was synthesized through co-precipitation process (Figure 4.1) method using nickel nitrate hexahydrate, cerium nitrate hexahydrate and samarium nitrate hexahydrate as the precursors. Stoichiometric amounts of nickel nitrate hexahydrate were dissolved in de-ionized water and separately cerium nitrate hexahydrate and samarium nitrate hexahydrate were thoroughly mixed in de-ionized water. Both solutions were then mixed with the concentration of the precursor solution was 0.5 M. This solution was stirred to obtain a transparent homogenous solution. Then poured 25% Ammonia Solution in the precursor solution until the precipitates are formed with a thick white slurry type resemblance. Now again stirred the solution consisted of precipitates and dried it on a hot plate at 200 ºC for 2 hrs. Pale yellow matter was obtained after the complete drying. Then ground that matter to form a fine powder and afterwards calcined the dried sample in a furnace at 800 ºC for 2 hrs with the heating rate of 5 ºC/min.

4.2.3 Synthesis of NiO-SDC at Different Calcination Temperature

Three samples of NiO-SDC were prepared at 600 ºC, 800 ºC and 1000 ºC.

The ceramic electrode material NiO-SDC was synthesized through co-precipitation process (Figure 4.1) method using nickel nitrate hexahydrate, cerium nitrate hexahydrate and samarium nitrate hexahydrate as the precursors. Stoichiometric amounts of nickel nitrate hexahydrate were dissolved in de-ionized water and separately cerium nitrate hexahydrate and samarium nitrate hexahydrate were thoroughly mixed in de-ionized water. Both solutions were then mixed with the concentration of the precursor solution was 0.5 M. This solution was stirred to obtain a transparent homogenous solution. Then poured 25% Ammonia Solution in the precursor solution until the precipitates are formed with a thick white slurry type resemblance. Now again stirred the solution consisted of precipitates and dried it on a

hot plate at 200 ºC for 2 hrs. Pale yellow matter was obtained after the complete drying. Then ground that matter to form a fine powder and afterwards calcined the dried sample in a furnace at 800 ºC for 2 hrs with the heating rate of 5 ºC/min.

4.2.4 Charaterization of NiO-SDC Variants

Phase identification and crystal structure of the synthesized anode material was determined by X-ray diffractometer (STOE & Cie GmbH Germany). XRD of powder sample was recorded using micro beam of CuKα radiation (λ = 1.5425 Å), with variable 2θ in the range of 10 to 80 degrees. The diffraction pattern was scanned in steps of 0.015°.

4.3 Syntheis of NiO-SDC with La and H_2O_2 Addition

4.3.1 Synthesis and Characterizaiton of NiO-SDC with La Addition

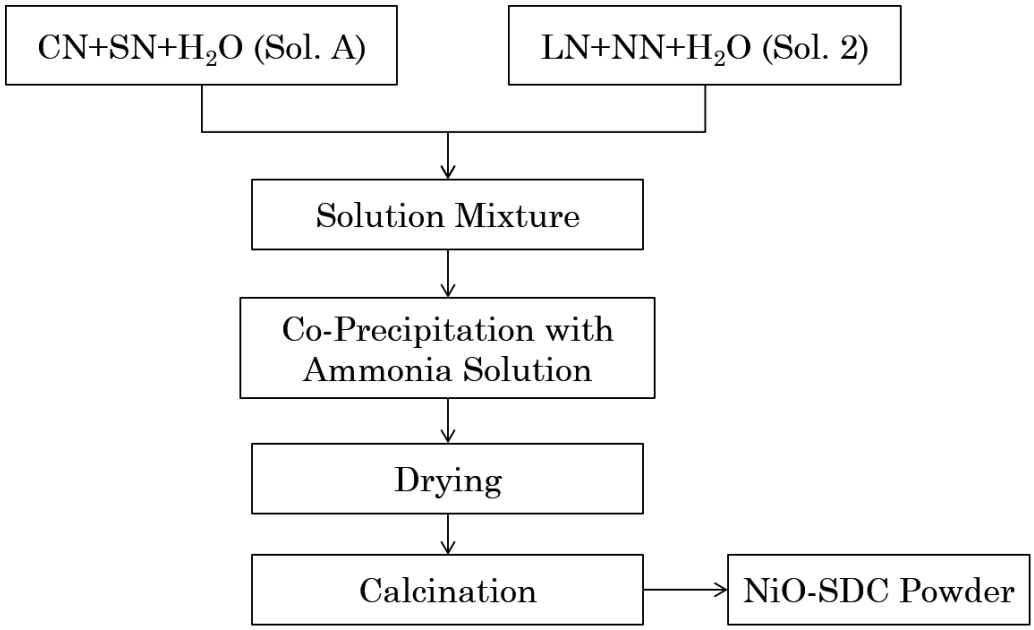

Figure 4.2: Flow Diagram of NiO-SDC Synthesis with Lanthanum Addition where LN, CN, SN and NN are Lanthanum, Cerium, Samarium and Nickle Nitrate Hexahydrates respectively

Lanthanum added NiO-SDC was synthesized through co-precipitation process (Figure 4.2) using nickel Lanthanum nitrate hexahydrate, nitrate hexahydrate, cerium nitrate hexahydrate and samarium nitrate hexahydrate as the precursors. Stoichiometric amounts of lanthanum nitrate hexahydrate and nickel nitrate hexahydrate were dissolved in de-ionized water and separately cerium nitrate hexahydrate and samarium nitrate hexahydrate were thoroughly mixed in de-ionized water. The concentration of the precursor solution was 0.5 M. Both solutions were then mixed and this solution was stirred to obtain a transparent homogenous solution. Then poured 25% Ammonia

Solution in the precursor solution until the precipitates are formed with a thick white slurry type resemblance. Now again stirred the solution consisted of precipitates and dried it on a hot plate at 200 ºC for 2 hrs. Pale yellow matter was obtained after the complete drying. Then ground that matter to form a fine powder and afterwards calcined the dried sample in a furnace at 800 ºC for 2 hrs with the heating rate of 5ºC/min.

Phase identification and crystal structure of the synthesized anode material was determined by X-ray diffractometer (STOE & Cie GmbH Germany). XRD of powder sample was recorded using micro beam of CuKα radiation (λ = 1.5425 Å), with variable 2θ in the range of 10 to 80 degrees. The diffraction pattern was scanned in steps of 0.015°. The morphological analysis and the particle size distribution of the prepared sample was observed by scanning electron microscopy (JEOL Analytical SEM). Thermal performance was analyzed by thermogravimetric and differential thermal analysis.

4.3.2 Synthesis and Characterization of NiO-SDC with Peroxide Inclusion

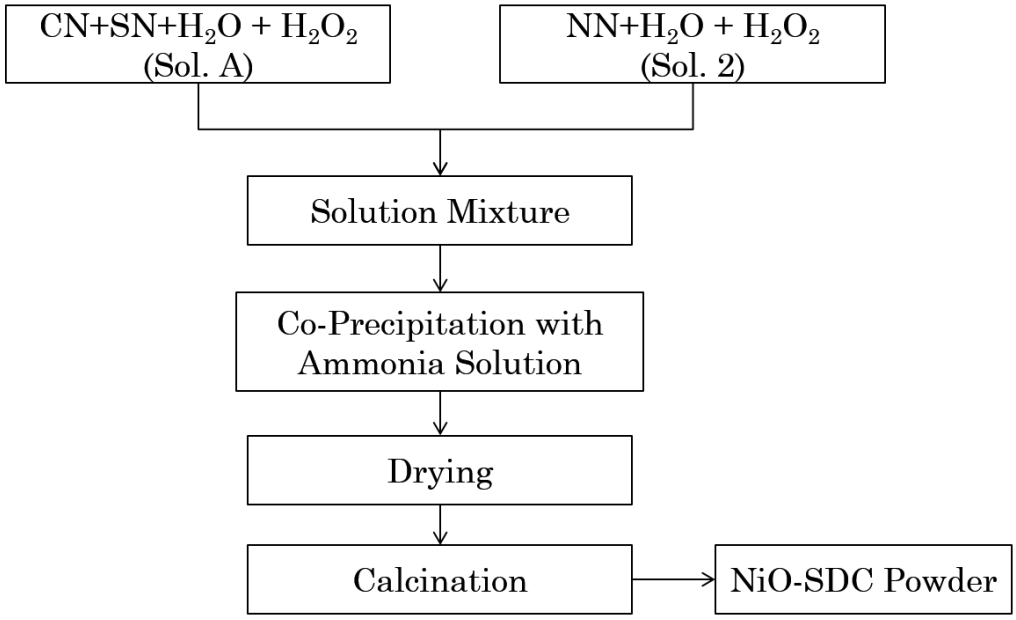

Figure 4.3: Flow Diagram of NiO-SDC Synthesis using Peroxide (H_2O_2) where CN, SN and NN are Cerium, Samarium and Nickle Nitrate Hexahydrates respectively

The ceramic electrode material NiO-SDC was synthesized through co-precipitation process (Figure 4.3) using nickel nitrate hexahydrate, cerium nitrate hexahydrate and samarium nitrate hexahydrate as the precursors [1]. Stoichiometric amounts of nickel

nitrate hexahydrate were dissolved in de-ionized water and separately cerium nitrate hexahydrate and samarium nitrate hexahydrate were thoroughly mixed in de-ionized water. Both solutions were treated with hydrogen peroxide then were intermixed mixed. This solution was stirred to obtain a transparent homogenous solution. Then poured 25% Ammonia Solution in the precursor solution until the precipitates are formed with a thick white slurry type resemblance. Now again stirred the solution consisted of precipitates and dried it on a hot plate at 200 ºC for 2 hrs. Pale yellow matter was obtained after the complete drying. Then ground that matter to form a fine powder and afterwards calcined the dried sample in a furnace at 800 ºC for 2 hrs with the heating rate of 5ºC/min.

Phase identification and crystal structure of the synthesized anode material was determined by X-ray diffractometer (STOE & Cie GmbH Germany). XRD of powder sample was recorded using micro beam of CuKα radiation (λ = 1.5425 Å), with variable 2θ in the range of 10 to 80 degrees. The diffraction pattern was scanned in steps of 0.015°. The morphological analysis and the particle size distribution of the prepared sample was observed by scanning electron microscopy (JEOL Analytical SEM). Thermal performance was analyzed by thermogravimetric and differential thermal analysis.

4.4 Chemical Compatibility Test of NiO-SDC Anode Composite Material and NDC Electrolyte

NiO-SDC and NiO were examined for chemical compatibility and was investigated via solid-state reaction process. Neodymium doped ceria (NDC) electrolyte is a promising candidate material for use in low temperature fuel cell applicatios (SOFC). The starting materials for this solid state reaction method are Neodymium doped ceria (NDC) and NiO-SDC. Both Neodymium doped ceria (NDC) and NiO-SDC were already synthesized in the lab by sol-gel and co-precipitation methods, respectively. 50 wt% of both NDC and NiO-SDC was mixed together and grounded in a pestle mortar equipment for about 1 hour. Then after fine grinding the sample was calcined at 800 °C for 180 minutes with a temperature shift 10 °C/min. Sample was then examined by XRD analysis for identification of new phase/ product (if any) during the synthesis.

New phase/ product formation was determined by X-ray diffraction equipment (STOE Germany). X-ray powder diffraction (XRD) of the sample was recorded using micro beam of CuKα radiation (λ = 1.5425 Å), with variable 2θ in the range of 10 to 80 degrees. The diffraction pattern was scanned in steps of 0.015°.

Summary

Initially, NiO-SDC cermet/ anode material was synthesized through co-precipitation process. Moreover, changes due to change in pH of medium, NiO concentration and calcination temperature on the phase structure and morphology of NiO-SDC have been studied. Afterwards, NiO-SDC was prepared with La addition to investigate the effect of La addition on the microstructure and thermal performance of NiO-SDC anode material. Furthermore, modified co-precipitation method was utilized to develop improved NiO-SDC and find the effects of peroxide addition on chemical and thermal properties of the NiO-SDC. Chemical compatibility test of NiO-SDC with NDC electrolyte was performed at 800 °C for 3 h in order to check the compatibility of these two materials. XRD, SEM along with TGA/DTA were employed to determine the microstructure and thermal properties of the anode materials.

References

[1] Z. Shao, W. Zhou, Z. Zhu, Advanced synthesis of materials for intermediate-temperature solid oxide fuel cells, Prog. Mater. Sci. 57 (2012) 804–874.

[2] I.M. Kolthoff, Theory of Coprecipitation - The formation and properties of crystalline precipitates, in: n.d.

[3] M. Ohring, Materials Science of Thin Films - Deposition & Structure, Second, n.d.

[4] R.M. Ormerod, Solid oxide fuel cells, Chem. Soc. Rev. 32 (2003) 17–28.

[5] A. Pappacena, P. Porreca, M. Boaro, C. de Leitenburg, A. Trovarelli, Effect of process modification and presence of H2O2 in the synthesis of samaria-doped ceria powders for fuel cell applications, Int. J. Hydrogen Energy. 37 (2012) 1698–1709.

Chapter 5

Results and Discussions

5.1 Study of NiO-SDC/ Base Material for SOFC Anode

We have synthesized materials based on various process parameters and investigated addition of La and H_2O_2. Detailed discussion are described in this chapter..

5.1.1 XRD Results of Various Process Parameters of NiO-SDC

Figure 5.1 shows the XRD indexing of the NiO and SDC nanoparticles prepared at the pH value of 9.5, 10 and 10.5. Phase peaks were identified, marked, and analyzed. These peaks described that the crystallites exhibited the cubic fluorite crystal structure (PDF Card # 78-0429 for NiO and 75-0158 for SDC). Further analyzation affirmed no formation of phases other than NiO and SDC There was no evidence of any other phases. The D_{XRD} of NiO and SDC at different pH values of 9.5, 10 and 10.5 were calculated using Scherrer equation. Table 5.1 shows the D_{XRD} calculated from XRD results.

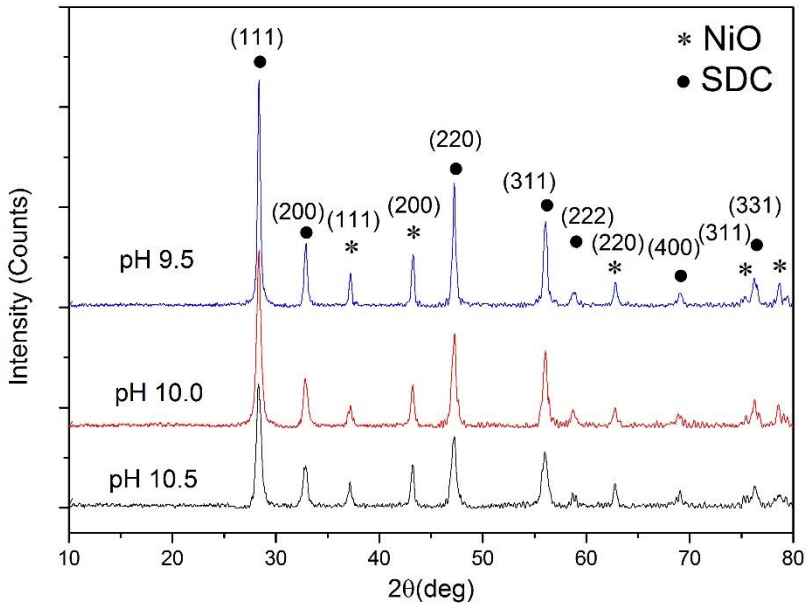

Figure 5.1: XRD patterns of NiO-SDC anode composite at pH = 9.5, 10 and 10.5.

Table 5.1: Crystallites sizes of NiO and SDC calculated from XRD at different pH

	Crystallite Size	
pH	**NiO**	**SDC**
9.5	25.4	27.1
10	28.8	32.4
10.5	33.1	36.6

The precipitation mechanism of metal cations happens through the formation of solvated cation complexes, hydrolysis, and condensation. The hydrolysis and condensation behavior of the solution is affected by the pH during co-precipitation and therefore, affects the crystallite size. With the increase in pH value the rate of hydrolysis decreases due to the gradual decrease in the concentration of the metal cations. The intensity and broadening of the peaks in the diffractogram is starting to increase by increasing the pH value. This shows that increase in pH facilitates in nucleation and growth of crystals. Therefore, crystallite size increases with the increase in pH value [1].

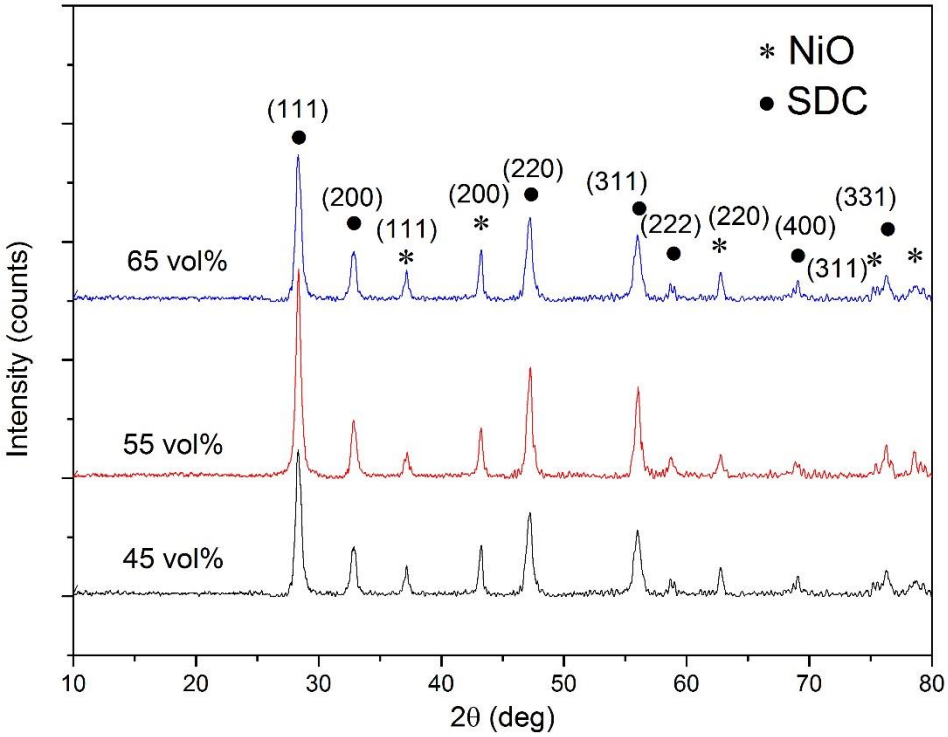

Figure 5.2: XRD patterns of NiO-SDC prepared at variable NiO concentration by volume

The XRD patterns of the synthesized powders with the NiO content of 45-65 vol% are shown in Figure 5.2. All the synthesized powders consist of SDC and NiO two crystal

phases without any other crystal phases, and the relative intensity of the diffraction peaks corresponding to the NiO phase increases with an increase in the NiO content. This means that the NiO-SDC composite powders have been successfully synthesized and the crystal phases of the synthesized NiO-SDC composite powders are unaffected by the NiO content. However, the resulted crystallite size and particle size of the synthesized NiO-SDC composite powders with different NiO content are different mentioned in Table 5.2 [2].

Table 5.2: Crystallites sizes of NiO and SDC calculated from XRD at NiO content

	Crystallite Size	
NiO Concentration	**NiO**	**SDC**
45 vol %	33.1	36.6
55 vol %	25.4	27.1
65 vol %	33.1	36.6

The crystallite sizes of NiO and SDC phases in the NiOeSDC composite powders were calculated from XRD line broadening analysis according to the Scherrer equation. Table 5.2 shows the crystallite sizes of NiO and SDC phases in the NiO-SDC composite powders with the NiO content of 45-65 vol%. It can be seen from Table 5.2 that the crystallite sizes of NiO and SDC slightly change at the NiO content of less than 50 vol% [3]. In contrast, at the NiO content of larger than 50 vol%, the crystallite sizes of NiO and SDC increase with increasing the NiO content. In addition, for all the NiO-SDC composite powders, the crystallite size of NiO is smaller than that of SDC, which indicates that the SDC crystallites grow more quickly than NiO crystallites. The similar observation was also reported in the synthesis of NiO-SDC composite powders by spray pyrolysis technique [4–7]. This also means that SDC is more likely to aggregate than NiO in the NiO-SDC composite powders.

Table 5.3: Crystallite sizes of NiO and SDC at different calcination temperatures

	Crystallite Size	
Calcination Temperature	**NiO**	**SDC**
600 °C	27.7	27.2
800 °C	32	19.5
1000 °C	46.4	31.3

The XRD results of NiO-SDC powders prepared at different calcination temperatures for 1 h are shown in Figure 5.3. With increasing calcination temperature, the powders slowly convert from amorphous phase to NiO and SDC crystal phase. The

crystallization of the amorphous oxides occurred at about 500 °C [8], and the oxidation of Ce^{3+} to Ce^{4+} had occurred up to 500 °C. No Sm_2O_3 crystal phase was found at any calcination temperature, indicating the direct formation of oxide solid solution ($Ce_{0.8}Sm_{0.2}O_{1.9}$). For the present results, the NiO and SDC phases were clearly detected with the XRD and no other phase was found, which indicate that the solid solution between NiO and CeO_2 or Sm_2O_3 was not formed.

Diffraction peaks of SDC and NiO became sharper and more intense with an increase in the calcination temperature, indicating a growth in the crystallite size with an increase in crystallinity of NiO-SDC powder. The crystallite size of SDC and NiO phases was calculated from XRD lines broadening analysis according to the Scherrer equation and is shown in Table 5.3. The crystallite sizes of NiO and SDC phases are 27 - 47 nm at 600-1000 °C, and increase quickly with an increase in the calcinations temperature. It is also noted that the NiO crystallite size is always larger than that of SDC at the same calcining conditions. Similar observation was also reported by the other researchers [7, 9]. This suggests that the NiO crystallites grow more quickly than SDC.

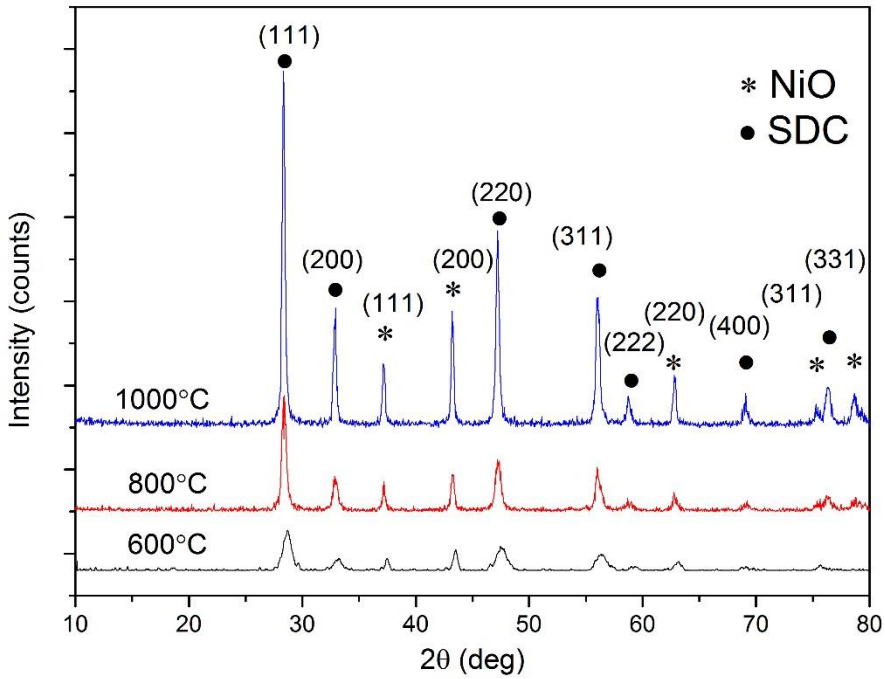

Figure 5.3: XRD patterns of NiO-SDC prepared at different calcination temperatures

5.1.2 SEM Anaylsis of NiO-SDC Composite Anode Material

Scanning electron microscopy was used to further analyze the morphology of as prepared NiO-SDC.

Figure 5.4 clearly shows that particles are well grown and distributed. No irregularity was observed which corresponded to equal distribution of NiO and SDC in the composite structure. NiO and SDC both have contributed into good homogenous structure. Therefore, with desired objectives, best stable structure is possible to achieve.

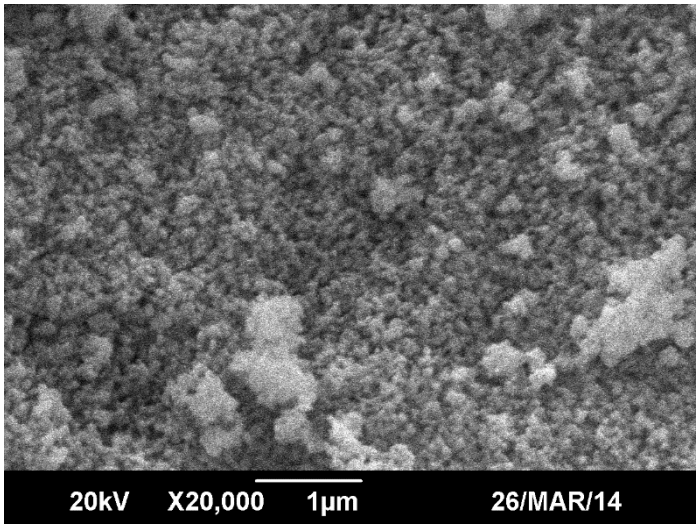

Figure 5.4: SEM images of NiO-SDC

5.1.3 TGA/DTA of NiO-SDC

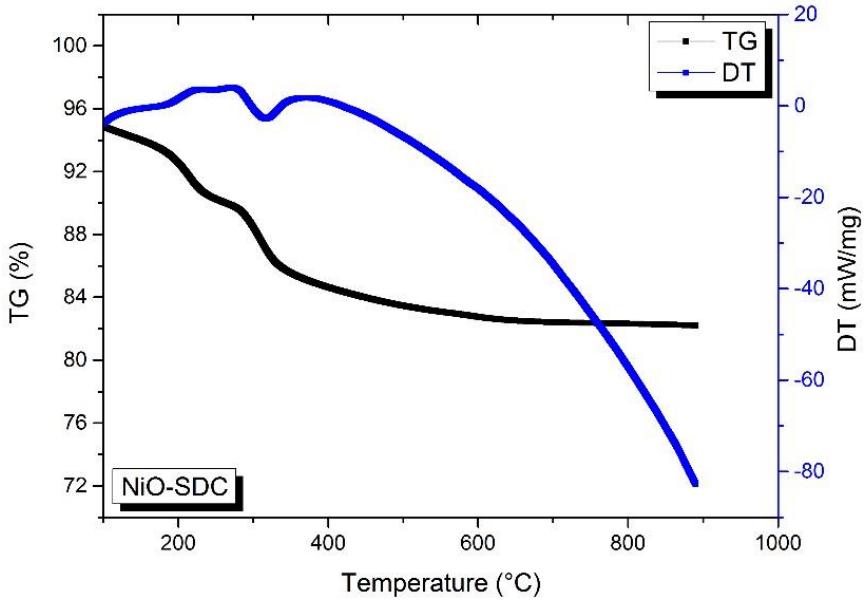

Figure 5.5: TGA & DTA curves obtained from NiO-SDC

Figure 5.5 shows the TG/DT curves of NiO-SDC cermet. Looking at TG curves of NiO-SDC, initial weight loss is being observed at temperatures below 100 °C. This weight loss indicates the removal of water and nitrates from powders. At temperatures

from 100 °C to 400 °C, a weight loss of 15.38% for NiO-SDC anode material was observed. This loss can be attributed to the removal of un-hydrolyzed $Ni(OH)_2$. A total of 17.81% weight loss for NiO-SDC, had been observed which is approximately same for both NiO-SDC and LaNiO-SDC. Weight loss tends to seize after 590 °C.

From DTA curves, we can observe sharp exothermic reaction peak for NiO-SDC, the appears at 314 °C. This exothermic peak indicates a phase change of sample from amorphous to crystalline. These results are consistent with XRD results.

5.1.4 Electrical Conductivity Measurement

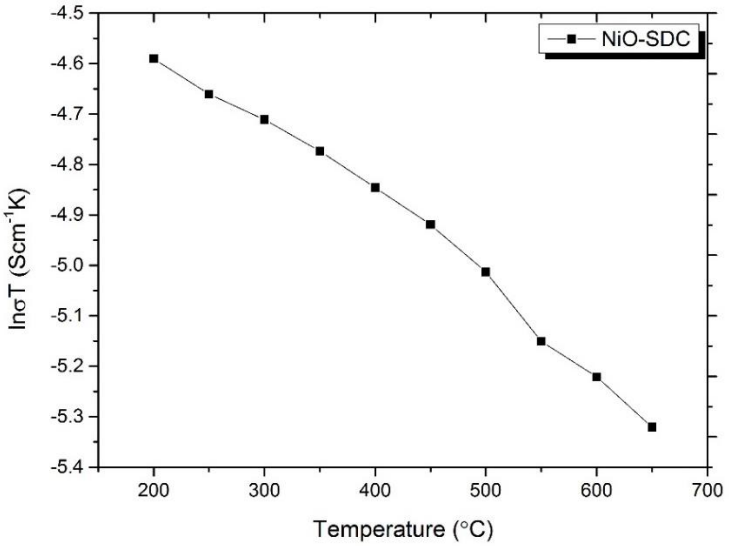

Figure 5.6: Arrhenius plot of the conductivity of NiO-SDC against Temperature

Figure 5.6 shows that conductivity of electrode increases with the rise in temperature. The calculated value of conductivity of NiO-SDC at 650 °C by using Arrhenius equation is 3.494×10^{-3} S/cm. Figure 5.6 shows the plot of conductivity of the prepared sample. As we are already aware of the fact that the ionic transport in such electrodes is due to hopping mechanism that gets facilitated as a result of increase in temperature.

5.2 Study of Effects of Lanthanum Addition in NiO-SDC

Figure 5.7 shows the XRD diffractograms of NiO-SDC with lanthanum inclusion (Ni(La)O-SDC) calcined at 1000°C for 1 hour. All peaks are associated to cubic fluorite crystal structure with the space group Fm-3m (225) (PDF Card # 78-0429 for NiO and 75-0158 for SDC).

Table 5.4: Results based on XRD patterns of Ni(La)O-SDC

	Crystallite Size	
La Addition	**NiO**	**SDC**
10 mol %	47.7	19.5
15 mol %	28.8	15.5
20 mol %	33.1	31.1

-

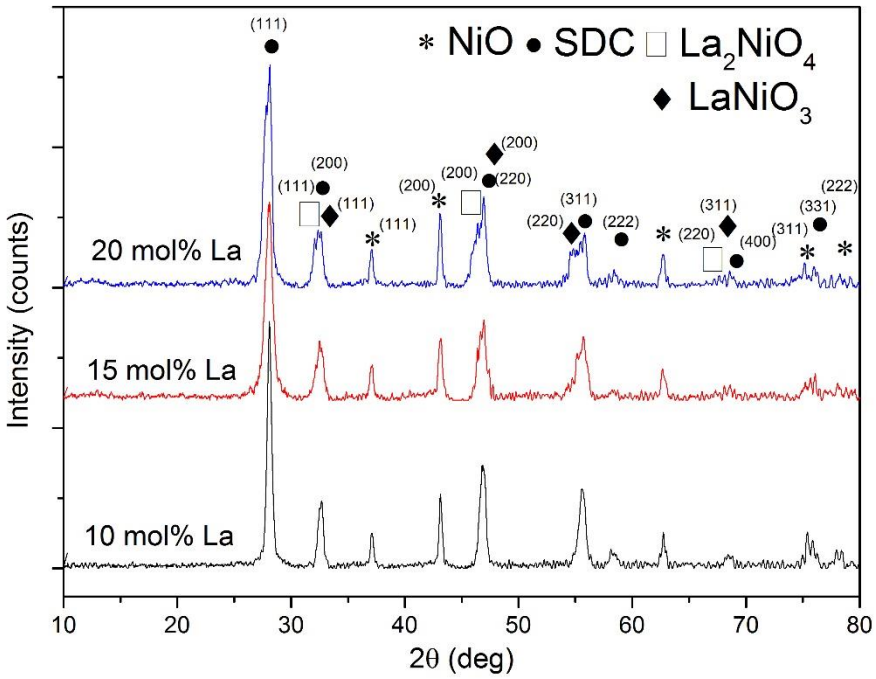

Figure 5.7: XRD patterns of NiO-SDC with Lanthanum Addition

Scanning electron microscopy was used to further analyze the morphology of prepared NiO-SDC, with La inclusion.

Figure 5.8 clearly show that particles are well distributed and diffused. It is evident that addition of La has improved the the overall homogeneity of microstructure as in Figure 5.8. The La has contributed into better distribution of NiO and SDC. Therefore, with the formation of required microstructure, best structurally stable structure can be achieved.

As the La did not appear clearly in XRD patterns therefore, energy dispersive spectroscopy (Figure 5.9) was performed to ensure presence of La in the sample pwders of LaNiO-SDC. It was demonstrated that the addition of La into NiO–SDC anode could effectively improve the performance and stability of the cell when operating on methane at temperatures between 500 and 600 °C [10]. La modification

of the nickel catalyst reduced the polarization resistance and increased the activity for methane [11].

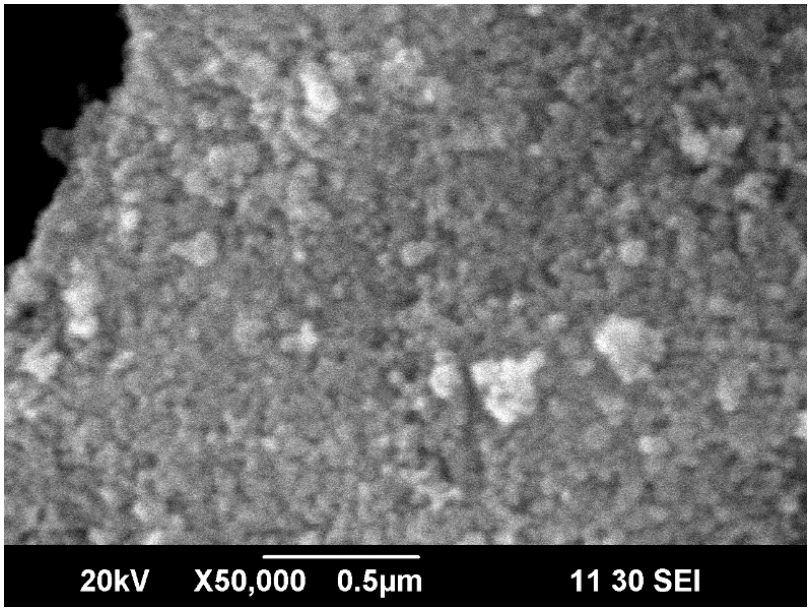

Figure 5.8: SEM images of NiO-SDC with La Addition

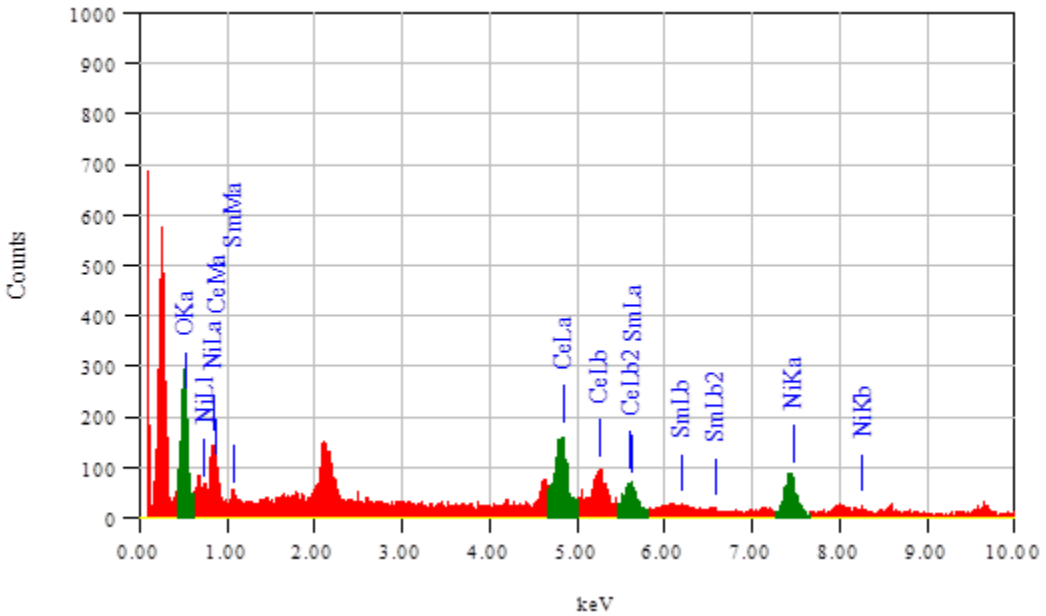

Figure 5.9: EDS images LaNiO-SDC

Figure 5.10 shows the TG/DT curves of LaNiO-SDC. Looking at TG curves of LaNiO-SDC, initial weight loss is being observed at temperatures below 100 °C. This weight loss indicates the removal of water and nitrates from powders. At temperatures from 100 °C to 400 °C, a weight loss 14.55% for LaNiO-SDC powder was observed. This loss can be attributed to the removal of un-hydrolyzed $Ni(OH)_2$. A total of 17.78% for

LaNiO-SDC had been observed which is lower than NiO-SDC. Weight loss tends to seize after 590 °C.

From DTA curves, we can observe sharp exothermic reaction peak appear at 318 °C for LaNiO-SDC. This exothermic peak indicates a phase change of sample from amorphous to crystalline. These results are consistent with XRD results.

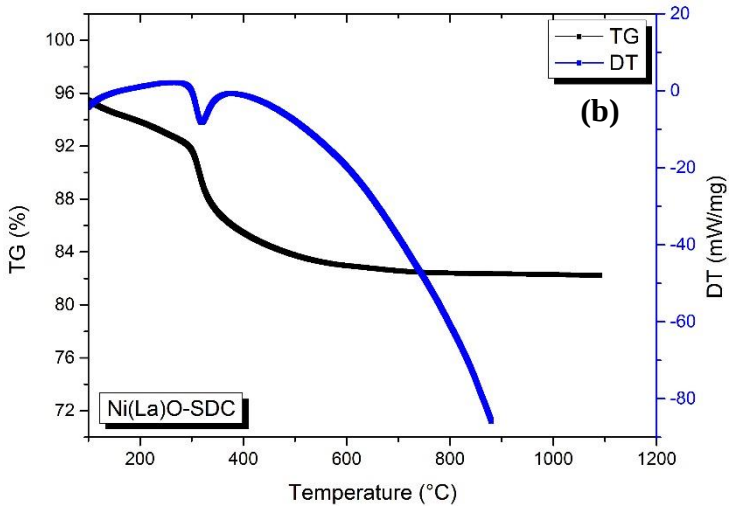

Figure 5.10: representing TG & DT curves obtained from LaNiO-SDC

5.3 Study of NiO-SDC Prepared Using H_2O_2

Table 5.5: XRD results based on NiO-SDC prepared using Peroxide

	Crystallite Size	
H_2O_2 Addition	**NiO**	**SDC**
05 mol %	33.1	16.4
10 mol %	47.7	24.0
15 mol %	28.5	27.1

Table 5.5 shows results based of XRD results of NiO-SDC prepared using peroxide. All the X-ray patterns of the powders obtained with using different amounts of H_2O_2 correspond to the fluorite structure, indicating that the crystallization of NiO and SDC begins during precipitation [12-15]. Diffraction peaks of powders precipitated with H_2O_2 are broader; thus the presence of this additive favors the formation of finer crystallites with respect to the conventional procedure [16]. Similar observations for an analogous composition and for pure ceria were explained [17, 18]. It was observed that the H_2O_2 addition was very effective improving the morphological and redox properties of the mixed oxide [19].

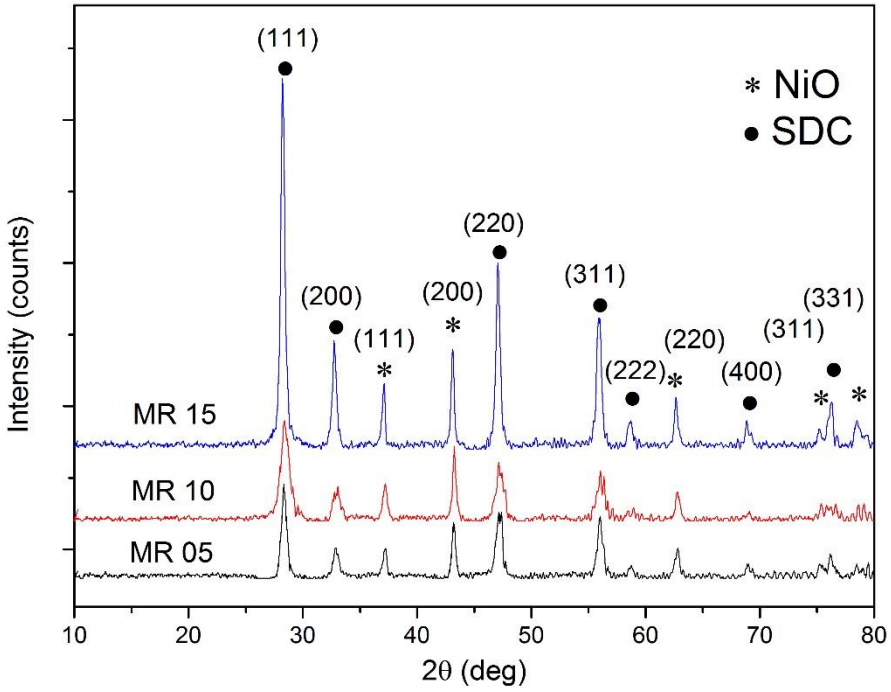

Figure 5.11: XRD patterns of NiO-SDC prepared using Peroxide

Scanning electron microscopy was used to further analyze the morphology of as prepared NiO-SDC, NiO-SDC with La inclusion and NiO-SDC using peroxide.

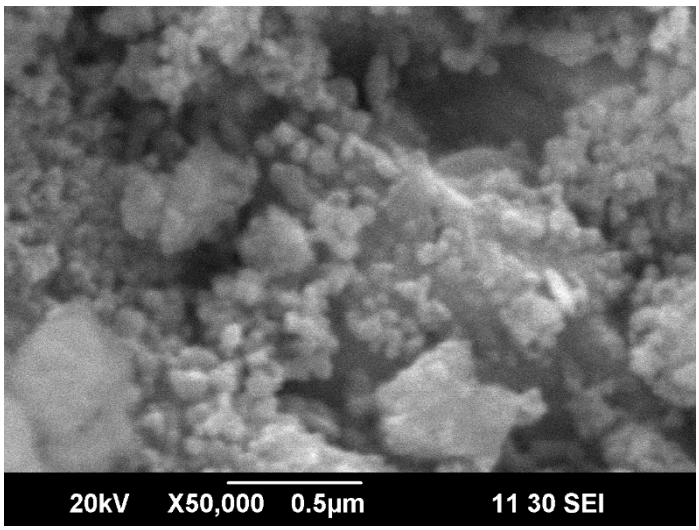

Figure 5.12: SEM images of NiO-SDC (using peroxide)

Figure 5.12 clearly shows that particles are well dispersed and homogenous. It can be observed that addition of peroxide has improved the densification. The small grains have contributed into better densification. Therefore, with proper configuration and mode of experiment best stable microstructure is possible to achieve.

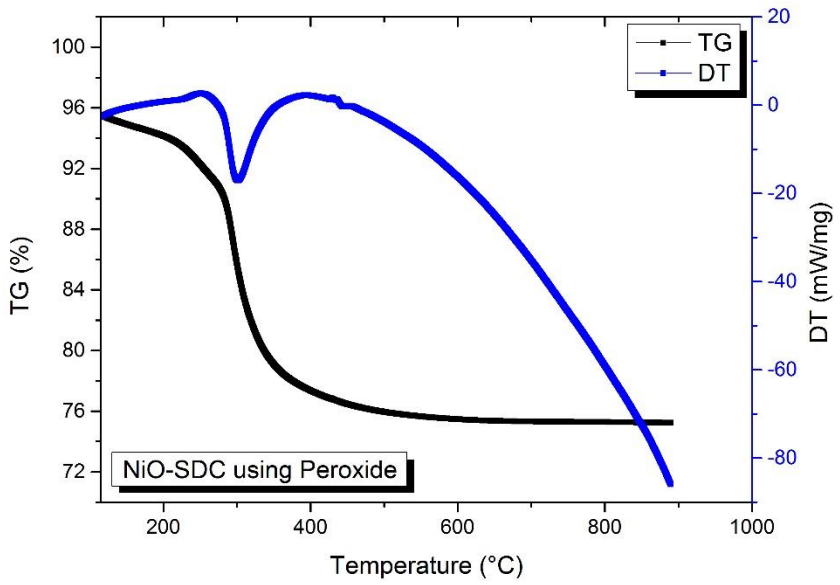

Figure 5.13: Representing TG & DT curves obtained from NiO-SDC (using H_2O_2)

Figure 5.13 shows the TG/DT curves of NiO-SDC (prepared using peroxide) cermet respectively. Looking at TG curve composite sample, initial weight loss is being observed at temperatures below 100 °C. This weight loss indicates the removal of water and nitrates from powders. At temperatures from 100 °C to 400 °C, a weight loss of 22.65% for NiO-SDC (prepared using peroxide) powder was observed which is highest among the as prepared NiO-SDC and LaNiO-SDC. This loss can be attributed to the removal of un-hydrolyzed $Ni(OH)_2$. A total of 24.78% weight loss for NiO-SDC (prepared using peroxide) powders has been observed which is more than both NiO-SDC and LaNiO-SDC. Weight loss tends to seize after 590 °C.

From DTA curves, we can observe sharp exothermic reaction peak. For NiO-SDC (prepared using peroxide) it appears at 302 °C. . This exothermic peak indicates a phase change of sample from amorphous to crystalline. These results are consistent with XRD results.

5.4 Chemical Compatibility Test of NDC and NiO-SDC

NDC electrolyte has recently evolved and there is not enough data available, that's why we carried out chemical stability test of NDC electrolyte material with the NiO-SDC anode to investigate whether both compounds remain stable at elevated temperature.

The experimentation is described in earlier section in Chapter 4. After mixing the , powders sintering was carried out at 800 °C. Figure 5.14 shows the XRD analysis of

prepared composite material. It is clear from the XRD pattern that both the compounds remained separate at the elevated temperature of 800 °C and no mixed phase was found between the two composites. That is why it can be depicted that both of these materials can be used in SOFC.

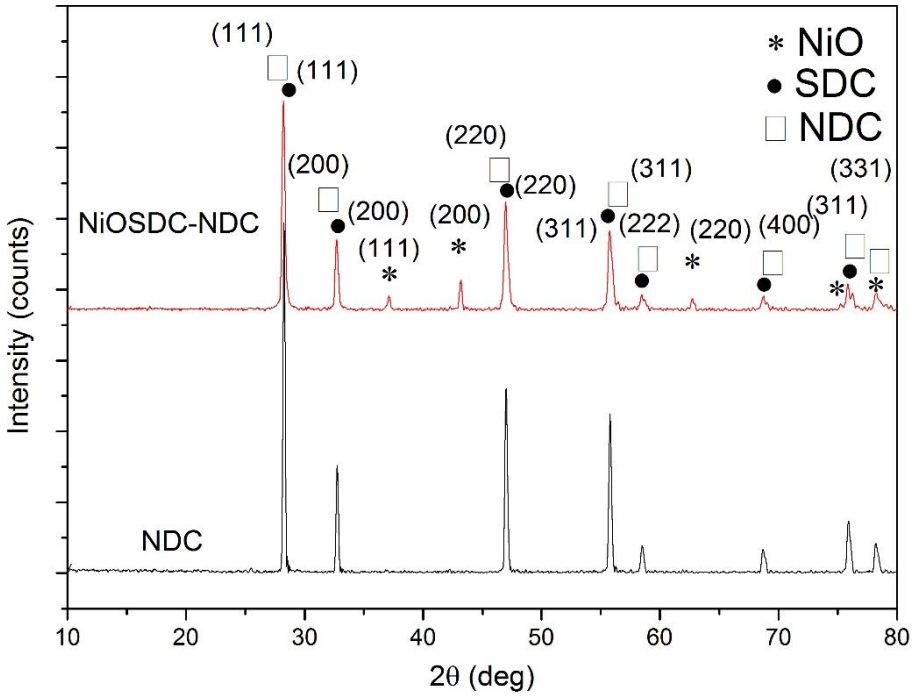

Figure 5.14: XRD patterns of NDC – NiO-SDC

5.5 Discussion of XRD Results Based on Crystallite Size

Table 5.6: Crystallites sizes of NiO-SDC, Ni(La)O-SDC & NiO-SDC using Peroxide

Powder Samples	Average Crystallite Size (nm)
NiO-SDC	33.76
La Addition NiO-SDC	33.50
H_2O_2 Addition NiO-SDC	35.85

The average crystallite size of all powder samples including as prepared NiO-SDC, Ni(La)O-SDC and NiO-SDC using peroxide is shown in Table 5.6. It is evident from the Table 5.6 that average crystallite is almost same for NiO-SDC and La added NiO-SDC but in case of H_2O_2 samples the crystallite increase. This is corresponding with the results of SEM of NiO-SDC and Ni(La)O-SDC. Slight difference in both the crystallites is due to strong chemical bonding of La with Ni and oxygen. H_2O_2 disrupts the M-O-M linkage and releases more hydrolysable Ce^{4+} and Sm^{4+}, which makes the

physical bonding more compact which causes agglomeration and increase the crystallite size.

5.6 Thermal Analysis of NiO-SDC, Ni(La)O-SDC and NiO-SDC (Using Peroxide)

Figure 5.15 (a), (b) and (c) shows the TG/DT curves of NiO-SDC, LaNiO-SDC and NiO-SDC (prepared using peroxide) cermet respectively. Looking at TG curves of all three samples, initial weight loss is being observed at temperatures below 100 °C. This weight loss indicates the removal of water and nitrates from powders. At temperatures from 100 °C to 400 °C, a weight loss of 15.38% for NiO-SDC, 14.55% for LaNiO-SDC and 22.65% for NiO-SDC (prepared using peroxide) powder is being observed. This loss can be attributed to the removal of un-hydrolyzed $Ni(OH)_2$. A total of 17.81% weight loss for NiO-SDC, 17.78% for LaNiO-SDC and 24.78% weight loss for NiO-SDC (prepared using peroxide) powders has been observed which is approximately same for both NiO-SDC and LaNiO-SDC. Weight loss tends to seize after 590 °C.

From DTA curves, we can observe sharp exothermic reaction peaks in both the graphs. For NiO-SDC, the exothermic peak appears at 314 °C, for LaNiO-SDC appears at 318 °C and for NiO-SDC (prepared using peroxide) it appears at 302 °C. These exothermic peaks indicate a phase change of samples from amorphous to crystalline. This corresponds to the XRD results, which indicated formation of no other phase in all NiO-SDC powder samples.

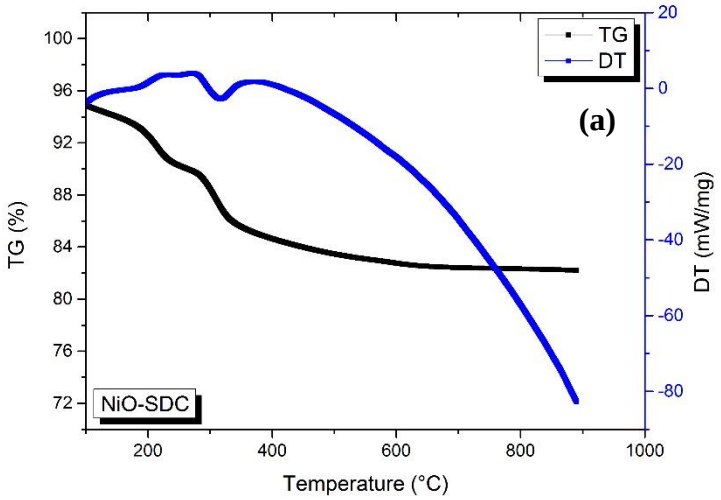

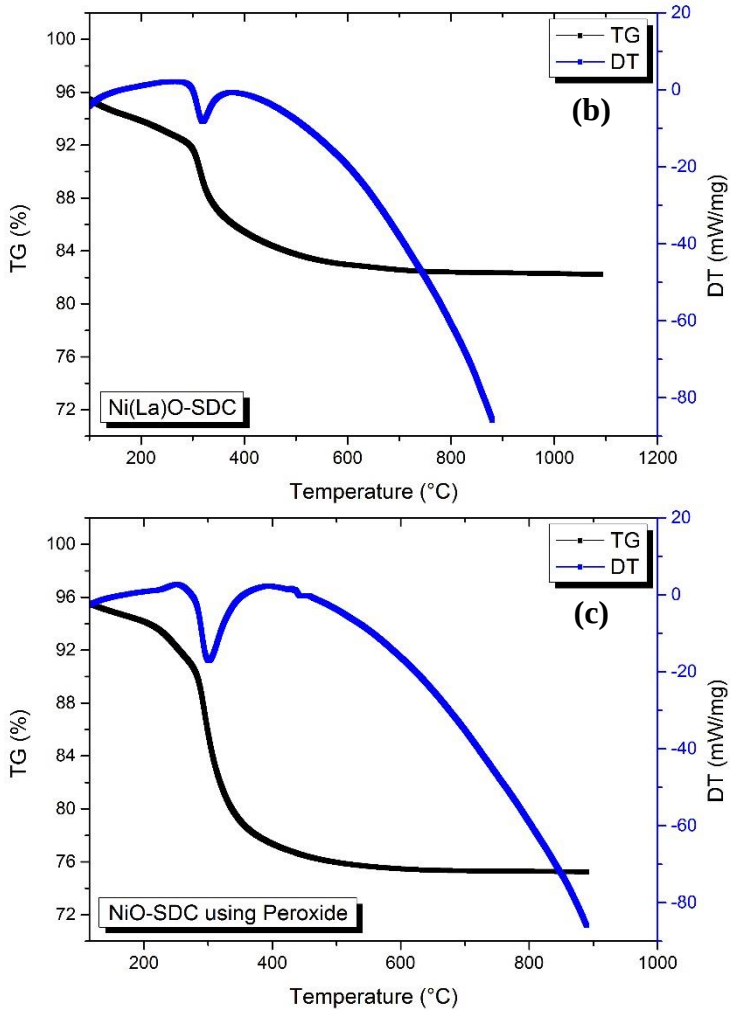

Figure 5.15: TG & DT curves of (a) NiO-SDC, (b) LaNiO-SDC and (c) NiO-SDC (using peroxide) respectively

References

[1] V. Esposito, E. Traversa, Design of Electroceramics for Solid Oxides Fuel Cell Applications: Playing with Ceria, J. Am. Ceram. Soc. 91 (2008) 1037–1051.

[2] C. Ding, T. Hashida, Synthesis and evaluation of NiO–Ce0.8Sm0.2O1.9 nanocomposite powders for low-temperature solid oxide fuel cells, Int. J. Hydrogen Energy. 36 (2011) 5567–5573.

[3] M. Chen, B.H. Kim, Q. Xu, O.J. Nam, J.H. Ko, Synthesis and performances of Ni–SDC cermets for IT-SOFC anode, J. Eur. Ceram. Soc. 28 (2008) 2947–2953.

[4] M. Chen, B.H. Kim, Q. Xu, O.J. Nam, J.H. Ko, Synthesis and performances of Ni–SDC cermets for IT-SOFC anode, J. Eur. Ceram. Soc. 28 (2008) 2947–2953.

[5] M. Kawano, H. Yoshida, K. Hashino, H. Ijichi, S. Suda, K. Kawahara, et al., Synthesis of matrix-type NiO–SDC composite particles by spray pyrolysis with acid addition for development of SOFC cermet anode, J. Power Sources. 173 (2007) 45–52.

[6] Q. Liu, X. Dong, C. Yang, S. Ma, F. Chen, Self-rising synthesis of Ni–SDC cermets as anodes for solid oxide fuel cells, J. Power Sources. 195 (2010) 1543–1550.

[7] H. YOSHIDA, H. DEGUCHI, M. KAWANO, K. HASHINO, T. INAGAKI, H. IJICHI, et al., Study on pyrolysing behavior of NiO–SDC composite particles prepared by spray pyrolysis technique, Solid State Ionics. 178 (2007) 399–405.

[8] C. Ding, H. Lin, K. Sato, T. Hashida, K. Tohji, N. Tsuchiya, et al., Synthesis of NiO-Ce[sub 0.8]Sm[sub 0.2]O[sub 1.9] Composite Nanopowders for Solid Oxide Fuel Cells, AIP Conf. Proc. 987 (2008) 30–34.

[9] X. Fang, Synthesis and properties of Ni–SDC cermets for IT–SOFC anode by co-precipitation, Solid State Ionics. 168 (2004) 31–36.

[10] D. Huang, Q. Xu, F. Zhang, W. Chen, H. Liu, J. Zhou, Synthesis and electrical conductivity of La2NiO4+δ derived from a polyaminocarboxylate complex

precursor, Mater. Lett. 60 (2006) 1892–1895

[11] A. Yan, M. Phongaksorn, D. Nativel, E. Croiset, Lanthanum promoted NiO–SDC anode for low temperature solid oxide fuel cells fueled with methane, J. Power Sources. 210 (2012) 374–380.

[12] A. Aguadero, J.A. Alonso, M.J. Mart?nez-Lope, M.T. Fern?ndez-D?az, M.J. Escudero, L. Daza, In situ high temperature neutron powder diffraction study of oxygen-rich La2NiO4+? in air: correlation with the electrical behaviour, J. Mater. Chem. 16 (2006) 3402.

[13] Wiley: X-Ray Diffraction Procedures: For Polycrystalline and Amorphous Materials, 2nd Edition - Harold P. Klug, Leroy E. Alexander, (n.d.).

[14] J.I. Langford, A.J.C. Wilson, Scherrer after sixty years: A survey and some new results in the determination of crystallite size, J. Appl. Crystallogr. 11 (1978) 102–113.

[15] A. Pappacena, P. Porreca, M. Boaro, C. de Leitenburg, A. Trovarelli, Effect of process modification and presence of H2O2 in the synthesis of samaria-doped ceria powders for fuel cell applications, Int. J. Hydrogen Energy. 37 (2012) 1698–1709.

[16] L. HUANG, S. CHEN, Y. ZHU, M. GONG, Y. CHEN, Preparation of Ce0.65Zr0.35O2 by co-precipitation: The role of hydrogen peroxide, J. Rare Earths. 31 (2013) 461–469.

[17] K. Higashi, K. Sonoda, H. Ono, S. Sameshima, Y. Hirata, Synthesis and sintering of rare-earth-doped ceria powder by the oxalate coprecipitation method, J. Mater. Res. 14 (1999) 957–967.

[18] B.P. Mandal, V. Grover, M.R. Pai, A.K. Tyagi, Improvement of physico-chemical properties by addition of H2O2: An extensive case study on the RE-doped ceria system (RE = Gd, Sm), J. Mater. Res. 24 (2009) 2845–2854.

[19] F.H. Scholes, C. Soste, A.E. Hughes, S.G. Hardin, P.R. Curtis, The role of hydrogen peroxide in the deposition of cerium-based conversion coatings, Appl. Surf. Sci. 253 (2006) 1770–1780.

Conclusions and Recommendations

Conclusions

In this work, efforts have been made for studying various parameters such as pH, NiO concentration by volume, calcination temperature, addition of Lanthanum (La) and Hydrogen Peroxide (H_2O_2), to develop high performance NiO-SDC composite anode. Observations from the x-ray diffraction results demonstrates that crystallites show an increment in their size with the rise in pH and calcination temperature but the alteration of NiO concentration influenced the average crystallite size. The average crystallite size in both the phases (NiO and SDC) increases with increase in the NiO concentration in all composite samples. Furthermore, no impurity phases have been found in the crystalline structure of synthesized NiO-SDC composite material. SEM results demonstrated that NiO-SDC powder samples are well dispersed but the particles exhibit irregular shape and size of the particles ranges from 50-65 nm.

Two different methods have been used to improve the NiO-SDC cermet. Firstly, NiO-SDC composite anode material by adding Lanthanum (La), Ni(La)O-SDC, was prepared by co-precipitation route. Cubic fluorite structure was observed and crystallite sizes, of both NiO and SDC, were found in the size ranges of 25 nm – 48 nm. La mix and disperse in the compound finely and no chemical reaction was observed with 10 mol% La or even with 15 mol% La. However, with 20 mol% La, there appears the onset formation of La_2NiO_4 and $LaNiO_3$. Secondly, NiO-SDC was synthesized via altered co-precipitation method with the inclusion of Hydrogen Peroxide (H_2O_2). Cubic fluorite structures was also observed in NiO-SDC prepared using H_2O_2 and crystallites of NiO and SDC were found in the size ranges of 20 nm - 48 nm. Addition of H_2O_2 promotes somewhat earlier crystallization and it also resulted in formation of refined crystals. Furthermore, the conductivity of NiO-SDC was also calculated at 650 °C and found to be 3.494×10^{-3} S/cm.

Last part contains chemical compatibility test of Neodymium Doped Ceria (NDC) electrolyte composite material and NiO-SDC. XRD characterization showed that both NDC and NiO-SDC remained separate at the elevated temperature of 800 °C and no mixed phase was found between the two composites. That is why it can be depicted that both of these materials can be used in SOFC applications. Therefore, these

research results can broaden the opportunities for applications in intermediate temperature solid oxide fuel cells (IT-SOFCs).

Recommendations

In the future, the electronic and ionic conductivity of NiO-SDC electrodes synthesized at various variants are required to be determined in order to optimize the reaction parameters during synthesis and to verify the results based on this study. It is also recommended to optimize the molar concentration of Lanthanum as an additive in NiO-SDC electrode to achieve the best possible stable structure with high performance because in this study only three compositions have been studied. Chemical compatibility test of NiO-SDC and NDC showed that both composites exhibit good matching of physiochemical properties so it is recommended to manufacture a button cell and/or symmetrical cell by using these two materials and test the performance of these cells up to intermediate temperature range, which will definitely be the novel research in this area.

Acknowledgements

First and foremost, I would like to express profound gratitude to my supervisor, Dr. Zuhair S. Khan, for giving me the opportunity to join Advanced Energy Materials and Fuel Cells Lab in CES, and for his invaluable support, encouragement, supervision and useful suggestions throughout this research work. His continuous guidance enables me to carry out my work successfully.

I am overwhelmed with the gratitude for the help and supervision by my co-supervisor, Dr. Mrs. Naveed K. Janjua, for all her professional guidance on research work and especially for her enormous help during my two months visit in Fuel Cells Lab at the Department of Chemistry in QAU, Islamabad.

I would like to thank my GEC members, Dr. M. Bilal Khan and Dr. Nasir Mehmood Ahmad, for the pleasant, effective and productive cooperation along with continuous encouragement and discussion.

Thanks to the PGP and Research Directorates of NUST for their financial support during my research work.

I would like to thank my group fellows in this lab, Mr. Mustafa Anwar, Mr. M. Akmal Rana, Mr. Kamal Mustafa and Miss Sehar Shakir for their continuous support and help during the last year of research. I will always remember the times we spent together in this lab and I wish them all the best in their future careers and lives.

Finally, I owe my deepest gratitude to my sweetest family: my parents, my sisters, my brother and my grand-parents, whose constant care, unconditional love, support and prayers helped me a lot during my whole educational career.

Annexure-A

Preparation of NiO-SDC Composites by a Modified Co-Precipitation Synthesis Method for Solid Oxide Fuel Cell (SOFC) Applications.

M. N. Akbar[a], M. Anwar[a], Zuhair S. Khan[a]*, Naveed K. Janjua[b]

[a]Advanced Energy Materials & Fuel Cells Lab, Centre for Advanced Studies in Energy, National University of Sciences and Technology Sector H-12, Islamabad-44000, Pakistan.
[b]Department of Chemistry, Quaid-i-Azam University, Islamabad-45320, Pakistan.
Email: zskhan@ces.nust.edu.pk

Keywords

Peroxide, Co-precipitation, Anode Microstructure, SOFC

Abstract

The fundamental step in the development of sustainable energy technologies is the effectuation of fuel cell energy systems in terms of new devices, materials and optimized processes for their production. Rare earth doped ceria oxides are suitable candidates for the new generation of cells but their cost effective production is of primal consideration as the price of rare earths is increasing. This work mainly involves the investigation of a novel method of co-precipitation by modifying synthesis with hydrogen peroxide. Some controlled parameters during synthesis process were the H_2O_2/M^{3+} molar ratio and the pH. Structural determinations of composite powders was done by X-Ray diffraction (XRD) and Scanning Electron Microscopy/Energy Dispersive X-Ray (SEM/EDX) techniques. Also, the studies were being carried out for the thermal analysis by Thermo Gravimetric Analysis (TGA) and the surface area & porosity by Brunauer Emmett Teller (BET) techniques. The synthesis approach used in this study was shown to be effective in the development of materials with properties exploitable for applications in catalysis and in Intermediate Temperature-Solid Oxide Fuel Cell (IT-SOFC) systems.

Introduction

A sustainable production of energy based on the use of H2 as transportation fuel and portable power requires the development of fuel cell and electrolyser technologies [1] as well as the development of new catalysts for H_2 production and its purification. In this perspective, RE-doped ceria catalysts with RE = Sm, Gd, Y, La have been attracting growing attention especially for their use as electrolyte or electrodes components in intermediate temperature solid oxide fuel cells and electrolysers (IT-SOFC, SOE) [1-7] and as catalysts for environmental and

energy production applications [8-11]. The physico-chemical properties of these oxides are dependent on their preparation approach [12-17]. There is a considerable interest in the development of versatile syntheses to engineer the powder properties suited to specific applications. Among the several ceria and RE/CeO_2 mixed oxides preparation syntheses, an inexpensive and flexible method commonly used is co-precipitation of the respective hydroxides from salt precursors followed by calcination [18-20]. With this approach the catalytic, morphological and structural properties of the final product can be modulated and controlled either by modifying the parameters of synthesis or by adding co-precipitant agents such as oxidizers [21,22], surfactants [23,24] and ligands [25]. In this regard, the addition of hydrogen peroxides deserves some attention. In fact, Woodhead proposes use of this additive for the production of ceria dispersions [26] and other studies demonstrate that it favours the production of nanocrystalline ceria [21, 27, 28]. In this case, the role of H_2O_2 is to convert the Ce^{3+} to the more easily hydrolysable Ce^{4+}, as well as to form cerium hydro peroxide complexes rather than simple hydroxides as oxide precursors. The presence of peroxo ligands would disrupt the formation of a compact network Ce-O-Ce, during the crystallization process, favouring the formation of highly dispersed nanocrystallites [21]. Hydrogen peroxide was shown to be a good additive for the stabilization of the tetragonal phase of ZrO_2 and ZrO_2 based electrolytes [29-31]. In the preparation of ceria and zirconia solid solutions for automobile catalyst applications, the interaction between the OOH hydroperoxyl ligand with both the cerium and the zirconium ions was found to improve the redox properties and the thermal resistance of these materials, which maintain a significant surface area and a high oxygen storage capacity even after calcination at 1373 K [32]. Recently it has been observed that the use of H2O2 also positively affected the production of rare earth-ceria mixed oxides contributing to an increase of their surface area and redox properties [33, 34].

In this study NiO-$Ce_{0.8}Sm_{0.2}O_{1.9}$ was prepared by conventional precipitation and by a modified route adding H_2O_2 before precipitation. The effect of critical parameter i.e., the amount of hydrogen peroxide was investigated and correlated with the structural and morphological characteristics of the calcined oxides. The aim of this study is to develop a flexible methodology which through the simple control of synthesis parameters allows us to generate materials with different functionalities. This could have particular relevance in the cost effective production of IT-SOFC devices, where this composition can be used both as an electrode component and electrolyte [35,36].

Experiemental

2.1 Synthesis

$Ce(NO_3)_3.6H_2O$ (99.99%), $Sm(NO_3)_3.6H_2O$ (99.95%) and $Ni(NO_3)_2.6H_2O$ (99.95%) were used as starting materials for the synthesis of NiO-$Ce_{0.8}Sm_{0.2}O_{1.9}$ (NiO-SDC) nanocomposite powders. $NH_3.H_2O$ were used as co-precipitation agent. The appropriate proportion of nitrate salts of Ce and Sm were dissolved in distilled water labelled as Sol-A while Ni nitrate salt was dissolved into distilled water labelled as Sol-B. Then Sol-A and Sol-B were mixed in and stirred at 60 °C and continuously stirred to form a homogenous solution at 60°C. After 30

minutes solution was let to cool till room temperature. $NH_3.H_2O$ solution was then added drop wise to the above solution mixture to form precipitate with stirring until the pH of >9 was reached. Finally, solution was dried and calcined at 800°C for 1 h to form NiO-SDC composite powders.

Then NiO-SDC was prepared by addition of peroxide before precipitation. The above process was modified by adding peroxide in molar ratio [H_2O_2/M^{3+}] of 5, 10 and 15. Rest of the process is the same except that it was not heated during stirrin because it was an exothermic reaction.

2.2 Characterization

Crystal phases of the synthesized powders were analysed by X-ray diffraction (PANalytical - X'Pert) using CuKa radiation (λ = 1.5425Å). The morphology and particle size of the synthesized powders were examined by Scanning electron microscopy (SEM, JEOL, Japan). Porosity measurements were done by BET while thermal performance was tested with TGA method.

Results and Discussions

X-Ray Diffraction

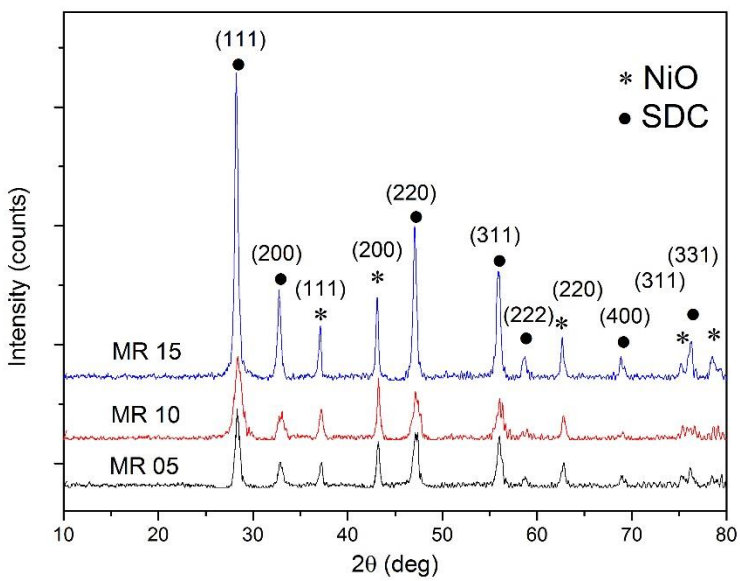

Figure 1 XRD patterns of NiO-SDC prepared with different molar ratio of H_2O_2

The NiO-SDC powders were analysed by XRD using a X-ray diffractometer with CuKα radiation. Crystalline phases were identified and crystallite sizes for NiO and SDC were calculated from the (1 1 1) reflection using the Scherrer equation[50]:

$$d = \frac{K\lambda}{Bcos(\theta_B)}$$

where *d* is the crystallite dimension, K is the Scherrer constant (equal to 1.1547 for the (111) plane in a cubic structure [51], λ is the wavelength of radiation (1.54056 A˚ for CuKa), *B* is the full width at half maximum height (FWHM) of the diffraction peak (in radians) and θ_B is the Bragg angle.

All the X-ray patterns of the powders obtained with using different amounts of H_2O_2 correspond to the fluorite structure, indicating that the crystallization of NiO and SDC begins during precipitation [52]. Diffraction peaks of powders precipitated with H_2O_2 are broader; thus the presence of this additive favors the formation of finer crystallites with respect to the conventional procedure[53]. Similar observations for an analogous composition and for pure ceria were explained [54,55]. Table 5.4 shows results based of XRD results of NiO-SDC prepared using peroxide. It was observed that the H_2O_2 addition was very effective improving the morphological and redox properties of the mixed oxide [24].

Scanning Electron Microscopy

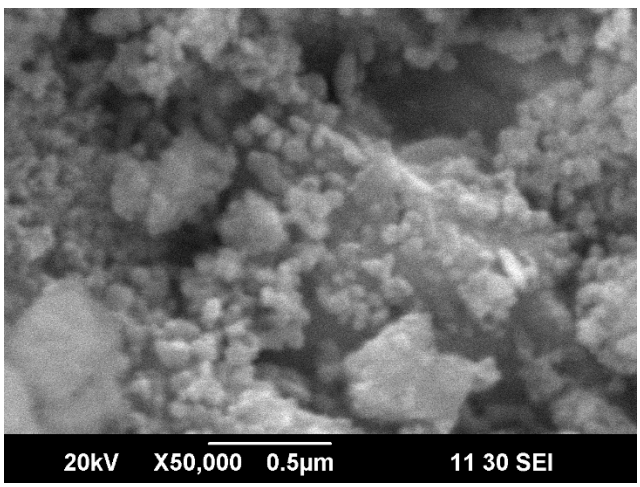

Figure 2 SEM micrograph of NiO-SDC prepared using H_2O_2

Scanning electron microscopy was used to further analyze the morphology of NiO-SDC using peroxide.

Fig. 2 clearly show that particles are well dispersed and homogenous. It can be observed that addition of peroxide has improved the densification.

The small grains have contributed into better densification. Therefore, if the desired microstructure can be formed, best stable structure is possible to achieve.

Conclusions

A method of co-precipitation of NiO-SDC via the addition of H_2O_2 was studied. The effect of the parameters of synthesis on the physico-chemical properties of the material were investigated in order to rationalize an easy approach capable of producing a versatile material for different applications in fuel cell technology. In particular, it was observed that the H_2O_2 addition was very effective in improving the morphological and structural properties of the mixed oxide.

References

[1] A. Pappacena, P. Porreca, M. Boaro, C. de Leitenburg, A. Trovarelli, Effect of process modification and presence of H2O2 in the synthesis of samaria-doped ceria powders for fuel cell applications, Int. J. Hydrogen Energy. 37 (2012) 1698–1709.

[2] M. YUE, M. CUI, N. ZHANG, Z. LONG, X. HUANG, Characterization of CeO2-ZrO2 mixed oxides prepared by two different co-precipitation methods, J. Rare Earths. 31 (2013) 251–256.

[3] F.H. Scholes, C. Soste, A.E. Hughes, S.G. Hardin, P.R. Curtis, The role of hydrogen peroxide in the deposition of cerium-based conversion coatings, Appl. Surf. Sci. 253 (2006) 1770–1780.

[4] L. HUANG, S. CHEN, Y. ZHU, M. GONG, Y. CHEN, Preparation of Ce0.65Zr0.35O2 by co-precipitation: The role of hydrogen peroxide, J. Rare Earths. 31 (2013) 461–469.

[1] Akbari-Fakhrabadi, R.E. Avila, H.E. Carrasco, S. Ananthakumar, R.V. Mangalaraja, Combustion synthesis of NiO–Ce0.9Gd0.1O1.95 nanocomposite anode and its electrical characteristics of semi-cell configured SOFC assembly, J. Alloys Compd. 541 (2012) 1–5.

[2] E. Antolini, J. Perez, The use of rare earth-based materials in low-temperature fuel cells, Int. J. Hydrogen Energy. 36 (2011) 15752–15765.

[3] M. Asamoto, S. Miyake, K. Sugihara, H. Yahiro, Improvement of Ni/SDC anode by alkaline earth metal oxide addition for direct methane–solid oxide fuel cells, Electrochem. Commun. 11 (2009) 1508–1511.

[4] H. Chen, K. Cheng, Z. Wang, W. Weng, G. Shen, P. Du, et al., Preparation of Porous NiO-Ce0.8Sm0.2O1.9 Ceramics for Anode-supported Low-temperatureSolid Oxide Fuel Cells, J. Mater. Sci. Technol. 26 (2010) 523–528.

[5] M. Chen, B.H. Kim, Q. Xu, O.J. Nam, J.H. Ko, Synthesis and performances of Ni–SDC cermets for IT-SOFC anode, J. Eur. Ceram. Soc. 28 (2008) 2947–2953.

[6] Y. Chen, S. Chen, G. Hackett, H. Finklea, J. Zondlo, I. Celik, et al., Microstructure degradation of YSZ in Ni/YSZ anodes of SOFC operated in phosphine-containing fuels, Solid State Ionics. 234 (2013) 25–32.

[7] C. Chioaru, I. Jitaru, M. Bicher, I. Mixed, SYNTHESIS AND CHARACTERIZATION OF NEW PRECURSORS FOR LANTHANUM NICKELATE, 70 (2008) 1–8.

[8] L.O.O. da Costa, A.M. da Silva, F.B. Noronha, L. V. Mattos, The study of the performance of Ni supported on gadolinium doped ceria SOFC anode on the steam reforming of ethanol, Int. J. Hydrogen Energy. 37 (2012) 5930–5939.

[9] C. Ding, H. Lin, K. Sato, T. Hashida, K. Tohji, N. Tsuchiya, et al., Synthesis of NiO-Ce[sub 0.8]Sm[sub 0.2]O[sub 1.9] Composite Nanopowders for Solid Oxide Fuel Cells, AIP Conf. Proc. 987 (2008) 30–34.

[10] C. Ding, T. Hashida, Synthesis and evaluation of NiO–Ce0.8Sm0.2O1.9 nanocomposite powders for low-temperature solid oxide fuel cells, Int. J. Hydrogen Energy. 36 (2011) 5567–5573.

[11] M.J. Escudero, I. Gómez de Parada, A. Fuerte, J.L. Serrano, Analysis of the electrochemical performance of MoNi–CeO2 cermet as anode material for solid oxide fuel cell. Part I. H2, CH4 and H2/CH4 mixtures as fuels, J. Power Sources. 253 (2014) 64–73.

[12] L. Fan, C. Wang, M. Chen, B. Zhu, Recent development of ceria-based (nano)composite materials for low temperature ceramic fuel cells and electrolyte-free fuel cells, J. Power Sources. 234 (2013) 154–174.

[13] M. Ferkhi, A. Ringuedé, A. Khaled, L. Zerroual, M. Cassir, La1.98Ni04±δ, a new cathode material for solid oxide fuel cell: Impedance spectroscopy study and compatibility with gadolinia-doped ceria and yttria-stabilized zirconia electrolytes, Electrochim. Acta. 75 (2012) 80–87.

[14] M.L. Ferrari, A.F. Massardo, Cathode–anode side interaction in SOFC hybrid systems, Appl. Energy. 105 (2013) 369–379.

[15] a. Fuerte, R.X. Valenzuela, M.J. Escudero, L. Daza, Study of a SOFC with a bimetallic Cu–Co–ceria anode directly fuelled with simulated biogas mixtures, Int. J. Hydrogen Energy. 39 (2014) 4060–4066.

[16] S. Goriparti, E. Miele, F. De Angelis, E. Di Fabrizio, R. Proietti Zaccaria, C. Capiglia, Review on recent progress of nanostructured anode materials for Li-ion batteries, J. Power Sources. 257 (2014) 421–443.

[17] J. Hanna, W.Y. Lee, Y. Shi, A.F. Ghoniem, Fundamentals of electro- and thermochemistry in the anode of solid-oxide fuel cells with hydrocarbon and syngas fuels, Prog. Energy Combust. Sci. 40 (2014) 74–111.

[18] J.-E. Hong, S. Ida, T. Ishihara, Decreased sintering temperature of anode-supported solid oxide fuel cells with La-doped CeO2 and Sr- and Mg-doped LaGaO3 films by Co addition, J. Power Sources. 259 (2014) 282–288.

[19] B.A. Horri, C. Selomulya, H. Wang, Electrochemical characteristics and performance of anode-supported SOFCs fabricated using carbon microspheres as a pore-former, Int. J. Hydrogen Energy. 37 (2012) 19045–19054.

[20] B.A. Horri, C. Selomulya, H. Wang, Characteristics of Ni/YSZ ceramic anode prepared using carbon microspheres as a pore former, Int. J. Hydrogen Energy. 37 (2012) 15311–15319.

[21] D. Huang, Q. Xu, F. Zhang, W. Chen, H. Liu, J. Zhou, Synthesis and electrical conductivity of La2NiO4+δ derived from a polyaminocarboxylate complex precursor, Mater. Lett. 60 (2006) 1892–1895.

[22] H.-N. Im, S.-Y. Jeon, M.-B. Choi, H.-S. Kim, S.-J. Song, Chemical stability and electrochemical properties of CaMoO3−δ for SOFC anode, Ceram. Int. 38 (2012) 153–158.

[23] A. Kirubakaran, S. Jain, R.K. Nema, A review on fuel cell technologies and power electronic interface, Renew. Sustain. Energy Rev. 13 (2009) 2430–2440.

[24] a. Lanzini, P. Leone, C. Guerra, F. Smeacetto, N.P. Brandon, M. Santarelli, Durability of anode supported Solid Oxides Fuel Cells (SOFC) under direct dry-reforming of methane, Chem. Eng. J. 220 (2013) 254–263.

[25] H. Li, C. Xia, Z. Zhou, M. Zhu, G. Meng, Improving the anode microstructure for SOFC with coprecipitated composite NiO/Ce0.8Sm0.2O1.9 powder, J. Mater. Sci. 41 (2006) 3185–3187.

[26] X.B. Li, H.Y. Wang, H.X. Gu, J. Wang, W.J. Zhang, T.G. Wang, Preparation of gradient Ni-SDC anode by tape casting and co-sintering, Sci. Sinter. 42 (2010) 153–159.

[27] E. Lorente, M. Millan, N.P. Brandon, Use of gasification syngas in SOFC: Impact of real tar on anode materials, Int. J. Hydrogen Energy. 37 (2012) 7271–7278.

[28] T. Mahata, S.R. Nair, R.K. Lenka, P.K. Sinha, Fabrication of Ni-YSZ anode supported tubular SOFC through iso-pressing and co-firing route, Int. J. Hydrogen Energy. 37 (2012) 3874–3882.

[29] S. Mekhilef, R. Saidur, A. Safari, Comparative study of different fuel cell technologies, Renew. Sustain. Energy Rev. 16 (2012) 981–989.

[30] S. Mhlanga, K. Mondal, Synthesis and study of carbon microspheres for use as catalyst support for cobalt, South African J. …. (2009) 304–308.

[31] P. Moçoteguy, A. Brisse, A review and comprehensive analysis of degradation mechanisms of solid oxide electrolysis cells, Int. J. Hydrogen Energy. 38 (2013) 15887–15902.

[32] E.P. Murray, T. Tsai, S.A. Barnett, A direct-methane fuel cell with a ceria-based anode, Nature. 400 (1999) 649–651.

[33] L. Nie, J. Liu, Y. Zhang, M. Liu, Effects of pore formers on microstructure and performance of cathode membranes for solid oxide fuel cells, J. Power Sources. 196 (2011) 9975–9979.

[34] G. Nurk, T. Huthwelker, a. Braun, C. Ludwig, E. Lust, R.P.W.J. Struis, Redox dynamics of sulphur with Ni/GDC anode during SOFC operation at mid- and low-range temperatures: An operando S K-edge XANES study, J. Power Sources. 240 (2013) 448–457.

[35] W.-P. Pan, Z. Lü, K.-F. Chen, X.-B. Zhu, X.-Q. Huang, Y.-H. Zhang, et al., Paper-Fibres Used as a Pore-Former for Anode Substrate of Solid Oxide Fuel Cell, Fuel Cells. 11 (2011) 172–177.

[36] S. Park, J. Lee, J. Han, Fabrication of anode supports for solid oxide fuel cells using nickel carbonate as a pore former, J. …. 13 (2012) 699–704.

[37] J. Patakangas, Y. Ma, Y. Jing, P. Lund, Review and analysis of characterization methods and ionic conductivities for low-temperature solid oxide fuel cells (LT-SOFC), J. Power Sources. 263 (2014) 315–331.

[38] B.B. Patil, V. Ganesan, S.H. Pawar, Studies on spray deposited NiO–SDC composite films for solid oxide fuel cells, J. Alloys Compd. 460 (2008) 680–687.

[39] M. Poon, O. Kesler, The influence of pore formers on the microstructure of plasma-sprayed NiO–YSZ anodes, J. Power Sources. 210 (2012) 204–217.

[40] M.K. Rath, M.-J. Lee, K.-T. Lee, Preparation of nano-structured Ni–Ce0.8Gd0.2O1.9 anode materials for solid oxide fuel cells via the water-in-oil (W/O) micro-emulsion route, Ceram. Int. 40 (2014) 1909–1917.